Fraunhofer IFAM

Universität Bremen

Effect of stress concentrations on the fatigue behaviour of structural adhesives

Dissertation

approved for the degree of

Doctor in Engineering

– Dr.-Ing –

Faculty of Production Engineering

Department of Production Engineering

University of Bremen

by

Vinicius Carrillo Beber

Bremen, March 2018

Fraunhofer IFAM

Universität Bremen

Einfluss von Spannungskonzentrationen auf das Ermüdungsverhalten von Strukturklebstoffen

Dem Fachbereich Produktionstechnik

der

Universität Bremen

zur Erlangung des Grades

Doktor-Ingenieur

Genehmigte

Dissertation

von

Vinicius Carrillo Beber

Bremen, März 2018

1. Referee

Prof. Dr. rer. nat. Bernd Mayer

Universität Bremen - Faculty of Production Engineering (FB4)

Wiener Straße 12 | 28359 Bremen - Germany

2. Referee

Prof. Dr. Lucas Felipe Martins da Silva

Faculty of Engineering of the University of Porto (FEUP)

Rua Dr. Roberto Frias | 4200-465 Porto – Portugal

Dissertation Defense Date: 09.03.2018

Eidesstattliche Versicherung

Hiermit versichere, ich Vinicius Carrillo Beber, dass ich diese Arbeit ohne unerlaubte fremde Hilfe angefertigt habe, keine anderen als die von mir angegebenen Quellen und Hilfsmittel benutzt habe und die den benutzten Werken wörtlich oder inhaltlich entnommenen Stellen als solche kenntlich gemacht habe.

_____	_____
Ort, Datum	Unterschrift

I would like to dedicate this doctoral dissertation to my aunt Maristela

Your love and dedication will live forever in our hearts

Abstract

With the increasing demand for lightweight components, structural adhesives have been playing a major role in the construction of multi-material joints with high stiffness and low weight. Under cyclic loading conditions the fatigue lifetime of structural adhesive joints is considerably affected by stress concentrations arising from notches.

The aim of the present research is to investigate the effect of stress concentrations on the fatigue behaviour of structural adhesives using numerical and experimental approaches with focus on the prediction of fatigue lifetime of notched specimens.

To achieve this purpose, un-notched and internally as well as externally notched bulk specimens were investigated. The notches introduced to the samples were chosen to cover a wide range of stress concentrations, stress gradients and stress triaxialities. For the investigations, two commercial toughened epoxy structural adhesives with similar tensile strength were employed. The mechanical properties of these adhesives differ mainly in terms of plastic deformation prior to failure.

The quasi-static and fatigue behaviour of adhesives under stress concentration conditions was evaluated. For this purpose, an innovative experimental set-up including cameras for test monitoring was built to provide information regarding stress-strain relation, stiffness degradation (*i.e.* damage evolution), total lifetime, and evolution of stress whitening (*i.e.* crazing) whilst allowing the detection of crack initiation. Numerical investigations were carried out by means of Finite Element Analysis (FEA) with 2D-plane strain and 3D models using the commercial software Abaqus ©.

Quasi-static tests under displacement control revealed that the tensile behaviour of adhesives is altered due to the presence of notches with a strong reduction of elongation at break for both adhesives. The adhesive which plastically deforms more strongly under high stresses, *i.e.* the more ductile adhesive, provided experimental evidence justifying the assumption of a supporting effect of the notch (*i.e.* higher maximum force with regards to the cross-sectional area). Conversely, the adhesive, which exhibits less plastic deformation prior to failure, has shown a reduction in tensile strength compared to un-notched samples. Prediction of failure stress using the equivalent plastic strain as failure criterion showed excellent agreement with experimental results, especially for 3D models, with average error of 5.5% for all notch types of both adhesives. Fracture surface analysis demonstrated the presence of stress whitening and voids close to the notch regions for both adhesives. These regions were correlated to higher

values of stress concentration and stress triaxiality using FEA. The more ductile adhesive underwent widespread stress whitening prior to failure, whereas in the less ductile adhesive this whitening was more localised.

Fatigue tests under constant amplitude and stress ratio of R = 0.1 revealed that fatigue strength is reduced in the presence of stress concentrations, especially in the high cycle fatigue range. This reduction is not only affected by the value of the maximum peak stress (stress concentration factor), but also by the size of the highly stressed region. A model was proposed to explain the behaviour of SN curves of notched specimens in which the slope is controlled by the size of the highly stressed region and the stress concentration factor translates the position of the curve.

The SN curves for crack initiation lifetime of both adhesives have indicated that most of the fatigue lifetime (60 to 95%) was spent on the crack initiation phase. Moreover, the crack initiation phase is shortened by an increasing stress concentration factor. The severity of this shortening is influenced by the mechanical properties of the adhesives (the most ductile adhesive was more sensitive) and by the level of applied stress. Experiments with externally notched specimens showed that the crack initiation causes a sudden increase of damage (i.e. reduction of stiffness) in the samples.

A method for lifetime prediction based on the stress-life approach and the Theory of Critical Distances (TCD) to account for the effects of stress concentrations on the fatigue lifetime was proposed. The critical distance length was obtained through a calibration process using experimental data, whose application for fatigue of adhesives, as done in the present work, is novel. Using the calibrated parameters the lifetime of three types of notched specimens was predicted. Prediction results have shown that the limitations of transferability of the stress-life approach can be overcome for notched specimens using the proposed prediction method with a proper choice of equivalent stress, geometrical model and definition of critical distance. The effectiveness of the proposed method in predicting the fatigue lifetime of notched specimens was evidenced by the good accuracy obtained with regards to experimental results (relative error less than 12%) for different notched specimens and different structural adhesives.

Keywords: Structural adhesives; Toughened epoxy; Fatigue behaviour; Lifetime prediction; Stress-life approach; Damage mechanics; Stress concentration; Notch

Zusammenfassung

Aufgrund der steigenden Nachfrage nach Leichtbaukonstruktionen spielen Strukturklebstoffe zunehmend eine wichtige Rolle bei der Fertigung von Multi-Material-Verbindungen mit hoher Steifigkeit und geringem Gewicht. Unter zyklischen Belastungen wird die Lebensdauer von Strukturklebverbindungen durch Spannungskonzentrationen, die durch Kerben entstehen können, erheblich beeinflusst.

Das Ziel der vorliegenden Forschungsarbeit ist es, die Auswirkung von Spannungskonzentrationen auf das Ermüdungsverhalten von Strukturklebstoffen numerisch und experimentell zu untersuchen mit dem Fokus auf einer rechnerischen Lebensdauervorhersage.

Um dies zu erreichen, wurden ungekerbte sowie innen- als auch außengekerbte Klebstoffsubstanzproben untersucht. Die in die Proben eingebrachten Kerben wurden so gewählt, dass ein weiter Bereich von Spannungskonzentrationen, Spannungsgradienten und Spannungs-Mehrachsigkeiten abgedeckt wurde. Für die Untersuchungen wurden zwei handelsübliche zähmodifizierte Epoxid-Strukturklebstoffe mit ähnlicher Zugfestigkeit eingesetzt. Die mechanischen Eigenschaften dieser Klebstoffe unterscheiden sich vor allem hinsichtlich der plastischen Verformung unter hohen Spannungen.

Das quasistatische und das Ermüdungsverhalten der Klebstoffe wurden unter dem Einfluss von Spannungskonzentrationen untersucht. Dazu wurde ein innovativer Versuchsaufbau mit Kameras für die Versuchsüberwachung entwickelt. Die Versuche lieferten Informationen über Spannungs-Dehnungs-Beziehungen, Steifigkeitsabfälle (d.h. Schadensentwicklung), Ermüdungslebensdauern und Weißbruchentwicklungen (d.h. Haarrissbildung). Zudem konnte die Rissentstehung beobachtet werden. Numerische Untersuchungen wurden an entsprechenden Modellen (2D- und 3D) mittels Finite-Elemente Analysen (FEA) mit dem kommerziellen Software-Paket Abaqus © durchgeführt.

Quasistatische Zugprüfungen unter Lageregelung zeigten, dass die Bruchdehnung der Klebstoffe aufgrund der Kerben stark verringert wird. Bei dem Klebstoff, der sich unter hohen Spannungen stärker plastisch verformt, d.h. beim duktileren Klebstoff, ergaben sich experimentelle Hinweise, die die Annahme einer Stützwirkung der Kerbe rechtfertigen. Die Maximalkraft bezogen auf die (ggf. durch die Kerbe reduzierte) Querschnittsfläche war bei den gekerbten Proben höher als bei den ungekerbten. Bei dem Klebstoff, der bei hohen

Spannungen weniger plastische Verformung zeigt, bevor er bricht, ergab sich im Vergleich zu ungekerbten Proben eine Verringerung der Zugfestigkeit.

Die rechnerische Vorhersage der Versagensspannung unter Verwendung der plastischen Vergleichsdehnung als Versagensgröße ergab eine ausgezeichnete Übereinstimmung mit den experimentellen Ergebnissen, insbesondere bei den 3D-Modellen. Für alle Arten von Kerben beider Strukturklebstoffe lag der mittlere Fehler unter 5.5%.

Bruchflächenanalysen zeigten Regionen mit Spannungsaufhellungen und Poren in der Nähe des Kerbgrunds bei beiden Klebstoffen. In den FEA Berechnungen wiesen diese Regionen hohe Spannungskonzentration und ein hohes Mehrachsigkeitsverhältnis auf. Der duktilere Klebstoff zeigte ausgedehnte Regionen von Weißbruch, während beim weniger duktilen Klebstoff die Regionen mit Weißbruch stärker lokalisiert waren.

Ermüdungsversuche mit konstanten Amplituden und einem Spannungsverhältnis von R = 0,1 ergaben, dass die Proben mit Spannungskonzentrationen, insbesondere im Bereich hoher Schwingspielzahlen, eine deutlich geringere Lebensdauer besaßen. Diese Reduktion wird nicht nur durch den Wert der maximalen Spannung (Spannungskonzentrationsfaktor) beeinflusst, sondern auch durch die Ausdehnung der hochbeanspruchten Regionen. Es wird ein Modell vorgeschlagen, mit dem die Charakteristik von Wöhlerlinien gekerbter Proben erklärt werden kann. Die Steigung der Linien wird durch die Ausdehnung der hochbeanspruchten Region bestimmt und der Spannungskonzentrationsfaktor bestimmt den Achsenabschnitt.

Die Wöhlerlinien für die Rissinitiierungslebensdauer beider Klebstoffe zeigten, dass der Großteil der Gesamtlebensdauer (60 bis 95%) auf die Rissinitiierungsphase entfiel. Die Rissinitiierungsphase wurde durch zunehmende Spannungskonzentrationsfaktoren verkürzt. Das Ausmaß der Verkürzung wurde durch die mechanischen Eigenschaften der Klebstoffe (der duktilere Klebstoff war empfindlicher) und die Höhe der Spannungsamplitude beeinflusst. Die Versuche an außen gekerbten Proben zeigten, dass die Rissinitiierung eine plötzliche Zunahme der Schädigung (d.h. Verringerung der Steifigkeit) verursacht.

Es wird ein Verfahren zur Lebensdauervorhersage schwingend belasteter Klebstoffsubstanzproben vorgeschlagen. Das Verfahren basiert auf lokalen Spannungen in Kombination mit Mittelungsansätzen (Theory of Critical Distance, TCD). Der Wert der kritischen Entfernung wurde durch die Kalibrierung experimenteller Daten erhalten, die so, wie sie hinsichtlich der Ermüdung von Klebstoffen in der vorliegenden Arbeit ausgeführt

wurde, neu ist. Mit Hilfe der kalibrierten Parameter wurde die Lebensdauer von drei Arten gekerbter Proben vorhergesagt. Die mit der vorgeschlagenen Methode vorhergesagten Ergebnisse zeigen, dass es möglich ist, Ansätze, die auf lokalen Spannungen und kritischen Entfernungen basieren zwischen unterschiedlichen gekerbten Geometrien bei geeigneter Wahl der Vergleichsspannungen, anzuwenden. Die Genauigkeit der Lebensdauervorhersagen ist sehr gut verglichen mit experimentellen Ergebnissen. Der relative Fehler lag unter 12% für die verschiedenen gekerbten Proben beider Strukturklebstoffe.

Stichwörter: Strukturelle Klebstoffe; Zähmodifiziertes Epoxid; Ermüdungsverhalten; Lebensdauervorhersage; Spannungslebensdauer-Ansatz; Schadensmechanik; Spannungskonzentration; Kerbe.

Acknowledgements

I would like to express my sincere gratitude to my advisor Prof. Dr. rer. nat Bernd Mayer for his support throughout the course of this work, and for the opportunity of staying at the Fraunhofer IFAM. I would like to thank Prof. Dr. Lucas da Silva for accepting the invitation to be part of this examination committee, and for his insightful comments and suggestions.

My special thanks to Dr. Markus Brede for providing me encouragement, opportunities and resources allowing me to collect experimental data, attend conferences and qualification trainings, which were relevant not only for this thesis but for my formation as a researcher. I am truly grateful to Dr. Bernhard Schneider for all the time spent on discussions and sharing of ideas as well as his constant motivation, permanent guidance and endless patience, without which, this work would not have been possible. For their aid and scientific inputs, I am grateful to the technicians and researchers of the OE419. Special thanks to my office colleagues M. Eng. Madlen Baumert and Dr. Olaf Hesebeck for always helping with German and FEA-related issues.

I would like to express my deepest gratitude to Dr. Welchy Leite Cavalcanti and to Dr. Michael Noeske. Their dedication to strengthen the cooperation between Brazil and Germany has changed the lives of many Brazilian students. This period of PhD work was made easier due to the time shared with Brazilian colleagues. In this regard, I would like to thank Pedro for his assistance and enthusiasm with the topic of fatigue of adhesives. I would like also to thank my friend Diogo for his constant listening and for his support with scientific writing.

I would like to thank God for the protection and for the opportunity of learning so much both personally and professionally during this journey as PhD Student. None of this would be possible without the support and love of my family even from far away. I love you all. My infinite gratitude to my parents, Irene and Roberto, for giving me always the best since the day I was born and for making me believe in my dreams; to my sister Vitória and my brother Lucas for their smiles and for making me feel the best person in the world. During this time as PhD student I had the opportunity to meet the love of my life, Stephani, to whom I am deeply grateful, for her care, her words of love and encouragement, and for always believing in me.

Finally, I would like to thank the financial support of the Brazilian Government (Coordination for the Improvement of Higher Education Personnel - CAPES) in the frame of the Science without Borders Program (BEX 13458 / 13-2).

Publication List

Published

(a) Beber VC, Fernandes PHE, Schneider B, Brede M, Mayer B (2017) Fatigue lifetime prediction of adhesively bonded joints: an investigation of the influence of material model and multiaxiality. **International Journal of Adhesion and Adhesives** 78:240-247

(b) Beber VC, Fernandes PHE, Schneider B, Brede M (2017) Effect of notch size on the fatigue damage behaviour of toughened epoxy adhesive specimens. **Journal of Adhesion** 93(1-2):113–126

(c) Beber VC, Fernandes PHE, Fragato JE, Schneider B, Brede M (2016) Influence of plasticity on the fatigue lifetime prediction of adhesively bonded joints using the stress-life approach. **Applied Adhesion Science** 4:5

(d) Beber VC, Schneider B, Brede M (2016) Influence of temperature on the fatigue behaviour of a toughened epoxy adhesive. **Journal of Adhesion** 92 (7-9):778–794

(e) Schneider B, Beber VC, Brede M (2016) Estimation of the lifetime of bonded joints under cyclic loads at different Temperatures. **Journal of Adhesion** 92 (7-9):795–817

(f) Carrillo Beber V, Taveira Caleiro L, Rossi de Aguiar K, Joswig J-O, Pereira Rodrigues Filho U, Noeske P-LM, Rischka K, Leite Cavalcanti W (2015) Molecular simulation on carbon dioxide fixation routes towards synthesis of precursors for innovative urethanes. **Applied Adhesion Science** 3:3

Not Yet Published

(g) Schneider B, Beber VC, Schweer J, Brede M, Mayer B (2017) An experimental investigation of the fatigue damage behaviour of adhesively bonded joints under the combined effect of variable amplitude stress and temperature variation. **International Journal of Adhesion and Adhesives** ***(Accepted)***

(h) Beber VC, Schneider B, Brede M, Mayer B (2017) Effect of temperature on the fatigue strength of a structural epoxy adhesive for automotive applications. **DVS Bericht** ***(Submitted)***

(i) Beber VC, Schneider B, Brede M, Mayer B (2017) On the fatigue behaviour of notched structural adhesives with regards to mechanical behaviour and stress concentration effects. **Procedia Engineering** ***(Accepted)***

Table of Contents

List of Acronyms

Acronym	Definition
BEA	Boundary Element Analysis
CDM	Continuum Damage Mechanics
CZM	Cohesive Zone Modelling
FDA	Finite Difference Analysis
FEA	Finite Element Analysis
FM	Fracture Mechanics
FSL	Fatigue Strength Loss
HCF	High cycle fatigue
IMS	Increase of Maximum Net Stress
LCF	Low cycle fatigue
LM	Line Method
PM	Point Method
SBR	Reduction of Strain at Break
TCD	Theory of Critical Distances

List of Figures

List of Tables

1. INTRODUCTION

1.1. BACKGROUND

In the last decades, adhesive bonding has become one of the main manufacturing technologies in several segments such as wind energy, automotive, aerospace, railway and shipbuilding industries [1]. This trend is related to the increasing demand for lightweight structures that is justified both economically (reduction of fuel consumption) and environmentally (reduction of harmful emissions) [2]. For instance, in the European Union (EU), regulations on automotive production have been set to reduce average emissions of CO_2 from about 140 g/km in 2010 to 95 g/km in 2020 with a perspective of an even stronger reduction for 2025 [3].

To produce lighter engineering structures, as seen in **Figure 1.1**, manufacturers have been using adhesive bonding to combine dissimilar materials, such as composites, metals, ceramics, and timber. Additionally, attributes including uniform load distribution, joint flexibility, hybrid joining, corrosion resistance and damping properties, make adhesive bonding a very attractive technology for several applications. This versatility can be noticed, for example, on the construction of aircrafts, where the Boeing 787 and the Airbus A350 have more than 50% of bonded structures [4]. In the case of load-bearing components, structural adhesives play a major role by providing constructions with high stiffness, low weight and enhanced fatigue properties [5].

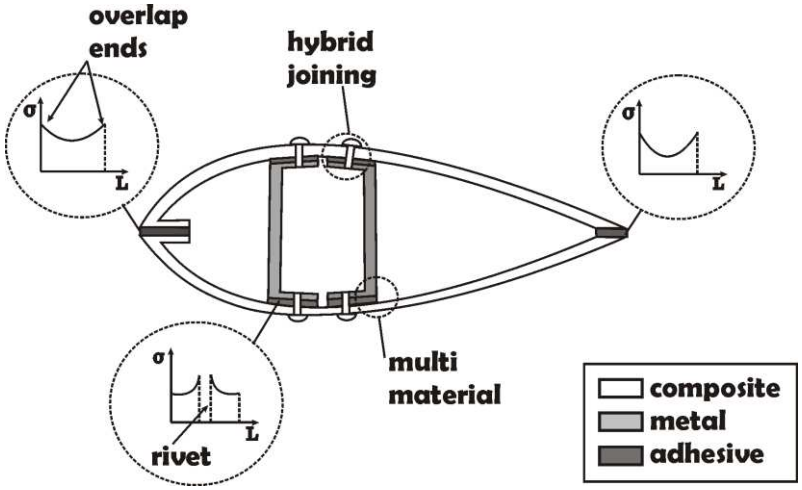

Figure 1.1 – Example of application of structural adhesive bonding in a rotor blade

Under service conditions, adhesively bonded structures are exposed to cyclic loads originated from different sources, *e.g.* rotation of turbines, vibration of engines, oscillations and impacts,

which make them susceptible to failure due to fatigue. For this reason, fatigue is a major cause of mechanical failure in engineering components [6]. Additionally, it is known that the loads leading to fatigue failure are generally much lower than the monotonic, quasi-static strength of materials and, in some cases, fracture occurs without previous visible evidence [7].

The process of fatigue can be divided into two phases: crack initiation and crack propagation. The initiation phase is related to the time (or number of cycles) necessary for the nucleation of one or more macro-cracks. Subsequently, the propagation phase starts with crack(s) growing until failure takes place. Due to the multiplicity of fatigue mechanisms, the distinction between the phases is very complex, and it may change according to the method used for measurement or detection. Actually, the modelling and monitoring of crack initiation is still an open topic in the literature [8]. Several factors may influence the dominance of initiation or propagation including type of loading, level of stress and joint geometry [9].

This intrinsic complexity of the phenomenon of fatigue makes it still difficult to accurately predict the in-service lifespan of bonded joints. This matter has been limiting a wider use of adhesively bonded joints for structural applications due to a tendency of over-conservative design [7,10]. Moreover, it is often common to include mechanical fasteners as additional safety precautions culminating in heavier and less optimised structures [11].

Another central issue on the design of components when dealing with fatigue is the presence of notches (*i.e.* stress raisers) [12], which arise from very common geometrical features such as holes, grooves and corners. Notches can affect fatigue performance for several reasons, namely: (i) highly stressed regions are commonly the preferable place for the initiation of cracks, (ii) generation of a triaxial state of stress and (iii) increasing of local strain rate [13,14]. In this regard, it is well-known that the mechanical behaviour of adhesives, being polymeric materials, depends on strain rate and triaxiality [15].

In the case of bonded structures, stress concentrations can also take place at the overlap ends of adhesive layers (**Figure 1.1**). For this reason, the topic of stress concentration becomes especially relevant for the durability of adhesively bonded joints [16]. Therefore, in order to improve safety and reliability in the design of bonded structures it is important to model and correctly predict the fatigue behaviour under stress concentration conditions.

However, it is hard to isolate the effect of stress concentration with the use of bonded joints due to the occurrence of adhesive failure, and the mechanical response of the adherends [17,18]. To circumvent the issue associated with adherends, the use of notched bulk adhesive

specimens is an alternative for mainly two reasons: (i) simplicity of production and (ii) mode of testing remains basically the same in comparison to un-notched specimens [6]. With the proper production of samples the use of bulk specimens has been extensively proved suitable for the modelling and analysis of adhesively bonded joints [17,19,20].

Regarding the fatigue modelling of adhesively bonded structures several methods are available. Stress-life approaches, for instance, rely on the relationship between stress and number of cycles to failure, expressed in the so-called SN curves. Under cyclic loading tested components might have shorter or longer fatigue lifetimes according to the level of applied stress. Taking this into account, it is usual to describe SN curves in two regions: (i) low cycle fatigue (LCF), where stresses are higher and lifetimes are shorter and (ii) high cycle fatigue (HCF), where stresses are lower and lifetimes are longer.

Stress-life approaches have been widely used due to their accuracy, simplicity and ease of application. Particularly nowadays with the support of computer-aided simulation (*e.g.* Finite Element Analysis – FEA), the calculation of stress became very easy even for complex structures, which makes this approach attractive for large scale industrial purposes [21]. However, this method still has some limitations, which include the lack of "transferability" between experimental data obtained from different joints configurations (*i.e.* different levels of stress concentration) and/or testing conditions. This transferability issue is often related to the difficulty of predicting the lifetime of samples with inhomogeneous stress distribution (*e.g.* single lap joint, notched specimens) using the data from samples with homogeneous stress distribution (*e.g.* dog bone specimen) [22].

Another important aspect of the understanding of the mechanisms of fatigue is related to the evolution of damage during cyclic loading. This information can be obtained with a damage mechanics approach. In this approach, fatigue damage is modelled as a function of a parameter that can be measured experimentally (*e.g.* stiffness). Hence, as the material is degraded, the value of this measured parameter tends to be reduced [23].

In this context, the present research work proposes to combine an innovative experimental approach (the use of notched bulk specimens) with numerical analysis (*i.e.* FEA) aiming to gain insights into the effect of stress concentrations on the fatigue damage behaviour of structural adhesives regarding SN curves, crack initiation lifetime and damage evolution.

By understanding these effects, it is intended to overcome the limitations of "transferability" related to the stress-life approach making it suitable for the lifetime prediction of samples of different structural adhesives with different levels of stress concentrations.

1.2. RESEARCH AIM

Within the background previously provided, the aim of the present research work is:

- To investigate the effect of stress concentrations on the fatigue behaviour of structural adhesives combining numerical and experimental approaches with focus on the prediction of fatigue lifetime of notched specimens using the stress-life method.

1.2.1. Specific objectives

In order to achieve the proposed research aim, the following specific objectives were set:

a) To generate quasi-static and fatigue experimental data of notched bulk structural adhesives with different levels of stress concentrations;
b) To develop a novel experimental set-up capable to monitor and capture the progression of damage and the nucleation (*i.e.* initiation) of cracks;
c) To set-up a numerical FEA-model including geometrical model, material model, boundary conditions, mesh and elements in order to simulate the mechanical behaviour of structural adhesives under stress concentration conditions;
d) To assess the effect of stress concentrations on the quasi-static tensile strength, strain at break and fracture behaviour of structural adhesives;
e) To assess the effect of stress concentrations on the fatigue behaviour of structural adhesives with regards to total lifetime, crack initiation lifetime, evolution of damage and fracture behaviour;
f) To evaluate the relationship between stress concentration, stress triaxiality and the process of fracture on structural adhesives;
g) To propose a model to describe the effect of stress concentrations on SN curves;
h) To propose an efficient, accurate and reliable approach based on the stress-life method for predicting the fatigue lifetime of notched specimens with different levels of stress concentrations.

1.3. RESEARCH METHODOLOGY

A research methodology was followed to ensure that results of the present research work were valid and reliable for several cases of fatigue involving structural adhesives. During the planning of the methodology some aspects were taken into account including:

a) Use of two different types of structural adhesives: assessment of the effect of different mechanical properties as regards to plastic deformation, tensile strength and stiffness;
b) Use of commercial adhesives: additional industrial relevance for the findings;
c) Use of bulk specimens: avoid the influence of adhesive failure whilst allowing the direct monitoring of crack formation/propagation and the change in the colour of the adhesives due to stress whitening;
d) Use of different types of notch (internal and external): stress concentrations with different stress triaxialities, size of highly stressed regions, stress gradients and maximum peak values;
e) Consideration of the whole fatigue range, which includes low and high cycle fatigue under constant amplitude loading;
f) Consideration of the total fatigue life, which includes crack initiation and crack propagation;

A summary of the applied methodology is described in **Figure 1.2**:

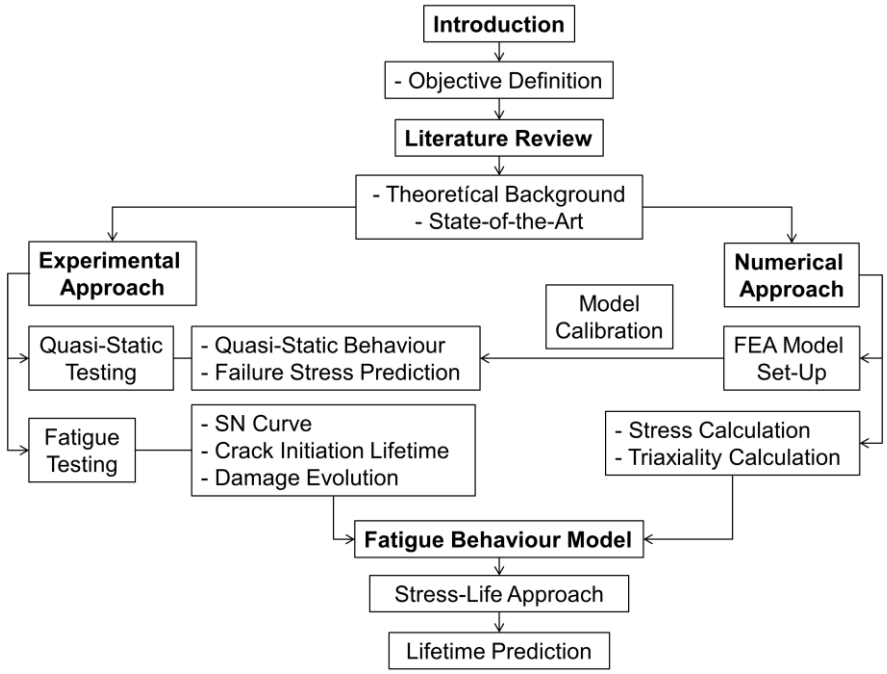

Figure 1.2 – Summary of the methodology applied in the present research work

1.4. THESIS OUTLINE

The present research work is divided in eight chapters which are summarised below:

- **Chapter 2** "Literature review". This chapter is concerned with a comprehensive literature review aiming to: (i) establish the theoretical framework for the investigation, (ii) describe key terminology/definitions, and (iii) evaluate the state-of-the-art on methods of fatigue modelling, experimental testing, and numerical investigations of structural adhesives.

- **Chapter 3** "Experimental methodology". This chapter is focused on the description of applied experimental methodology, which includes: selection of structural adhesives, manufacturing of samples, and experimental set-up for quasi-static and fatigue tests.

- **Chapter 4** "Numerical methodology". In this chapter the numerical methodology related to the Finite Element Analysis applied in the present research work is described, including: definition of geometry, definition of material model, definition of failure criterion, boundary conditions, meshing and element choice.

- **Chapter 5** "Quasi-static behaviour of structural adhesives". This chapter is focused on the investigations regarding the quasi-static behaviour of structural adhesives under the effect of stress concentration due to the presence of notches. Findings regarding tensile strength and strain at break were related to stress distributions, stress triaxiality and mechanical properties of the adhesives. The FEA model established in Chapter 4 was used to predict the failure stress of both adhesives under different levels of stress concentration.

- **Chapter 6** "Fatigue behaviour of structural adhesives". This chapter is concerned with the understanding of the fatigue behaviour of adhesives under the effect of stress concentrations. Un-notched, internally notched and externally notched specimens were analysed by means of SN curves (total lifetime and crack initiation), damage evolution curves and fractography. Findings were correlated to numerical simulations of stress concentration and stress triaxiality

- **Chapter 7** "Fatigue lifetime prediction of notched specimens". This chapter presents the process of set-up of the method for predicting the fatigue lifetime of notched specimens. The method is based on the stress-life approach and the Theory of Critical Distances to account for the effect of stress concentration on the fatigue lifetime of adhesives. The validation of the method was carried out by comparing predicted fatigue lifetimes with experimental results of notched specimens with different levels of stress concentration.

- **Chapter 8** "Conclusions and outlook". This final chapter has the purpose of reviewing the main findings of previous chapters whilst highlighting the novel contributions of the present research work to the field of fatigue of structural adhesives. Finally, some suggestions about topics for future research are given.

2. LITERATURE REVIEW

In this chapter a comprehensive literature review is presented regarding the following topics: adhesive bonding technology (**Section 2.1**), fatigue of structural adhesives (**Section 2.2**), calculation of stress (**Section 2.3**), notches and stress concentrations (**Section 2.4**), fatigue modelling approaches for structural adhesives (**Section 2.5**) and experimental techniques (**Section 2.6**).

2.1. ADHESIVE BONDING TECHNOLOGY

Adhesive bonding technology has been used by humans to manufacture tools and machines for a long period of time. Practically every usable material can be joined by this surface-to-surface technology. In the beginning, adhesives were manufactured from natural polymers (*e.g.* fish glue). With the advent and continuous development of synthetic polymers, such as the phenol-formaldehydes (1910`s) and the epoxies (1950`s), adhesive bonding was spread in several fields of application [1,23].

When compared to other joining techniques adhesive bonding presents several advantages: adherends are not necessarily affected by heat, very thin adherends can be joined allowing flexible joints, and optimised corrosion and sealing properties can be obtained [7,23]. At the same time, as any technology, adhesive bonding has some limitations which include: susceptibility to ageing due to radiation, moisture or chemical exposure and, often, the requirement of surface cleaning preparation and, in the case of hot curing adhesives, the necessity of fixture devices during the waiting period for hardening [1].

According to the DIN 923 [24] an adhesive is "a non-metallic substance which can join two substrates together via bonding to the substrate surfaces (adhesion) and via its own internal strength (cohesion)". Substrates which are joined by the adhesive are referred to as *adherends*. The basic elements of an adhesively bonded joint are depicted in **Figure 2.1**.

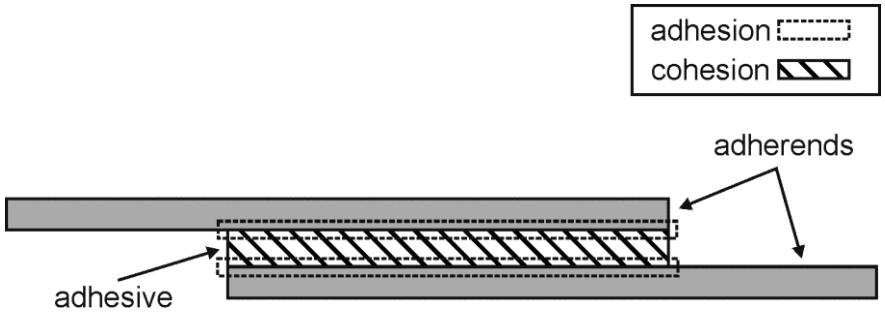

Figure 2.1 – Basic elements of an adhesively bonded joint

Under stress (mechanical, chemical, thermal) any of these elements of an adhesively bonded joint might fail. Depending on which of these elements failed, the types of failure modes can be classified as shown in **Figure 2.2**.

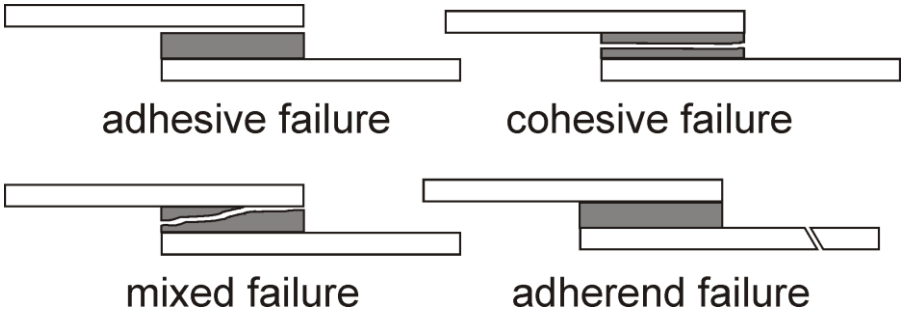

Figure 2.2 – Failure modes of adhesively bonded joints

The type of failure strongly depends on the type of adhesive, the type of adherend, the surface treatment, the type of loading and environmental conditions. For instance, a poor surface treatment will probably lead to an adhesive failure. On the other hand, for example, the combination of stiff adhesives (*e.g.* epoxides) with wooden adherends will lead to an adherend failure.

2.1.1. Theories of adhesion

Adhesion is "the attraction between two substances resulting from intermolecular forces that establish between them" [23]. Adhesion is one of the main factors acting on the strength of an adhesive joint since forces involving adhesion are much stronger than the cohesive strength of the adhesive [25]. Historically, several classical theories are available to explain the phenomenon of adhesion. Some of these theories are summarised below [1,23,25]:

- Mechanical theory: it states that adhesion is provided due to the amount of mechanical interlocking between the adhesive and the surface of the adherend. Thus, the mechanical theory is commonly related to the effect of surface roughness on the adhesion strength.
- Diffusion theory: it is relevant to explain adhesion between polymers, in which mutual interdiffusion of polymer molecules occur across the interface. The conditions for this interdiffusion are chain mobility and polymer compatibility.
- Electrostatic theory: it considers that adhesion is promoted by the transfer of electrostatic charge between the adhesives and the adherend.

- Adsorption theory: it is the most widely accepted theory of adhesion and recognised as a promoter of adhesion between all types of materials. In the adsorption theory adhesion is promoted through the contact and consequent formation of either primary (*e.g.* covalent) or secondary (*e.g.* van der Waals) bonds between adhesives and adherends.

2.1.2. Classification of adhesives

Adhesives can be classified by several properties, *e.g.* physical form (liquid, paste, film), chemical form (epoxy, acrylic, polyurethane), type of adherend to be bonded (metal, wood, composite) and end use (automotive, aerospace, dental). One of the methods of classification of adhesives is by their hardening, *i.e.* curing, process. This is seen in **Figure 2.3**:

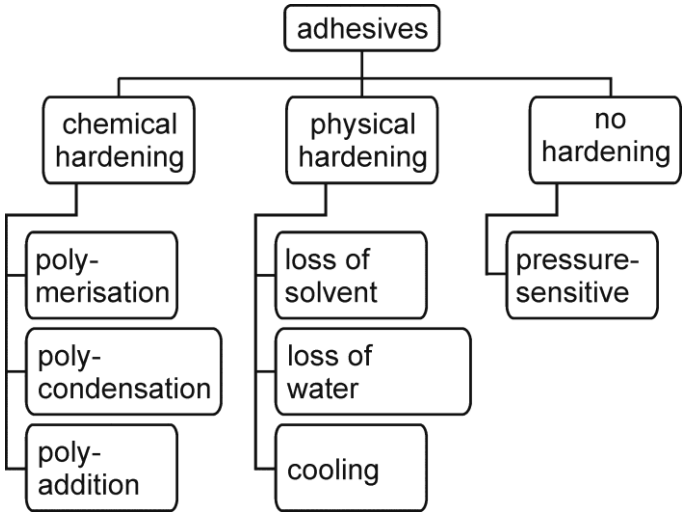

Figure 2.3 – Classification of adhesives according to hardening manner - Adapted: Adams et al. [1]

After curing the mechanical behaviour of adhesives varies drastically with regard to their final macromolecular structure. For example, the classification of the adhesives according to their macromolecular structure and some respective properties is described in **Table 2.1**.

Table 2.1 – Classification of adhesives according to macromolecular structure - Adapted: Habenicht [26]

thermoplastic	**thermoset**	**elastomer**
amorphous or partially crystalline	amorphous	amorphous
no crosslinking	narrow crosslinking	wide crosslinking

The presence of narrow cross-linking between molecular chains alters significantly the mechanical properties of adhesives. This is related to the hindering of the relative movement of chains relative to each other, which makes it impossible to draw out single molecules; hence, thermosets are much stiffer than thermoplastics and elastomers [27]. For this reason, thermosets are the most common type of polymer used for the conception of adhesives designed for structural applications [25].

2.1.3. Structural adhesives - toughened epoxy adhesives

In the case of load-bearing joints the term structural adhesive as defined by Adams *et al.* [23] can be used when "the load to be carried is substantial enough that the adhesive provides for the major strength and stiffness of the structure". Within the class of structural adhesives, epoxy-based adhesives are the most relevant and versatile [25]. The most common type of epoxy resin used for engineering applications is the DGEBA (diglycidyl ether bisphenol A) [23]. The molecular structure of DGEBA is shown in **Figure 2.4**.

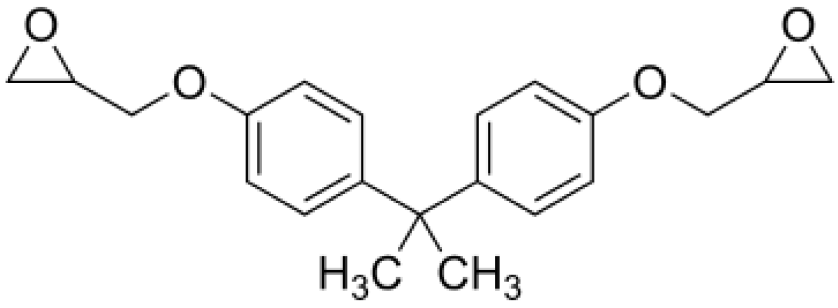

Figure 2.4 – Molecular structure of DGEBA (epoxy resin)

Epoxy resins are highly cross-linked and amorphous (thermosets - **Table 2.1**). Their microstructure provides a combination of high stiffness with high chemical, thermal, and corrosion resistance. However, single-phase (*i.e.* neat) epoxy resins are usually very brittle and readily to crack. In the past these undesirable shortcomings limited the range of applications for epoxy-based adhesives. For this reason, toughened (*i.e.* modified) epoxy adhesives were developed to provide a microstructure capable of withstanding impact and promote energy absorption [28].

The principle of toughening relies on the incorporation of secondary "elastic" particles into an epoxy matrix. This incorporation leads to a multiphase microstructure with higher fracture toughness and higher peel and shear strength and, consequently, better suited for structural applications [15].

In order to maximise toughening effects, two requirements are needed. The first requirement is that toughening particles must be compatible with the matrix meaning that liquid particles must be soluble in the uncured matrix. However, toughening particles must precipitate out during the cure, which induces phase separation (*i.e.* multiphase formation). The second requirement is that the toughening particles must be reactive with the epoxy groups of the matrix [29].

Regarding the effect of toughening on modified epoxies two important mechanisms have been identified as demonstrated by Kinloch *et al.* [30]: (i) localised cavitation and subsequent void growth at the toughening particle or at the particle/matrix interface, as well as, (ii) plastic shear yielding in the epoxy matrix.

These mechanisms can be seen in the stress-whitening region in a fractured surface of a toughened epoxy. These surfaces are characterized by many small holes which are larger than the original particle size and by yielding (*i.e.* plastic deformation) of the polymer matrix near the particles (evidenced by bevelled edges of the voids). The holes are the consequence of the dilatation of the original toughening particles. The shear yielding is initiated by the intense tri-axial stress state around the particles causing large deformations in the matrix [29]. Yee and Pearson [31,32] investigated rubber-toughened DGEBA-based epoxies proposing a model to describe their deformation mechanisms, which is shown in **Figure 2.5**:

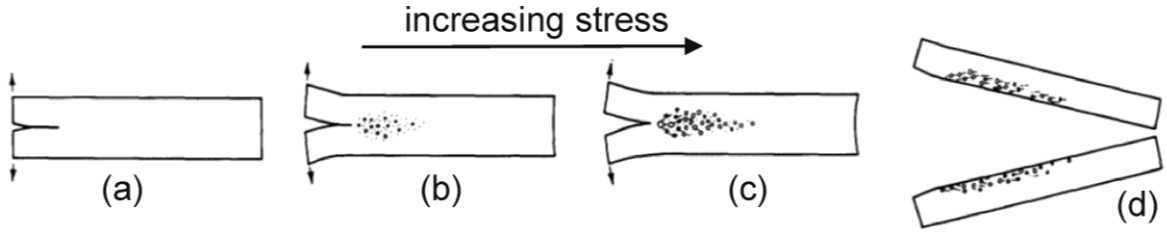

Figure 2.5 – Effect of toughening under increasing stress - Adapted: Pearson and Yee [31]

According to this model with an increasing stress, the presence of the rubber particles ahead of crack tip induces a tri-axial stress field that causes a high hydrostatic tension around the particles. Consequently, dilatation promotes their cavitation and the enlargement of the resultant voids. On increasing the load voids continue to grow and the region characterised by shear band extends its dimensions. The crack propagating through the voided plane increases the fracture path along with energy dissipation. Plastic deformation increases due to particle-particle interaction until the final fracture of the material. Another known characteristic of

toughened epoxies, and very relevant for design purposes, is the presence of two glass transitions temperatures: one for the matrix and other for the toughening particles [30,33].

2.1.4. Types of joint configurations

With regard to mechanical loading, adhesive joints can be subjected to different types of stresses (**Figure 2.6**). Due to the polymeric nature of adhesives, some stresses can be more critical than others. For instance, under service conditions peel and cleavage should be avoided [1].

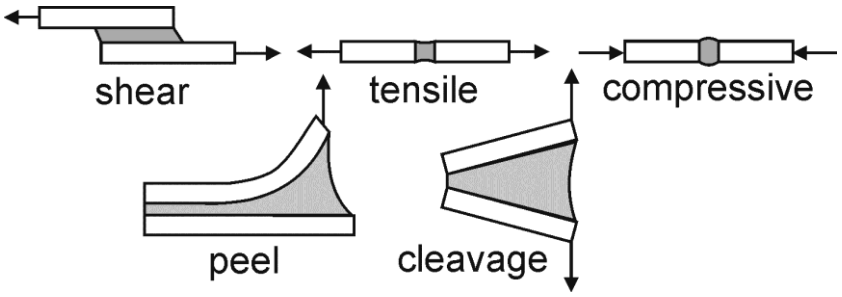

Figure 2.6 – Types of joint stresses. Adapted: Pethrick [34]

Therefore, the proper characterisation of the mechanical behaviour of adhesives under different types of stress is a key aspect for understanding of the long term durability of bonded joints [35]. In this regard a diverse range of joint configurations have been developed for testing of adhesive properties under different types of stresses. Some of these joint configurations are shown in **Figure 2.7**:

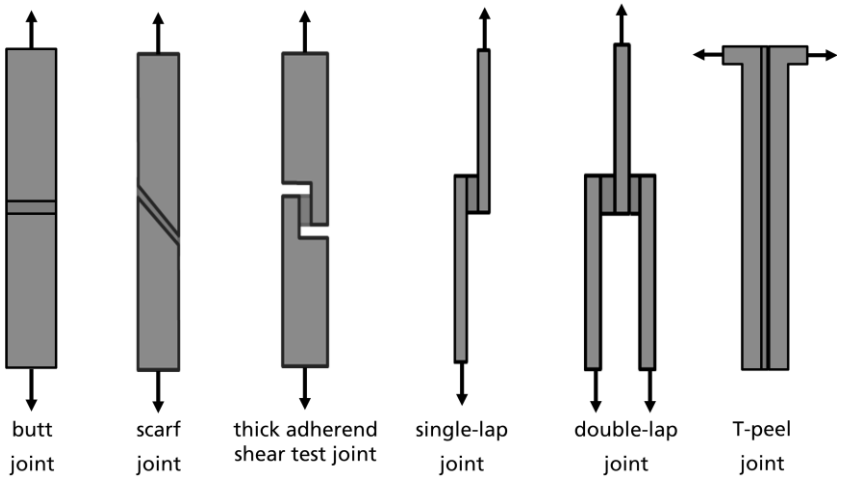

Figure 2.7 – Some types of joint configurations

Butt joints, when loaded under tension, present a state of nearly homogeneous tensile stress within the adhesive layer [22]. In scarf joints the angle between load and bonding surface

controls the ratio of tensile and shear stresses [33]. Thick adherend shear test (TAST) joints are commonly used to assess the shear strength of adhesives [35]. They present a much more homogeneous state of stress compared to single-lap joints (SLJs). Single lap joints have been widely investigated due to their similarity with joints found in practical applications (thin adherend sheets). When subjected to traction this type of joint tends to bend causing a bending moment that induces peel stresses at the overlap ends [36]. This region with highly concentrated stresses is usually the locus for the initiation of failure [7].

Differences in the state of stress among different joint configurations are known to alter their fatigue behaviour under cyclic loading [22]. These alterations on the fatigue behaviour can be seen in SN curves (*e.g.* **Figure 2.15**), which is one of the topics for the next sections (*i.e.* **Section 2.3.3**).

2.2. FATIGUE

Fatigue can be defined as the failure of a material subjected to cyclic loads which in most of the cases are much lower than the monotonic strength of a material [37]. The topic of fatigue has been widely studied for metals since the 19th century with the pioneering work of Wöhler [38]. One of his main conclusions was that in the process of fatigue "the stress amplitude is the most important parameter for fatigue life, but a tensile mean stress also has a detrimental effect" [39]. Historical breakthroughs in the study of fatigue are listed in **Table 2.2**

Table 2.2 – Some historical breakthroughs in the study of fatigue

author (year)	**breakthrough**
Wöhler (1858) [38]	first systematic investigation of fatigue
Basquin (1910) [40]	log-log relationship for SN curves
Griffith (1921) [41]	fracture mechanics (brittle fracture)
Miner (1945) [42]	cumulative damage (variable amplitude)
Coffin [43] / Manson [44] (1954)	effect of plastic strain (low cycle fatigue)
Neuber (1958) [45] / Peterson (1959) [46]	effect of stress concentrations (notch fatigue)
Paris (1961) [47]	fracture mechanics applied to fatigue
Elber (1968) [48]	effect of crack closure

The increase on the number of research works regarding the study of fatigue of adhesives is closely related to a more broad use of this type of material for engineering applications which started around the early 70's [8,49].

2.2.1. General concepts

For a better understanding of the present work it is helpful to define some general concepts and terminologies regarding cyclic loading and fatigue. A typical sinusoidal cyclic load with constant amplitude is presented in **Figure 2.8**:

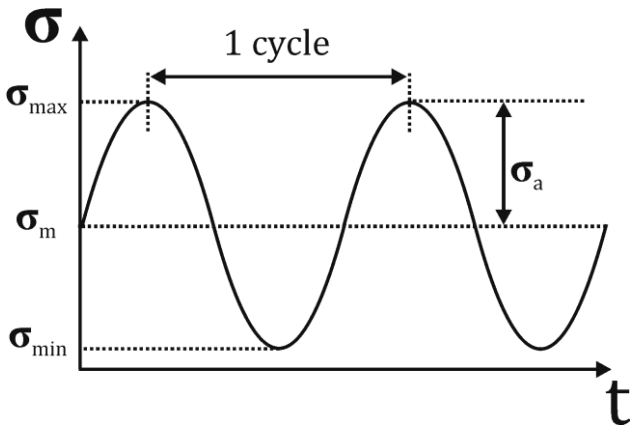

Figure 2.8 – General form of a sinusoidal cyclic load

Based on the maximum (σ_{max}) and the minimum stress (σ_{min}) within a cycle, the stress amplitude (σ_a), the mean stress (σ_m) and the stress ratio (R) can be obtained from **Equations (2.1)**, **(2.2)** and **(2.3)**:

$$\sigma_a = \frac{\sigma_{max} - \sigma_{min}}{2} \tag{2.1}$$

$$\sigma_m = \frac{\sigma_{max} + \sigma_{min}}{2} \tag{2.2}$$

$$R = \frac{\sigma_m - \sigma_a}{\sigma_m + \sigma_a} = \frac{\sigma_{min}}{\sigma_{max}} \tag{2.3}$$

The applied stress ($\sigma(t)$) at any given time (t) can be obtained from **Equation (2.4)**:

$$\sigma(t) = \sigma_m + \sigma_a \sin(\omega t) \tag{2.4}$$

Here $\omega = 2\pi f$ is the angular frequency (in radians) while f is the frequency (in Hz) that determines the number of cycles per one second. Due to their viscoelastic nature, adhesives are highly sensitive to heating under high frequencies, which can lead them to thermal fatigue or even melting [49].

A fundamental form of representing the fatigue behaviour of a material (or a joint) is by means of SN curves (or *Wöhler* plots), which are obtained from experimental testing. In such a plot the stress amplitude (σ_a) is related to the number of cycles to failure (N_f). The curve is obtained by fitting experimental data points. A typical fitting procedure relies on the use of the Basquin's exponential law [40] according to **Equation (2.5):**

$$\sigma_a = S_0 N_f^{-\left(\frac{1}{B}\right)} \tag{2.5}$$

Here S_0 and B are constants. By plotting an SN curve in a log-log chart, a linear correlation between the stress amplitude and the number of cycles to failure is obtained (**Figure 2.9**).

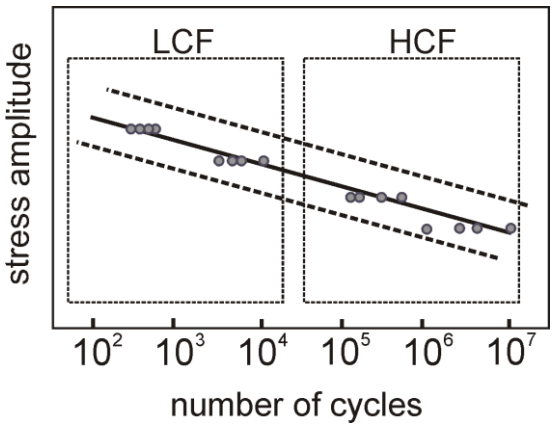

Figure 2.9 – Representative SN curve in a double log chart with experimental data points

It is usual to divide the fatigue lifetime into two regions. The first region ($10 < N_f < 10^4$), the so-called *low cycle fatigue* (LCF), has the following characteristics: applied stresses are high, lifetimes are short and significant plastic deformations occur during cycling. Conversely, in the second region ($N_f > 10^4$), which is referred to as *high cycle fatigue* (HCF): applied stresses are lower, lifetimes are longer and deformations are predominantly elastic [1,23,37]. The exact region where this transition occurs is still under discussion in the literature [27]. In some cases of very low stresses fatigue failure might not occur [23].

Scatter of experimental data points is another inherent characteristic of fatigue (*i.e.* SN curves). To indicate the scatter of fatigue tests it is common to plot scatter bands (dashed lines in **Figure 2.9**) around the SN curve which are related to confidence level and probability of failure [37]. By applying a logarithm in both sides of the Basquin's relationship in **Equation (2.5)**, a linear relationship between the stress amplitude and the number of cycles to failure could be obtained:

$$\log \sigma_a = \log S_0 - \frac{1}{B} \log N_f \tag{2.6}$$

With this approach the SN curve becomes a line with S_0 as the y-intercept of the SN curve, and the term *B* representing the inverse negative slope of the SN curve. The slope of an SN curve is closely related to the severity of the process of fatigue [50]. A steeper slope indicates a more severe process of fatigue because a small increase in stress amplitude will cause a great reduction of fatigue lifetime. In order to compare the severity of fatigue for different types of samples the concept of fatigue strength loss is very helpful. The fatigue strength loss (*FSL*) is defined based on the slope (parameter *B*) of the SN curve. It represents the percentage of the fatigue strength which is reduced every factor of 10 in the fatigue lifetime [50]:

$$FSL = 100\left(1 - 10^{-\frac{1}{B}}\right) \tag{2.7}$$

For example, a *FSL* of 45% indicates that moving a factor of 10 in the lifetime in an SN curve (*e.g.* from 1,000 cycles to 10,000 cycles) the fatigue strength is reduced 45%. For this reason, higher values of *FSL* are associated with more severe process of fatigue.

2.2.2. Fatigue crack initiation and propagation

The number of cycles to fatigue failure (N_f) can be divided into two parts: the number of cycles for crack initiation (N_i) and for crack propagation (N_p) as seen in **Equation 2.8**.

$$N_f = N_i + N_p \tag{2.8}$$

The determination of which phase is more dominant on fatigue lifetime is still a topic of debate among researchers [19]. This is related to the difficulty to clearly define the exact time for the complete formation of cracks. Mostly, a crack nucleates from micro-defects within the structure of the material. With the evolution of cycles, these micro-defects continue to grow until a macro-crack is formed [37]. Subsequently, the crack propagation phase begins. Therefore, the ratio between initiation and propagation is dependent on how a "macro-crack" is defined, measured, and also on the resolution of the method used for its detection. Several factors can influence the dominance of initiation or propagation, *e.g.* surface finishing, joint geometry, stress concentrations, internal flaws and applied stress (**Figure 2.10**) [8].

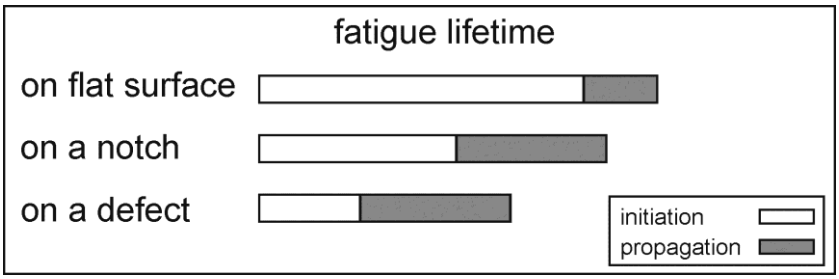

Figure 2.10 – Factors influencing on crack initiation - Adapted: Richard and Sander [51]

However, it is widely recognised that the initiation phase is considerably more sensitive to these influences. The influence of most of these factors is more evident in the high cycle fatigue, because they are generally overruled during low cycle fatigue due to plastic deformation. For this reason, high cycle fatigue results usually present higher scatter [37]. Moreover, macro crack growth under low-cycle fatigue (high stresses) is limited because small cracks will already induce complete failure of the material.

During high-cycle fatigue significant macro-crack propagation takes place [37]. Fracture mechanics models are used to describe the phenomenon of crack propagation. In these models, once the crack is formed and a certain threshold is attained (G_{th}) crack propagation starts to occur [37,52]. The crack can propagate in one or in a mix of the modes presented in **Figure 2.11**.

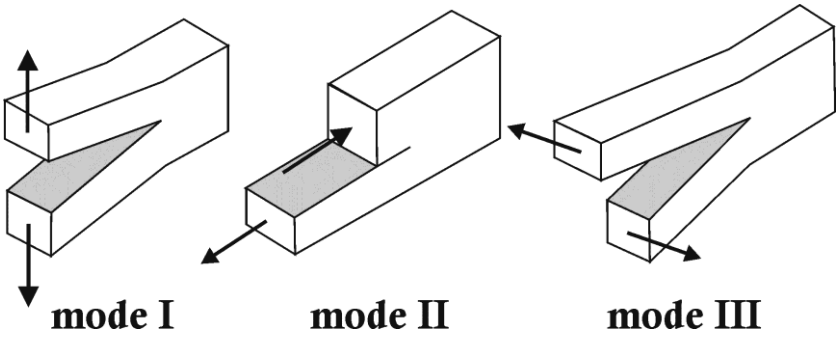

Figure 2.11 – Crack opening modes

With an increasing number of cycles, as the crack propagates, the material releases the stored energy to form new surface for the crack. A typical form of representing this correlation is by means of crack growth rate (da/dN) and energy release rate (G). Initially, the crack growth is stable and the relationship ($da/dN = f(G)$) can be linearly modelled by the Paris's law. After a certain limit the increase of crack length (a) becomes unstable and fracture occurs very fast until the critical energy release rate (G_c) is reached and the material fails.

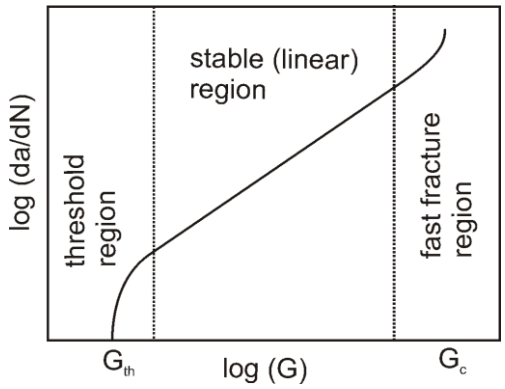

Figure 2.12 – Typical crack propagation chart

2.2.3. Factors influencing on the fatigue behaviour of structural adhesives

Due to the diversity of applications of adhesive bonding systems, investigations have been extensively conducted to determine which factors influence the fatigue behaviour of structural adhesives. These factors may include: surface treatment, material parameters, joint geometry, curing parameters and loading conditions.

A review on the topic of fatigue of adhesives was published by Abdel-Wahab [8], in which the main developments on fatigue modelling between 1975 and 2011 were discussed. More recently, Costa *et al.* [53] presented a review on the effect of environmental factors (*e.g.* temperature and moisture) on the fatigue response of adhesive joints.

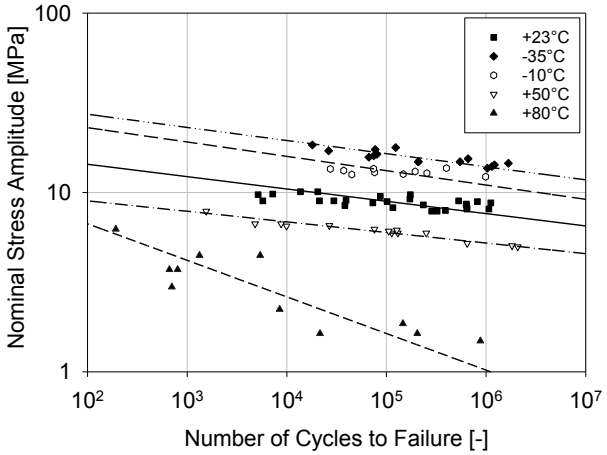

Figure 2.13 – Effect of temperature on the fatigue strength of a bulk specimen of a toughened epoxy adhesive - Adapted: Beber et al. [33]

The effect of temperature has been the focus of study of several authors [5,23,54]. For the case of fatigue of toughened epoxies, Beber *et al.* [33] have assessed the influence of temperature (ranging from -35°C to +80°C) on the fatigue behaviour of bulk specimens and

bonded joints. Conclusions were that fatigue strength is reduced with an increase of temperature as shown in **Figure 2.13**.

Another influencing factor on the fatigue behaviour of structural adhesives is the stress ratio (*e.g.* Crocombe and Richardson [55], Underhill and Duquesnay [56]). A typical plot showing the effect of stress ratio (R) on the SN curves of bulk specimens of a toughened epoxy adhesive is shown in **Figure 2.14**.

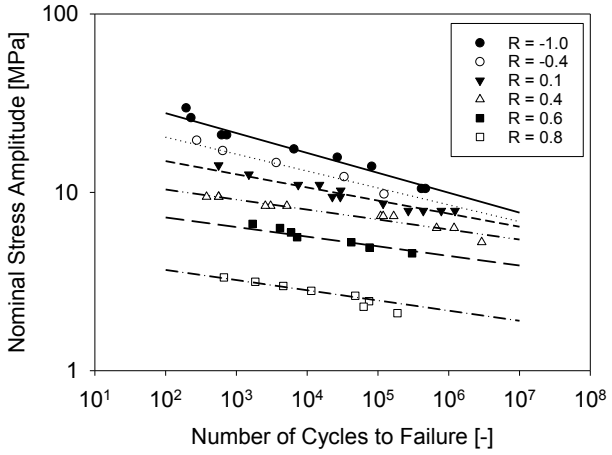

Figure 2.14 – Effect of stress ratio on the fatigue strength of a bulk specimen of a toughened epoxy adhesive - Adapted: Bornemann et al. [57]

Since fatigue tests are expensive and time consuming it is desirable to have methods to reduce the number of tests for different stress ratios. Fatigue results at different stress ratios (and the same fatigue lifetime) can be correlated with the aid of a Haigh-Diagram, in which the stress amplitude is plotted as a function of the mean stress [58]:

$$\sigma_a = \frac{1-R}{1+R}\sigma_m \tag{2.9}$$

As stated previously, the state of stress within a material alters significantly its fatigue behaviour [59]. For instance, the influence of stress distribution on the fatigue response of structural adhesives has been reported since the 60`s (*i.e.* Wang [60]).

In the case of adhesively bonded joints, the influence of a triaxial state of stress in the adhesive layer has been the focus of a considerable number of works, *e.g.* Ishii *et al.* [61] and Imanaka *et al.* [62]. The stress triaxiality is defined in terms of the hydrostatic pressure and the von Mises stress (see **Section 2.3.1**). By means of a chart - "hydrostatic pressure *vs* von Mises stress" - it is possible to visualise that different joint configurations have different

values of hydrostatic pressure and Von Mises stress, which affects directly their fatigue lifetime (*N*) (**Figure 2.15**).

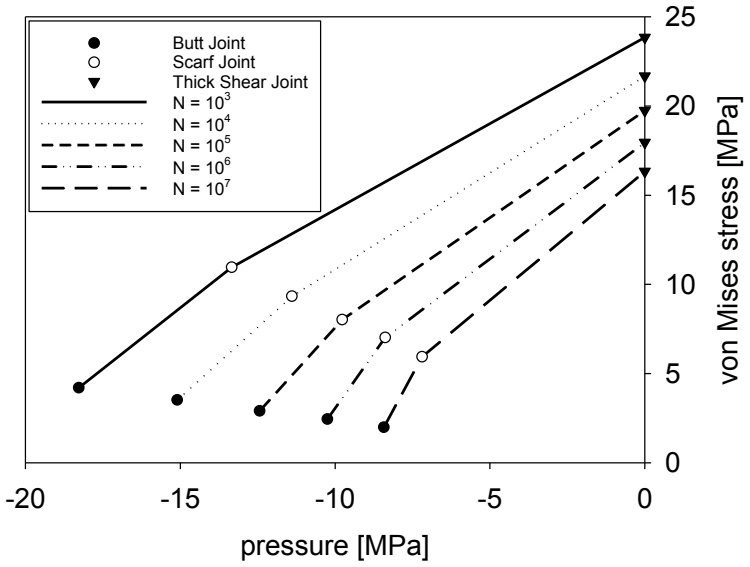

Figure 2.15 – Hydrostatic pressure and Von Mises stress diagram for the fatigue lifetime of bonded joint of a toughened epoxy - Adapted: Baumgartner et al. [54]

These evidences confirm the key role that is played by the calculation of stress in the modelling of fatigue lifetime. Therefore, the calculation of stress in structural adhesives is the next topic in the present literature review.

2.3. CALCULATION OF STRESS IN STRUCTURAL ADHESIVES

2.3.1. Stress representation

The state of stress in any point of an adhesive can be described using tensorial notation by a stress tensor as given in **Equation (2.10)**. The stress tensor is made of normal stresses (σ_{ii}) and shear stresses (τ_{ij}).

$$\sigma_{ij} = \begin{pmatrix} \sigma_{11} & \tau_{12} & \tau_{13} \\ \tau_{21} & \sigma_{22} & \tau_{23} \\ \tau_{31} & \tau_{32} & \sigma_{33} \end{pmatrix} \tag{2.10}$$

By coordinate rotation of the reference system it is possible to derive a stress representation where shear stress components (τ_{ij}) are zero. This new tensor, the maximum principal stress tensor (σ_{ij}^{MP}), has only normal stress components named principal stresses ($\sigma_I, \sigma_{II}, \sigma_{III}$) as seen in **Equation (2.11)**.

$$\sigma_{ij}^{MP} = \begin{pmatrix} \sigma_I & 0 & 0 \\ 0 & \sigma_{II} & 0 \\ 0 & 0 & \sigma_{III} \end{pmatrix} \tag{2.11}$$

When the tensor of maximum principal stresses has only one non-zero component the state of stress is named *uniaxial stress*. This occurs, for instance, in a uniaxial tensile loading of un-notched bulk specimens. However, when two or more maximum principal stresses are non-zero, the state of stress is named *triaxial* or *multiaxial* [59]. Stress triaxiality can be induced due to external loading (*e.g.* combined tension and bending) or due internal effects (*e.g.* presence of notches) [63]. The present work will focus on stress triaxiality induced by internal effects caused by notches.

For fatigue modelling purposes, a common approach to deal with triaxial stresses is to define an *equivalent stress* (σ_{eq}) to be used as a comparative parameter between the state of stress of different loading configurations. The equivalent stress is a function of the stress tensor which is chosen so that it characterises the severity of the stress, *e.g.* under quasi-static loading the material fails at a certain value of the equivalent stress, and under cyclic loading each value of equivalent stress corresponds to a certain fatigue lifetime.

For instance, the maximum principal stress (σ_{MP}) has been widely applied as an equivalent stress for adhesives [64]:

$$\sigma_{MP} = \max(\sigma_I, \sigma_{II}, \sigma_{III}) \tag{2.12}$$

From the principal stresses ($\sigma_I, \sigma_{II}, \sigma_{III}$) another equivalent stresses, namely, the hydrostatic stress (σ_H) and the von Mises stress (σ_{VM}), can be calculated:

$$\sigma_H = \frac{\sigma_I + \sigma_{II} + \sigma_{III}}{3} \tag{2.13}$$

$$\sigma_{VM} = \sqrt{\frac{1}{2}\left[(\sigma_I - \sigma_{II})^2 + (\sigma_{II} - \sigma_{III})^2 + (\sigma_I - \sigma_{III})^2\right]} \tag{2.14}$$

Using these variables (σ_H and σ_{VM}) the stress triaxiality (η) is defined as follows

$$\eta = \frac{\sigma_H}{\sigma_{VM}} \tag{2.15}$$

Another useful equivalent stress is the Drucker-Prager stress [65], which in its linear form contains one material parameter (β) and is calculated from:

$$\sigma_{DP} = \sigma_{VM} + \sigma_H \tan(\beta) \tag{2.16}$$

The linear Drucker-Prager equivalent stress (σ_{DP}) includes the effect of hydrostatic stress, which is widely known to alter the mechanical behaviour of adhesives [66,67]. The importance of the stress triaxiality (η) regarding modelling purposes will be highlighted in the following sections.

2.3.2. Analytical calculation of stress

Analytical (or closed form) models for the calculation of stress have been extensively developed in order to provide useable and direct solutions for design when computational power was not advanced as today [36].

In the analytical calculation of stress of notched components, the early efforts of Neuber [45] and Peterson [46] to quantify the stress concentration around notches are widely regarded. For bonded joints, the stress concentrations arising at the overlap ends of single lap joints (SLJs) have attracted the attention of several researchers. For instance, the shear-lag model proposed by Volkersen [68] was a ground-breaking work in the calculation of shear stresses for SLJs.

Still dealing with SLJs, Goland and Reissner [69] were able to introduce the calculation of peel stresses and the effect of non-linear material behaviour was considered by Hart-Smith [70]. A review presented by da Silva *et al.* [36] has shown a literature survey containing the main breakthroughs regarding the calculation of stress for adhesively bonded joints.

The use of analytical models is not exclusive for SLJs. In this sense, Bigwood and Crocombe [71] proposed an elastic model for the calculation of stress of more generalised joint configurations, Hart-Smith [72] have calculated the stress in double-lap joints and Gleich [73] has proposed an analytical solution for the stress in scarf joints.

Nevertheless, with the increasing complexity of materials and geometries as well as the evolution of computational power, numerical methods have become the leading method for calculation of stresses [11].

2.3.3. Numerical calculation of stress

Several numerical methods are available for calculation of stress, namely the boundary element analysis (BEA), the finite difference analysis (FDA), and the finite element analysis (FEA). Among these, FEA has been well established for decades and it is the most employed method in the field of adhesive bonding [11].

As shown in **Figure 2.16**, FEA relies on the discretisation of a continuum domain (*i.e.* the geometry) into smaller sub-domains (the elements) to numerically solve a range of boundary problems [23]. Each element has a defined number of nodes. Every node has a certain number of degrees of freedom (dof's). The dof's determine the directions (translation and rotation) in which the nodes are allowed to move. One node could be totally free (all dof's are free), partially free (some dof's are free) or totally constrained (all dof's are zero). A node could have up to six dof`s, *i.e.* three for translation and three for rotation.

Two adjacent elements are connected to each other by connecting nodes. These connecting nodes share the same dof's. At the end, the initial domain is characterised by a finite number of elements, nodes, and dof`s. A field quantity (*e.g.* stress, strain) of each element is interpolated, usually by a polynomial form, from the values of the nodes.

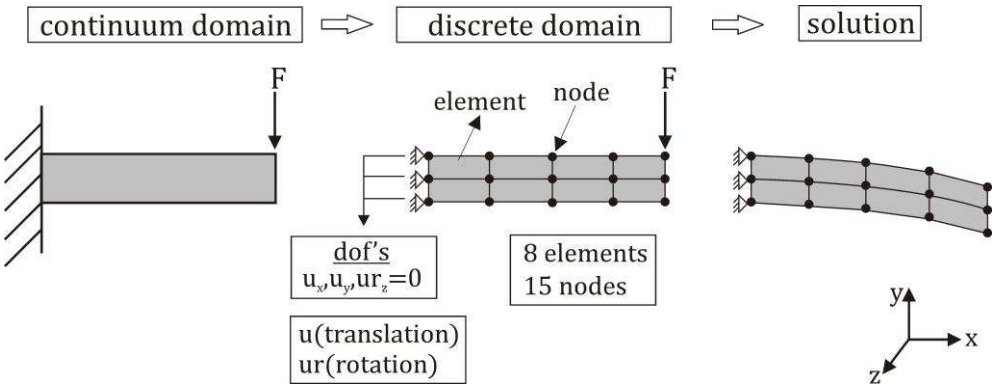

Figure 2.16 – Example of discretisation of a continuum domain for finite element analysis

Stress analysis of adhesive joints using FEA has been growing since the pioneering works of Adams *et al.* [74–76]. Nowadays, with the easy access to commercial software packages, FEA is a consolidated technique for the calculation of stress for quasi-static and fatigue conditions allowing the inclusion of several effects such as moisture and temperature [11,77]. Moreover, FEA can be used with each method of fatigue modelling that will be discussed in **Section 3.2**. However, to ensure an accurate calculation of stress using FEA much care is needed with

regard to definition of boundary conditions, definition of material behaviour, mesh refinement, element distortion, and suitable choice of type of element [11].

2.4. NOTCHES AND STRESS CONCENTRATION

In engineering components notches are originated from very common geometrical features (*e.g.* holes, grooves, corners), which makes the occurrence of stress concentrations almost unavoidable [78]. In the case of bonded joints, stress concentrations might occur at singularity regions, such as the overlap ends of single lap joints [16].

With the aid of stress trajectories, which run in the direction of the maximum principal stress, stress concentrations in a notched component can be observed in **Figure 2.17**. For an un-notched specimen (a) the trajectories run in parallel. Conversely, in the presence of a notch (b, c, d), these trajectories are altered and in the region where they move closer to each other a stress concentration region arises [27,37].

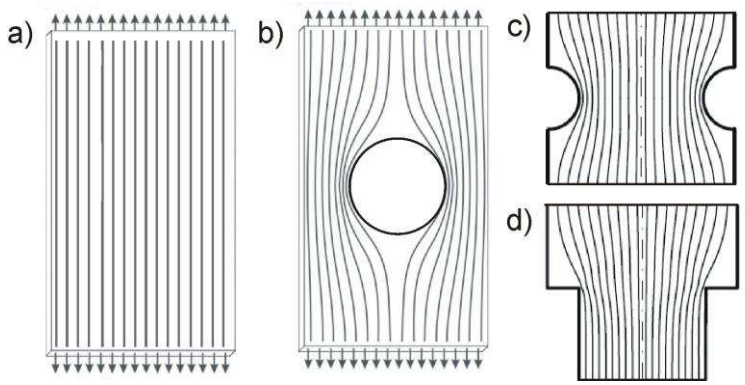

Figure 2.17 – Effect of notches on the stress trajectories: (a) unnotched, (b) internal notch, (c) external notch and (d) contraction

In the case of a finite value of stress concentration (*i.e.* excluding singularities), the stress concentration factor (k_T) can be used to numerically quantify the effect of stress concentrations [79]:

$$k_T = \frac{\sigma_{peak}}{\sigma_{nom}^{net}} \tag{2.17}$$

It represents the ratio between the maximum peak stress inside the material (σ_{peak}) and the nominal net stress (σ_{nom}^{net}):

$$\sigma_{nom}^{net} = \frac{F}{t(w-d)} \tag{2.18}$$

Where F is the applied force, w is the width of the sample and d is the diameter of the internal notch (**Figure 2.18**). Higher values of k_T indicate a higher notch-induced stress concentration.

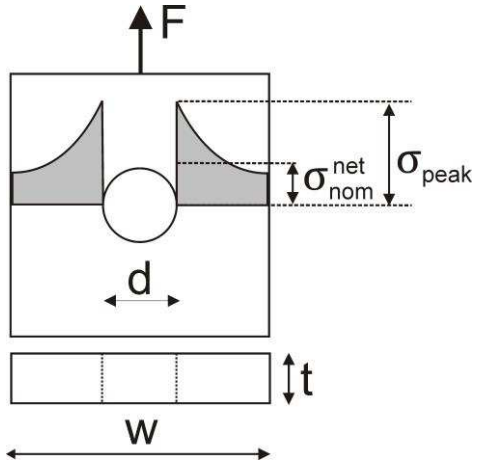

Figure 2.18 – Variables used for the definition of the elastic stress concentration factor

With the introduction of stress concentration within the structure, the distribution of stress is no longer homogeneous and stress gradients arise around notches [80]. Siebel and Steiler [81] and Irwin [82] were among the first researchers to address the role of stress gradients in fracture processes. In their works they stated that a sharp gradient implies a less severe situation than a low gradient.

In this regard, given a distribution of stress ($\sigma(x)$) as a function of distance (x) from the notch, the relative stress gradient (G_σ) quantifies how quickly the stress decreases from the peak stress at certain distance (X):

$$G_\sigma = \frac{1}{\sigma_{peak}} \frac{d\sigma}{dx}\bigg|_{x=X} \tag{2.19}$$

The concept of the highly stressed volume (*Werkstoffvolumenkonzept*, in German) [83,84] is used to formulate the effect of stress gradients on the mechanical behaviour of materials. This concept states that the smaller the highly stressed volume is, the greater the fatigue strength is.

This volume is quantified in terms of the region in which the stress is higher than a certain percentage (*e.g.* 90%) of the peak stress as illustrated in **Figure 2.19**. One advantage of the

highly stressed volume concept is that it is based both on statistical effects (Weibull distribution) and support effects (stress gradient) [85].

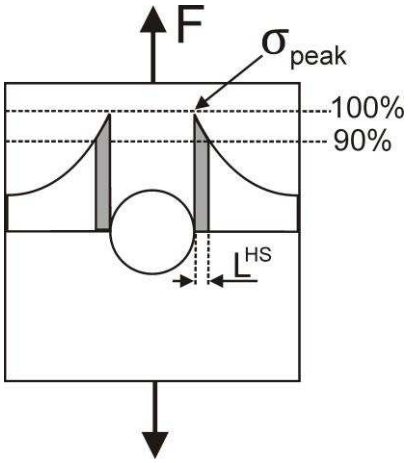

Figure 2.19 – Highly stressed volume concept

The high stress volume in the length direction (L^{HS}) is defined as follows (for a percentage of 90% of the peak stress):

$$\sigma(L^{HS}) = 0.9\sigma_{peak} \tag{2.20}$$

The effect of stress concentrations (caused by notches) on the mechanical behaviour of components is dependent on the level of applied stress [80]. Moreover, the presence of notches also generates a triaxial state of stress in the vicinity of the notch (even under uniaxial loading) [86]. The next sections are dedicated to the discussion of some research works that investigated the effect of notch-induced stress concentration and stress triaxiality on the mechanical behaviour of structural adhesives under quasi-static and fatigue conditions.

2.4.1. Effect of notches on the quasi-static behaviour of structural adhesives

Takano and Nielsen [14] investigated the stress-strain behaviour of a wide range of notched polymer specimens. Their conclusion was that the introduction of notches decreased the ultimate tensile strength of polymers and the elongation at break is even more reduced especially for ductile polymers.

Kinloch and Williams [87] studied the fracture and crack blunting mechanisms of a set of notched epoxy resin specimens including rubber toughened ones. They applied a critical distance criterion to model the failure behaviour obtaining a good agreement with experimental data.

Hertzberg *et al.* [52] explained the effect of notch strengthening (increase on the tensile strength in the presence of a notch) with the aid of *Weibull statistics* concluding that the volume of material that experiences the maximum stress is reduced for notched specimens. Therefore, the presence of the notch limits the size of region in which the crack may initiate. Another explanation to the strengthening exhibited by some ductile notched materials is related to the presence of considerable plastic deformation under high levels of stress, which hinders the material being deformed increasing its strength. Therefore, different behaviours under notched conditions might be expected between ductile and brittle materials.

Notch strengthening was observed by Sobieraj *et al.* [13] during the investigation of notched PEEK samples under monotonic loading. A dramatic change in the fracture mechanism with notching due to cavitation and void formation was observed. They proposed the following model to explain the higher amount of voids around smaller notches:

(i) cavitation is related to the hydrostatic stress;
(ii) due to stress concentrations just the region around the notch yields (plastic deformation), the yielded zone at the notch root is constrained by the un-yielded material around it;
(iii) this condition causes a triaxial stress field in the yielded zone, and the smaller the notch radius is, the greater the hydrostatic stress (*i.e.* stress triaxiality) is;
(iv) the greater the stress triaxiality in the plastic zone is, the greater the void growth rate is.

Katnam *et al.* [88] focused their work on a ductile two-part toughened epoxy paste adhesive. They demonstrated the formation of a stress-whitening region around the notches and that failure stress was increased by an increasing triaxiality ratio. Rodriguez *et al.* [89] assessed the fracture strength of a brittle DGEBA-based epoxy resin showing that the failure load increased with an increasing notch radius moving from a sharp crack to a blunt notch behaviour.

2.4.2. Effect of notches on the fatigue behaviour of structural adhesives

Under cyclic loading conditions the fatigue notch factor (k_F) is defined as the ratio of the fatigue strength of an un-notched specimen to that of a notched specimen under the same experimental conditions and the same number of cycles [79].

The notched behaviour of materials under quasi-static and fatigue conditions is distinct due to several reasons [79,80]: (i) plastic deformation effects and (ii) volume of highly stressed material. Consequently, some materials are more sensitive to notching than others. The notch sensitivity factor can be introduced to quantify how much the fatigue strength of a component is reduced in the presence of a notch [79]. The notch sensitivity varies between 0 (no sensitivity) to 1 (full sensitivity) [79,90]. From k_F and k_T it is possible to calculate the notch sensitivity (q):

$$q = \frac{k_F - 1}{k_T - 1} \tag{2.21}$$

Sobieraj *et al.* [12] investigated the fatigue behaviour of PEEK in circumferentially grooved round bar specimens with 3 different notch sizes. They observed that an increase in notch severity was accompanied by a reduction in fatigue strength, a steeper slope of SN curves, and a higher damage rate.

Several researchers have shown the reduction of the effect of stress concentration in the low cycle fatigue range for a wide range of materials: Mortazavian and Fatemi [91] for a PBT thermoplastic, Zhou and Mallick for a fibre reinforced polyamide [92], and Hoey and Taylor [93] for PMMA.

2.4.3. Theory of Critical Distances

Due to stress concentrations, the distribution of stress in the vicinity of the notch is not constant (**Figure 2.17**). Moreover, the consideration of only the peak stress for calculation the of fatigue lifetime of notched specimens have been shown, in many cases, to produce over-conservative predictions [63,94,95]. Therefore, based on the concept that fatigue takes place in a process zone; averaging methods have been developed to address the effect of stress concentration on the mechanical behaviour of notched components.

The Theory of Critical Distances (TCD), originally proposed in the works of Neuber [45] and Peterson [46] and brought back in the recent years by Taylor [96], has been well established as a stress averaging method to assess fracture both in quasi-static and fatigue conditions in a wide range of materials [95]. It relies on a length parameter, namely the *critical distance*. The critical distance determines the size of the process zone in which fatigue occurs defining a representative value of the stress causing the damage within the process zone [97].

One of the challenges when dealing with the TCD is the choice of the critical distance, it could be a function of the type of material [63] or the type of joint configuration [98,99]. Approaches for its determination have been presented by Hoey *et al.* [93], Susmel *et al.* [104], Khoramishad *et al.* [101], and Akhavan-Safar *et al.* [102].

The choice of a suitable equivalent stress (**Section 2.3.1**) is a crucial step in the use of the TCD. Several equivalent stress have been applied for the fracture of adhesives, namely: maximum principal stress, peel stress, shear stress and von Mises stress (this one with less success for not accounting for the hydrostatic stress dependence of adhesives) [64].

By averaging an equivalent stress (σ_{eq}) within a critical distance (L), an effective stress (σ_{eff}) is obtained which can be used for prediction purposes (**Figure 2.20**).

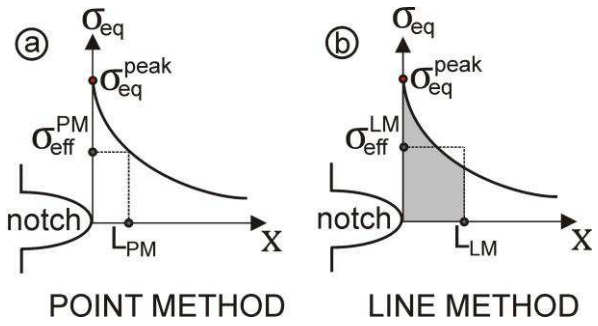

Figure 2.20 – Theory of Critical Distances: (a) Point Method, (b) Line Method

The TCD comprises several methods that consider the averaged stress in a point, in a line, in an area or in a volume [95]. In the present work, as shown in **Figure 2.20**, two of these methods will be used: the Point Method (PM) and the Line Method (LM).

1) in the Point Method (σ_{eff}^{PM}) the effective stress is considered to be the equivalent stress in a point determined by a critical distance (L_{PM}) from the notch:

$$\sigma_{eff}^{PM} = \sigma_{eq}\left(L_{PM}\right) \tag{2.22}$$

2) in the Line Method (σ_{eff}^{LM}) the effective stress is considered to be the equivalent stress averaged in a line with a length determined by a critical distance (L_{PM}) from the notch:

$$\sigma_{eff}^{LM} = \frac{1}{L_{LM}} \int_{0}^{L_{LM}} \sigma_{eq}\left(x\right) dx \tag{2.23}$$

In the case of adhesives, Crocombe [100] applied a stress criterion based on an averaging method in order to predict the failure load of single-lap joints obtaining good predictions for ductile adhesives. More recently, critical distance based methods have been employed for single lap joints to successfully predict the effect of overlap length and substrate thickness (Khoramishad et *al.* [101]), and bondline thickness (Akhavan-Safar *et al.* [102]). The investigations involving critical distance based methods for prediction of fatigue lifetime are described in **Section 2.5.1**.

2.5. FATIGUE MODELLING APPROACHES

The main objectives of fatigue modelling are to accurately predict the fatigue lifetime and to assess the rate of change of fatigue related parameters (*e.g.* crack length, stiffness degradation). Fatigue modelling is intimately related to a criterion to be established for the failure analysis of the adhesive. The chosen criterion is to be compared with a material property (*e.g.* ultimate tensile strength, fracture toughness) in order to assess the failure stress (quasi-static load) or the fatigue strength (cyclic load).

2.5.1. Continuum mechanics - total-life approach

The total-life approach relies on the use of stress (stress-life method) or strain (strain-life method) to define the failure of the material making it a continuum mechanics based criteria. The *stress-life method* requires a reference SN curve (obtained experimentally) to provide a relationship between stress amplitude and fatigue lifetime [37].

In the stress-life method for the prediction of fatigue lifetime for a given nominal stress amplitude, the effective stress related to this nominal stress must be calculated *(e.g.* using critical distance methods, **Section 2.4.3**). Then, using the calculated effective stress the fatigue lifetime is determined by means of the reference SN curve [7]. One advantage of the stress-life approach is the simplicity of its usage; especially, considering FEA stress calculation, which allows an easy correlation between calculated stress and fatigue lifetime [11].

Abdel Wahab *et al.* [103] predicted the fatigue threshold in CFRP-epoxy lap joints using an averaging criterion based on the maximum principal stress. The value of stress was taken from a distance from the singularity point to avoid mesh sensitivity. Still dealing with averaging methods, Susmel *et al.* [63] presented a review of the use of theory of critical

distances (TCD) for fatigue applications (**Section 2.4.3**). The TCD was shown to be valid for uniaxial and multiaxial fatigue and for low and high cycle fatigue.

Spaggiari *et al.* [21] applied TCD-based and stress gradient methods to estimate, with the support of FEA, the fatigue lifetime of a hydraulic control valve showing the potential of this method for engineering industrial components.

For the fatigue of adhesives, Schneider *et al.* [22] used the maximum principal stress to predict the fatigue lifetime of scarf, thick adherend and SLJs at different temperatures using a linear-elastic material model. They concluded that the homogeneity of stress distributions in the adhesive layer has a direct influence on the accuracy of the lifetime predictions. Beber *et al.* extended this analysis including elasto-plastic material models [98] and multiaxiality considerations [104]. They were able to improve the quality of predictions, especially for SLJs.

It is known that the hydrostatic stress can influence the mechanical behaviour of adhesives [67]. To address this influence, an approach based on the combination of hydrostatic and von Mises stress was successfully applied to predict the lifetime of several types of adhesive joints in a wide range of temperatures in several joint projects comprising German research institutions (including the Fraunhofer IFAM) [54,57].

However, one of the main challenges when dealing with the stress-life approach is the transferability between SN curves of joint configuration with different stress concentrations, loading conditions (stress ratio) [23].

For this reason, the choice of suitable equivalent stress (**Section 2.3.1**) is again very important. At the same time, stress-life approaches do not allow the possibility of predicting damage evolution or the assessment of residual strength. These limitations have been addressed in the literature with the use of damage based analysis, such as Miner [42] and Mesmacque *et al:* [105].

2.5.2. Fracture mechanics

The fracture mechanics (FM) approach is employed predominantly to model the crack propagation phase (**Section 2.2.2**), by assuming that crack initiation occurs during the early stages of fatigue cycling or an initial crack already exists. The number of cycles to failure can be obtained by integration of a fatigue crack growth law, *e.g.* a Paris-like law. The crack

propagation law is integrated from an initial (a_i) to a final crack size (a_f) as seen in **Equations (2.24)** and **(2.25)**

$$\frac{da}{dN} = f(\Delta\Gamma) = C(\Delta\Gamma)^m \tag{2.24}$$

$$N_f = \int_{a_i}^{a_f} \frac{da}{f(\Gamma)} \tag{2.25}$$

Where C and m are material properties and $\Delta\Gamma$ is a fracture mechanics quantity (*i.e.* energy release rate).

Kinloch and Osyemi [106] predicted with good accuracy the fatigue lifetime of single-lap joints using a fracture mechanics approach based on the strain energy release rate of a DCB specimen. Abdel Wahab *et al.* [107] used a generalised technique based on FEA to predict the fatigue crack propagation lifetime in bonded structures. Pirondi and Moroni [108] applied a fracture mechanics-based model in order to predict fatigue failure of adhesive joints.

An inherent limitation of the fracture mechanics approach is the incapability to account for the crack initiation phase, which in some structural adhesives can be significant [25].

2.5.3. Continuum damage mechanics

In the Continuum Damage Mechanics (CDM) approach, a damage variable (D) is defined to quantify the state of damage within the material. The damage variable can be associated with a quantity (*e.g.* stiffness, tensile strength) that is degraded with the evolution of number of cycles [23].

The damage parameter is zero for an undamaged material. With the formation of cracks and micro-voids, the damage parameter increases. Finally, the damage parameter reaches the value of one for a fully damaged material. According to this theory, the initiation of a macro-crack occurs at a certain level of damage (between 0 and 1). This approach presents the advantage of monitoring of damage evolution and the possibility (with a proper modelling) of assessment of the residual strength of the structure.

Abdel-Wahab *et al.* [109] proposed a CDM approach within a thermodynamic framework to predict the number of cycles to failure of composite bonded joints. In this model the damage rate ($\partial D / \partial N$) is calculated as a function of the equivalent stress range ($\Delta\sigma_{eq}$) as follows:

$$\frac{\partial D}{\partial N} = \alpha^{AW}\left[\frac{\Delta\sigma_{eq}}{(1-D)}\right]^{\beta^{AW}+m^{AW}} R_v^{\beta^{AW}/2} \tag{2.26}$$

Here α^{AW}, β^{AW} and m^{AW} are material parameters that should be fitted to experimental data, and R_v is the triaxiality function calculated from:

$$R_v = \frac{2}{3}(1+\nu) + 3(1-2\nu)\frac{\sigma_H}{\sigma_{VM}} \tag{2.27}$$

Which is defined as function of Poisson`s ratio (ν), hydrostatic stress (σ_H) and von Mises stress (σ_{VM}). To obtain the number of cycles to failure (N_f) the **Equation (2.26)** can be integrated in case of proportional loading from $D = 0$ to $D = 1$. Rearranging the variables it is possible to see that:

$$N_f = \frac{\Delta\sigma_{eq}^{-\beta^{AW}-m^{AW}} R_v^{-\beta^{AW}/2}}{\alpha^{AW}(\beta^{AW}+m^{AW}+1)} \tag{2.28}$$

Imanaka *et al.* [110] developed an isotropic CDM model combined with a kinetic law to describe the evolution of fatigue damage in a butt joint. The calculated damage (D_{calc}) was compared to experimentally obtained damage ($D_{\exp}$) that was considered to be a function of the measured stiffness:

$$D_{\exp}(N) = 1 - \frac{E(N)}{E_0} \tag{2.29}$$

In this approach the damage in the early stages of fatigue increased gradually with an increasing number of cycles. With the evolution of cycles, the slope of degradation started to increase with a faster increase approaching the final cycles. The samples always failed at a critical damage (D_c) less than 1.

Matzenmiller and Kurnatowski [111] proposed a law to describe the evolution of fatigue damage as a function of number of cycles. In their model, damage parameters could be obtained by fitting of fatigue experimental data from SN curves.

Shenoy *et al.* [112] proposed a unified model to predict the fatigue behaviour of adhesively bonded joints, in which the evolution of fatigue damage in the adhesive material was defined as a power law function of the micro-plastic strain.

Several authors have proposed elasto-plastic damage models to predict fatigue lifetime, such as Shenoy *et al.* [113], Graner Solana *et al.* [114], Katnam *et al.* [115] and Shen *et al.* [116].

2.5.4. Cohesive zone modelling

Cohesive Zone Modelling (CZM) approaches are based on the original works of Barenblatt [117] and Dugdale [118]. These approaches are formulated from the observation that with an increasing separation between two atomic planes within the material (or at the interface) the cohesion forces initially grow, eventually reaching a maximum value. Then, these forces start to decrease and eventually are reduced to zero [11].

This method combines stress-based failure criteria to determine crack initiation and fracture mechanics based criteria for damage propagation. Cohesive zone models follow a traction-separation constitutive law to predict failure initiation, damage, and failure [11].

Regarding the fatigue modelling using CZM, in general, there are three different approaches to account for the evolution of damage during fatigue cycles. The first is the cycle by cycle approach. This means that the fatigue model is numerically integrated over time for each cycle. It provides very detailed information of the degradation process even for complex loading histories [119]. However, it demands an extensive computational effort becoming impractical for complex structures or for high cycle fatigue. The second approach is the jump cycle strategy, using cyclic extrapolation techniques (e.g. Turon *et al.* [120], Ural *et al.* [121]). Finally, the third approach is based on maximum load conditions [11].

More recently, Khoramishad et al. [9] investigated the effect of load ratio on the fatigue behaviour of adhesively bonded joints using both experimental and numerical approaches, in which progressive damage of the adhesive material was modelled using a cohesive zone approach with a bilinear traction-separation

2.6. EXPERIMENTAL TECHNIQUES

The main topics regarding experimental techniques will be discussed in the following sections. Historically, a real breakthrough for fatigue testing equipment occurred around the 50's with the advent of closed-loop fatigue machines allowing a feedback signal from the specimen to monitor the load on the specimen. With this feedback, the fatigue load (*i.e.* stress) could be regulated by a computer-controlled system [37].

2.6.1. Use of bulk specimens

In the present work the investigation of the effect of stress concentrations will be done using notched bulk adhesive specimens (**Section 1.1**). In the literature several research works have been produced with the use of bulk specimens, some of them are discussed here.

Morin *et al.* [18] proposed a failure criterion for structural adhesives based on the triaxiality stress ratio and strain rate, which was derived from bulk specimens under different loading tests.

Abdel-Wahab *et al.* [19] and Hilmy *et al.*[122] found bulk adhesive specimens proper for the determination of damage parameters for a fatigue damage model for bonded joints. A damage evolution law was proposed from experimental results using a robust optimisation process using least square method for fitting the data.

Chen *et al.* [20] used bulk specimens to investigate the fracture toughness in mode I and mode III of a brittle and a ductile adhesive. Mixed-mode criteria were proposed for the experimental results showing good agreement with the strain energy theory.

Burst *et al.* [17] studied the matter of comparing *in-situ* (bonded joint) and bulk material properties. They concluded that bulk specimens are suitable for the design and analysis of adhesively bonded joints.

2.6.2. Monitoring of damage and crack initiation/propagation

Two techniques have been commonly used to monitor damage and cracks in adhesives, namely: back–face strain technique and video-microscopy. The back-face strain technique has been applied with success for bonded joints in several studies such as Zhang *et al.* [123], Crocombe *et al.*[124] and Shenoy *et al.* [125].

However, for the case of bulk materials the video-microscopy is much more suitable allowing the direct monitoring of fatigue-related phenomena (*e.g.* cracking, crazing and damage). Moreover, it is simple using video-microscopy to synchronise the computer and testing machine enabling the synchronisation between image acquisition and load application. Several authors have used video-microscopy for monitoring purposes of adhesives such as Dessurealt and Spelt [126] and Azari *et al.* [127].

Court *et al.* [128] used transparent PMMA adherends to observe crack propagation inside the joints using a video camera. They found that that crack initiation dominated the fatigue lifetime.

Other authors (*e.g.* Quaresimin and Ricotta [129] and Khoramishad *et al.* [130]) used in situ video-microscopy techniques to support fatigue modelling methods for adhesively bonded joints by providing a method to quantify the ratio between crack initiation and crack propagation.

2.6.3. Fracture surface analysis

Fracture surface analysis is another very important experimental technique to support the fatigue and fracture of structural adhesive. Many authors have applied fractography techniques to gain insights into the mechanics of material failure.

Sander *et al.* [51] classified the fracture behaviour due to cracks into three categories: surface crack, corner crack and through crack. This behaviour also suffers alteration in the presence of notches due to drilling according to **Figure 2.21**.

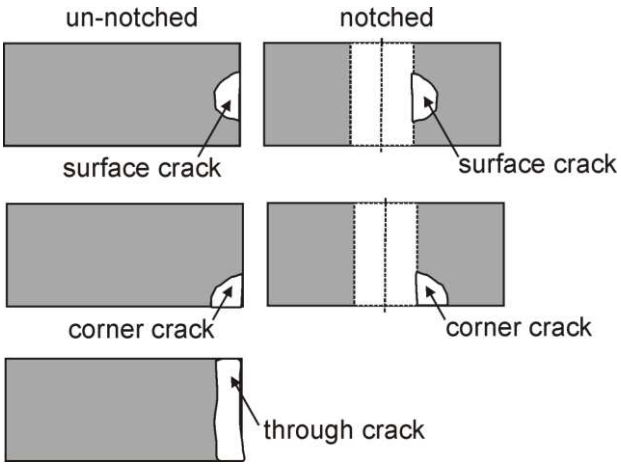

Figure 2.21 – Types of crack on fractography

Tsuji *et al.* [131] examined the failure of notched specimens in polycarbonate (PC) to evaluate the location of the crack initiation sites, concluding that cracks always initiate within the region with high plastic deformation.

Several researchers have used fractography analysis to assess the fracture behaviour of toughened adhesives such as Kinloch *et al.* [30], Pearson and Yee [31] and Huang and Kinloch [15]. They observed that the main mechanisms of toughening are related to localised cavitation followed by void growth and plastic shear yielding (**Section 2.1.3)**.

Sobieraj *et al.* [132] investigated the notched behaviour of highly crosslinked polyethylene. They revealed, with the use of fractography from a scanning electron microscope, that notching altered the deformation and the micromechanism of fracture by allowing craze formation, which was not observed in un-notched specimens.

2.7. SUMMARY

In the present section the key concepts and terminologies related to adhesive bonding technology, fatigue, calculation of stress, notches and stress concentration, fatigue modelling approaches, and experimental techniques were revised.

The technological relevance of structural adhesives (especially toughened epoxies) was presented. The effect of stress concentrations on the quasi-static and fatigue behaviour of structural adhesives was revised and discussed. In this regard, the present literature review revealed a lack of studies involving: (i) the relationship between stress concentrations and mechanical properties of structural adhesives, and (ii) the relationship between crack initiation and stress concentration.

State-of-the art literature research showed that the fatigue behaviour of structural adhesives is highly dependent on the state of stress within the material, especially under stress concentration conditions. Furthermore, it was discussed how notches could induce the formation of highly stressed regions and a multiaxial state of stress in the vicinity of the notch. Therefore, the use of the concept of equivalent stress can be very helpful by providing a comparative parameter between the state of stress of different loading configurations.

These evidences highlight the importance of precise calculation of stress for modelling purposes. In this regard, the finite element analysis has been proven to be most suitable method for calculation of stress for adhesives. At the same time, the theory of critical distance was shown to be an efficient method to address the inhomogeneity of stress (*i.e.* stress concentration) within a structure regarding quasi-static and fatigue predictions of notched specimens.

Main approaches for fatigue modelling were revised, namely: total-life, fracture mechanics, continuum damage and cohesive zone modelling. Their advantages and limitations were discussed based on research works found in the literature. Total-life approaches are the most straightforward method for fatigue lifetime prediction, but they still suffer from transferability issues between SN curves of joint configurations with different stress concentration and lack

damage evolution assessment. Fracture mechanics approaches are useful to calculate the propagation of crack. However, they have an inherent limitation of non-accounting for the crack initiation lifetime. Continuum damage mechanics approaches rely on a measurable parameter (*e.g.* stiffness) to account for the evolution of damage. Cohesive zone modelling uses stress-based failure criterion to determine crack initiation and fracture mechanics based criterion for damage propagation allowing the modelling of both phases.

With regards to experimental techniques, the advantages related to the use bulk adhesive specimens have been widely validated in the literature. To address the challenging task of crack initiation and damage monitoring, video microscopy have been proven to have suitable capabilities. Finally, studies have shown the potential of fractography analysis to understand the fracture mechanisms of notched components.

3. EXPERIMENTAL METHODOLOGY

The present chapter is concerned with the description of the experimental methodology applied for achieving the objectives set in **Chapter 1**. The present description was divided into the following topics: adhesive selection, sample manufacturing, experimental set-up, online monitoring during testing, stiffness degradation measurements and fractography. An overview of the experimental methodology is shown in **Figure 3.1**.

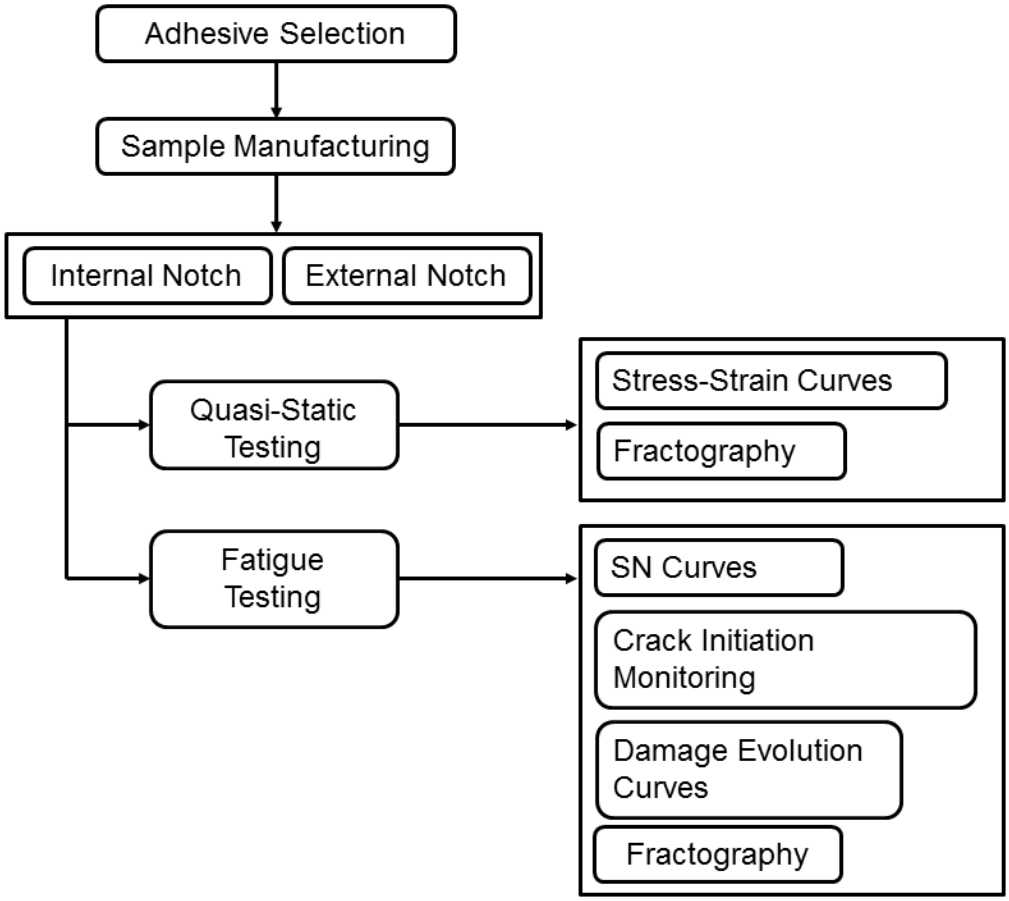

Figure 3.1 – Overview of experimental methodology

3.1. SELECTION OF STRUCTURAL ADHESIVES

Two commercial toughened epoxy adhesives designed for structural applications were employed for the present research work. Throughout the next chapters these adhesives will be named: RB-T adhesive (commercial name DOW Betamate 1496v©) and PU-T adhesive (commercial name SikaPower® -498). The idea behind using commercial adhesives of different manufacturers is to ensure that results found in this work are relevant for industrial (*i.e.* large scale) applications.

Both adhesives are made of a DGEBA-based epoxy resin. Regarding curing conditions they are both single components adhesives with hot cure. One of the main differences between the adhesives is the type of particles used as toughening element: one is rubber (RB-T adhesive) [133] and the other is polyurethane (PU-T adhesive) [134]. More information regarding the adhesives is available in **Table 3.1.**

Table 3.1 – Main characteristics of adhesives used in the investigation

adhesive	toughening particle	resin	composition	curing conditions
RB-T	rubber	DGEBA	single component	180°C / 30min
PU-T	polyurethane	DGEBA	single component	175°C / 20min

The selection of adhesives was done with the purpose to have different mechanical properties as shown in **Table 3.2**. Since different stress concentration are to be expected at notched specimens (**Section 3.2.1**), the objective is to correlate the effect of different stress concentrations in the adhesives to their mechanical properties.

Table 3.2 – Mechanical properties of adhesives [133,134]

adhesive	RB-T adhesive	PU-T adhesive
E [MPa]	1600	2120
Elongation at Break [%]	15	5
Tensile Strength [MPa]	32	30
Lap Shear Strength [MPa]	30	30

When comparing the adhesives the following characteristics are noticeable: they have similar tensile strength, but one adhesive (RB-T) is *more ductile* (*i.e.* higher elongation at break) and the other (PU-T) is *stiffer* (*i.e.* higher Young's Modulus, *E*). These mechanical properties have been shown to have an influence on the mechanical behaviour of notched specimens of polymers and adhesives [14,88]. Representative stress-strain curves of the adhesives are illustrated in **Figure 3.2**. These curves were obtained from quasi-static tests, which are discussed in more detail in **Chapter 5**.

The aim of showing a preview of these curves here in the experimental methodology is to display the differences between the adhesives. Moreover, it is shown that with the applied manufacturing process (detailed in **Section 3.2**) it is possible to achieve higher elongations at break than as the ones given by the suppliers, an evidence of the quality of the manufacturing process.

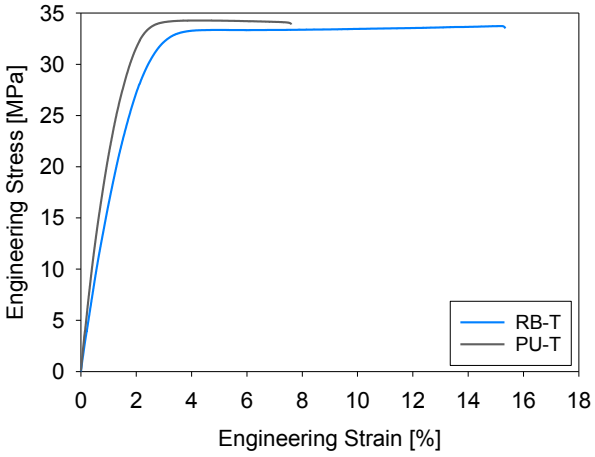

Figure 3.2 – Representative stress- strain curves of adhesives used in this work

3.2. MANUFACTURING OF BULK ADHESIVE SPECIMENS

Since both adhesives are single components with hot cure, the steps to manufacture bulk adhesive specimens were the same. The only differences are related to temperature and time of cure as could be seen in **Table 3.1**. The process of manufacturing was developed with a twofold aim: (i) to produce samples with a minimum amount of voids (since they are natural stress raisers) and (ii) to ensure reproducibility of samples, so that the only difference between them will be the type of introduced notch. The manufacturing process followed the guidelines of ISO 15166 [135]. A general scheme of the manufacturing set-up is shown in **Figure 3.3**.

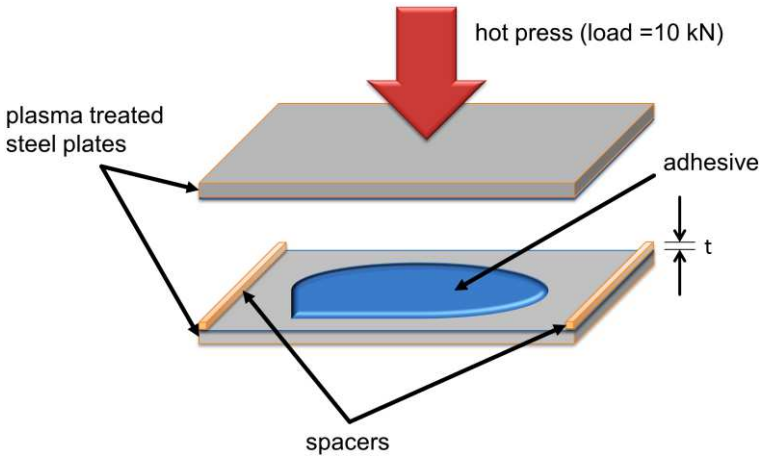

Figure 3.3 – Scheme of sample manufacturing set-up

To initiate the manufacturing process the adhesive cartridges were heated to 55°C (as recommend by suppliers) in order to obtain a suitable viscosity of the adhesives for application with a pneumatic-gun with pressure control. Then, the manufacturing process followed the steps shown in **Figure 3.4**:

a) The adhesive was applied on an anti-stick plasma treated steel plate. Spacers were placed between the plates to set the desired sample thickness (5 mm). Then, the adhesive was covered with a second plate.
b) Since mechanical properties of bulk adhesive specimens are highly influenced by temperature and time of cure [18], the curing was performed in a hot-press with a controlled load of 10 kN.
c) After curing, the produced adhesive plates were ready to be milled into dog-bone shaped samples.

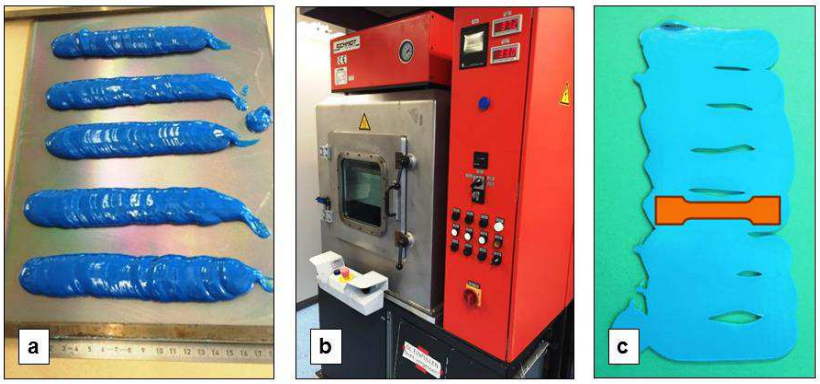

Figure 3.4 – Steps of sample manufacturing | (a) adhesive application, (b) curing under controlled load, and (c) adhesive plates to be milled

From the cured adhesive plates, the bulk adhesive specimens were milled into geometries provided in **Figure 3.5** with two different types of notches: (a) internal and (b) external.

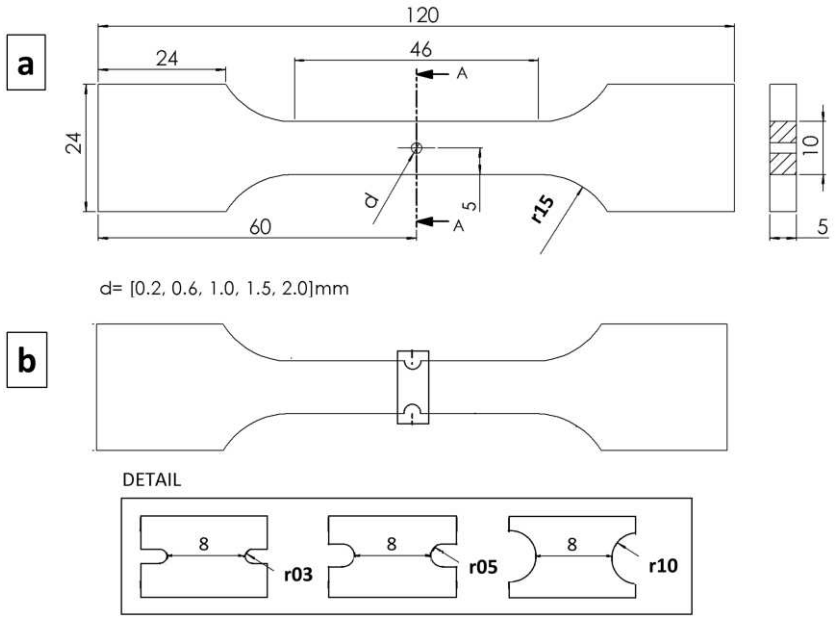

Figure 3.5 – Geometry of notched specimens: (a) internal notch and (b) external notch

3.2.1. Choice of notches

In engineering applications the types of notches are very diverse. In this regard, the present research work used different types of notches to cover a broad range of possibilities. To achieve this, two types of notches were investigated: internal notches (referred to as *dXX*) and external notches (referred to as *rXX*). Here *dXX* is related to the diameter of an internal notch and *rXX* is related to the radius of an external notch.

As explained in **Section 2.4**, the introduction of a notch can affect the quasi-static/fatigue behaviour of a specimen for several reasons: onset of stress concentrations (peak stress), formation of a stress gradient, creation of a triaxial state of stress, creation of a highly stress region, and reduction of cross-section. The size of notches was designed to address these issues in order to have a broad vision of the effect of stress concentrations. From the geometry of the samples it is possible to analytically calculate the elastic stress concentration factor [136] if the material behaviour is considered to be linear elastic.

With the use of internal notches the reduction of cross section, the size of highly stressed region, and the stress concentration factor changed according to the diameter of the notch as shown in **Table 3.3**. Moreover, it is expected that the smaller the diameter is, the greater the stress gradient is.

Table 3.3 – Internal notches: stress concentration factor and reduction of area

notch type	**d02**	**d06**	**d10**	**d15**	**d20**
internal diameter size [mm]	0.2	0.6	1.0	1.5	2.0
stress concentration factor, k_T [-]	2.94	2.83	2.73	2.62	2.52
reduction of original area [%]	2.0	6.0	10.0	15.0	20.0

By using external notches the aim was to have different stress concentration factors and gradients but with the same cross-section (**Table 3.4**). Additionally, with external notches it is possible to obtain a wider range of stress concentrations as compared to the internal notches [136].

For both types of notches different states of triaxial stress are to be expected. Some representative examples of the notched specimens can be seen in **Figure 3.6** (internal notch) and **Figure 3.7** (external notch). The internal notches were introduced to the samples using a drilling machine. The external notches were produced with a milling machine.

Table 3.4 – External notches: stress concentration factor and reduction of area

notch type	**r03**	**r05**	**r10**
external radius size [mm]	0.3	0.5	1.0
stress concentration factor, k_T [-]	3.90	3.16	2.42
reduction of original area [%]	20.0	20.0	20.0

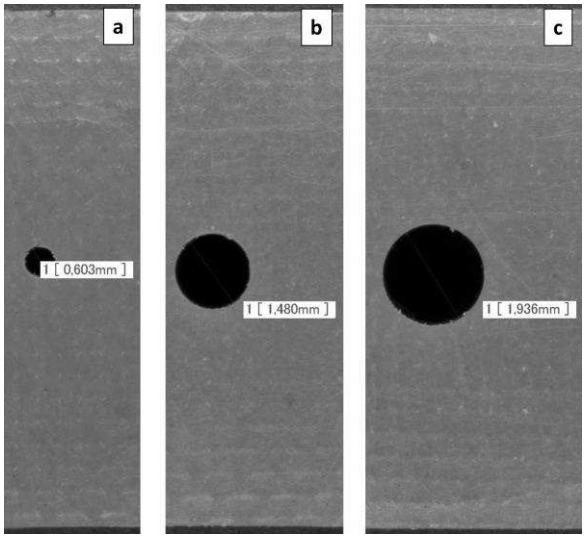

Figure 3.6 – Example of internally notched specimens: (a) d06, (b) d15 and (c) d20

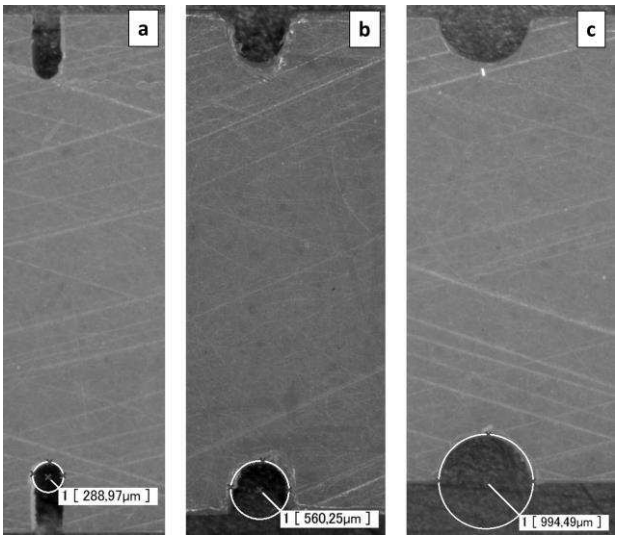

Figure 3.7 – Example of externally notched specimens: (a) r03, (b) r05 and (c) r10

3.3. EXPERIMENTAL SET-UP

Mechanical tests (quasi-static and fatigue) were carried out in an electrodynamic testing machine Instron® E3000 with a load capacity of ± 3 kN. Testing procedures followed guidelines provided in the book edit by da Silva *et al.* [35]. The values of the applied load

could be obtained directly from the testing machine, whereas displacement values were measured with a clip-on extensometer MTS® 632.17C-20 mounted on the tested sample. The devices used in this investigation are shown in **Figure 3.8**.

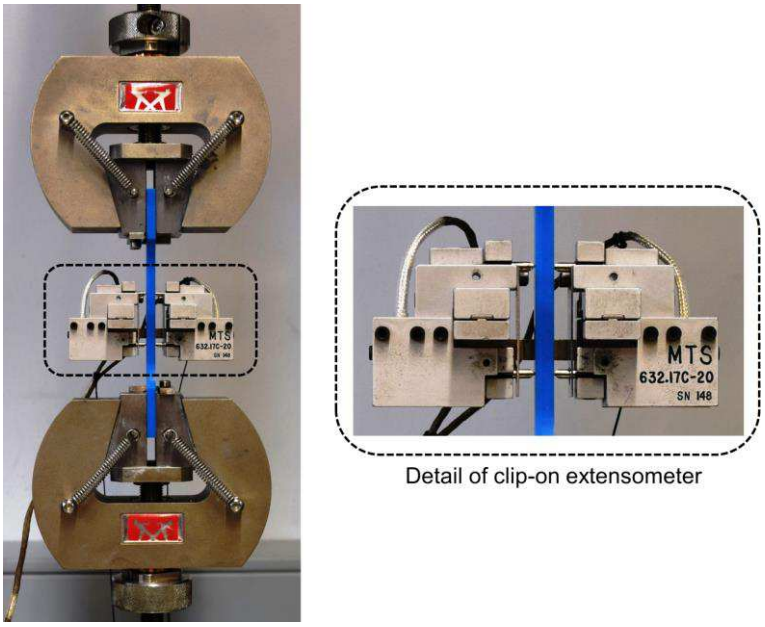

Figure 3.8 – Mechanical testing device for quasi-static and fatigue experiments

Samples were tested until complete failure. The samples that broke outside the notch region, at a bubble or at a manufacturing defect were discarded.

3.3.1. Quasi-static testing

Quasi-static testing was carried out using displacement control. The objectives of the quasi-static tests were:

a) to provide input data for material models for FEA (*e.g.* Young´s modulus);
b) to assess the effect of displacement rate on quasi-static strength and fracture behaviour of un-notched specimens;
c) to assess the effect of stress concentrations (notches) on quasi-static strength and fracture behaviour of structural adhesives.

In **Figure 3.9**, the main topics related to the quasi-static tests including structural adhesives, type of notches and displacement rate of testing are summarised.

Since stress concentrations can cause a local increase of strain rate, the tests under different displacement rates with un-notched samples was conducted to provide insights into how the

investigated adhesives are affected by strain rate alterations. Results and analysis of quasi-static tests are given in **Chapter 5**.

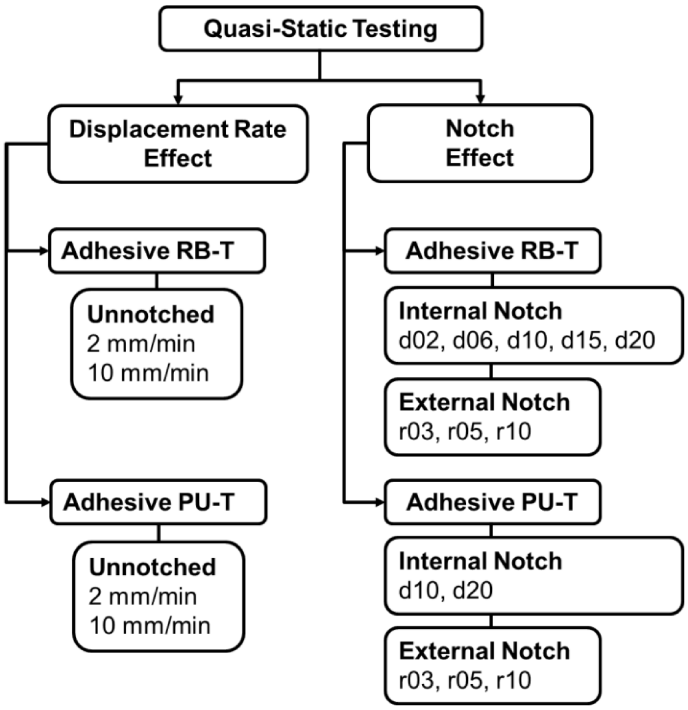

Figure 3.9 – General scheme of quasi-static testing

3.3.2. Fatigue testing

Fatigue tests were performed in accordance with the ISO12107 [137] under constant amplitude with force control in a cyclic tension-tension loading with sinusoidal shape, stress ratio (R = 0.1) and a frequency of 5 Hz. This frequency was defined to obtain the highest possible frequency (for reduction of testing time) whilst avoiding the risk of thermal heating affecting fatigue results. This choice was based on earlier studies by our research group [54,111].

Stress amplitudes were defined to capture lifetimes from low to high cycle range ($10^3 < N_f < 2.10^6$). The statistical analysis of the data was carried out based on the ASTM E739 [138] with a 95% confidence interval and a 50% probability of failure. A summary with the main points related to the fatigue testing is shown in **Figure 3.10**.

The objectives of fatigue tests were:

a) to generate fatigue data with different levels of stress concentration for fatigue modelling;

b) to develop an experimental set-up capable of monitoring and capturing the progression of damage and the formation of cracks;

c) to assess the effect of stress concentrations on the fatigue behaviour of structural adhesives with regard to total lifetime, crack initiation lifetime, progression of damage and fracture pattern.

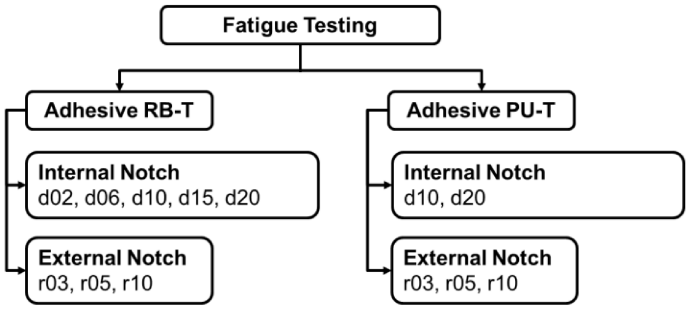

Figure 3.10 – General scheme of fatigue testing

In the beginning of cyclic loading a certain amount of cycles was necessary for the controlling system algorithm of the machine to adapt to the actual stiffness of the sample under test. Therefore, in the first cycles there was a difference between the *set value* of load and the *actual value* of load. The *set values* of load were reached by the controlling system after some feedback cycles. This adjusting process is depicted in **Figure 3.11**, where the differences between *actual* and *set values* of maximum (F_{max}) and minimum applied forces (Fmin) during cyclic loading are shown.

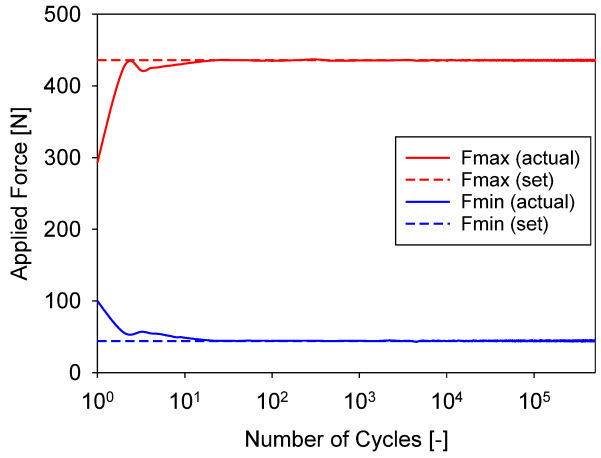

Figure 3.11 – Differences between set and actual values of applied force

Due to this difference in the beginning of the tests, the data related to the first 10 cycles of fatigue testing were not considered for stiffness calculations. This procedure was conducted by other researchers without compromise of the analysis of fatigue damage behaviour [19].

As mentioned before, structural adhesives can be sensitive to strain rate during testing. Fatigue tests were performed in low and high cycle fatigue range. Consequently, there was a range of stress amplitudes. An example of this stress amplitude variation is presented in **Figure 3.12**.

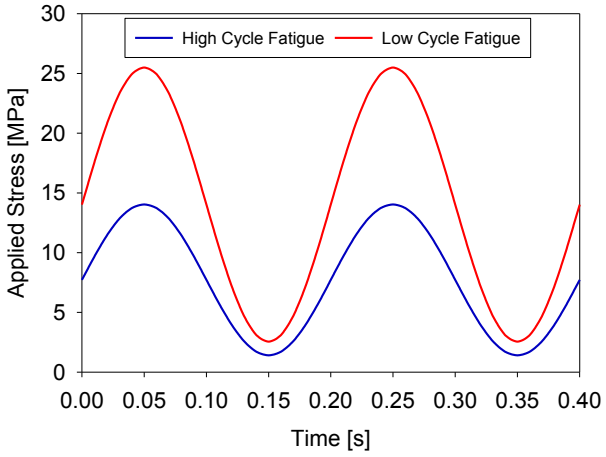

Figure 3.12 – Stress amplitude variation for low and high cycle fatigue range for an externally notched specimen (r03)

Since frequency of tests was kept the same, differences on strain rate between low and high cycle fatigue are to be expected. However, in the cases of the present study these differences are around a factor of two or three, which is not high enough to critically influence fatigue results.

3.4. ONLINE MONITORING OF CRACK INITIATION

Under fatigue loading the exact determination or definition of crack initiation is very complex and depends strongly on the defined criterion, or on the measuring device used for its detection. For bonded joints the monitoring of crack initiation is troublesome due to the thin layer of adhesive which difficult visualisation [8].

On the other hand, in the case of bulk specimens this monitoring can be performed directly, especially for notched specimens in which localised stress concentration make the onset of cracks more clear. Another advantage of online monitoring of mechanical testing is the possibility of observing the evolution of damage through the crazing (stress whitening) of the samples under test [65].

Two different monitoring systems were used in the course of the present research work. The first monitoring was employed to provide insights into crack initiation process and evolution

of damage. The second system (hereinafter referred to as "enhanced system") was totally integrated and synchronised with the load controlling system of the mechanical testing machine, which allowed a very good detection of crack initiation. Details of both monitoring systems are described in the next sections.

3.4.1. First monitoring system

In the first monitoring system shown in **Figure 3.13** two different USB video-cameras, a Microsoft® LifeCam Cinema and a Logitech® HD C615, were installed close to each side of the samples being tested. An image was taken for every cycle of testing in order to evaluate the cracking behaviour and plastic deformation.

Figure 3.13 – Experimental set-up of the first monitoring system

The first monitoring system was very useful to differentiate the crack propagation mode and to evaluate the size of damage zone and plastic deformation (to see whether it was localised or more generalised). However, since it took one photo per cycle, a lot of storage space was necessary. For instance, in a hypothetical case of one million cycles two million pictures must be taken, which requires an enormous amount of storage space.

A representative set of images obtained from the first monitoring system is shown in **Figure 3.14**:

a) beginning of test – no damage
b) early stage of crack propagation – generalised plastic deformation
c) final state of crack propagation – crack wide open

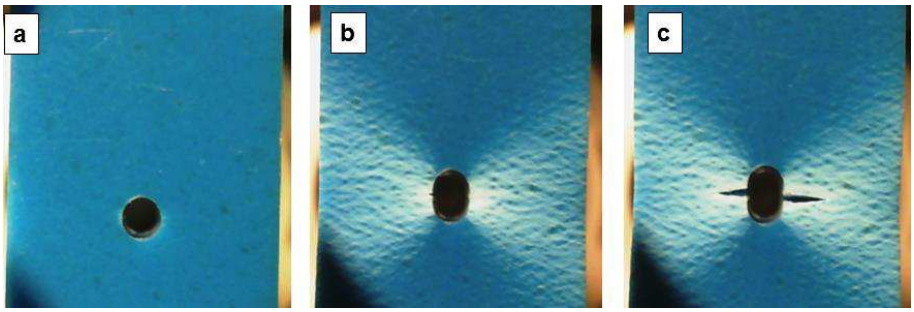

Figure 3.14 – Set of images from the first monitoring system: (a) test beginning, (b) early stage of crack propagation, and (c) final stage of crack propagation

The main drawback of the first monitoring system was the lack of synchronism with the load controlling system of the testing machine. Consequently, in the earlier stages of crack initiation it was hard to visualise an opened crack because the time when the picture was taken was not necessarily the point of maximum load of the cycle (where cracks are clearly visible). For this reason, the enhanced monitoring system was developed in order to establish a synchronism between pictures and maximum load (*i.e.* crack opening).

3.4.2. Enhanced monitoring system

The enhanced monitoring system was set-up using two Imaging Source® Industrial Cameras with CMOS Sensor (Model DMK 23UX236). The cameras were installed close to each side of samples being tested. The experimental set-up using the enhanced monitoring system is shown in **Figure 3.15**.

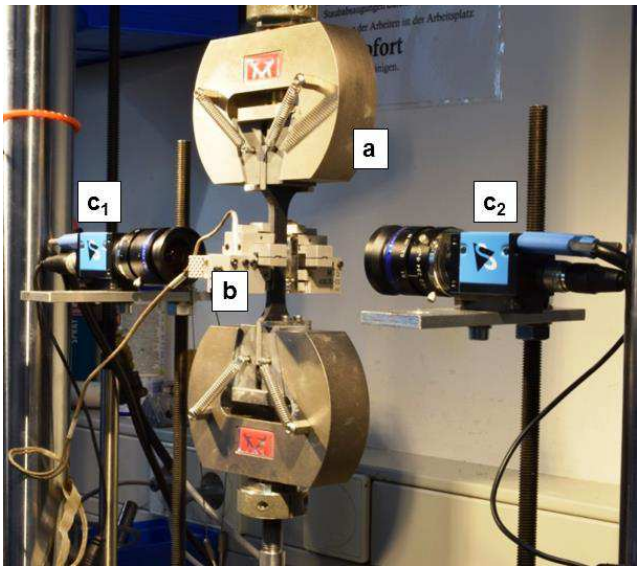

Figure 3.15 – Mechanical testing device for quasi-static and fatigue experiments | (a) cross-head of testing machine, (b) clip-on extensometer, and (c) cameras for monitoring

The advantage of this system was the possibility of image acquisition of the samples at the maximum force of the cyclic loading, which is the best position to observe the crack initiation. Using the controlling software of the testing machine a loop system was programmed to take a photo after a defined number of cycles. This looping was done with two aims: (i) to reduce storage space and (ii) to synchronise image acquisition and maximum load.

To achieve the second aim, the test was stopped during image acquisition. A photo was taken every ΔN = 250 cycles. This looping process is depicted in **Figure 3.16**.

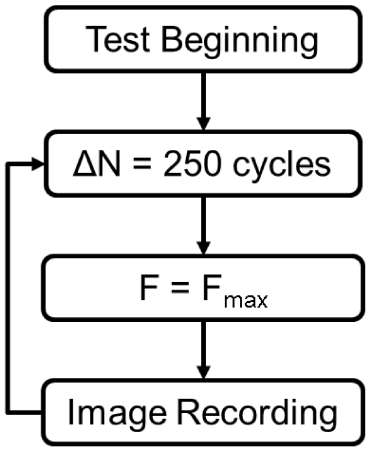

Figure 3.16 – Looping process for image recording for monitoring of crack initiation

A representative set of images obtained with the enhanced monitoring system is shown in **Figure 3.17**, where it is possible to observe

a) beginning of test – no crack
b) crack initiation – localised cracking
c) final stage of crack propagation – generalised cracking

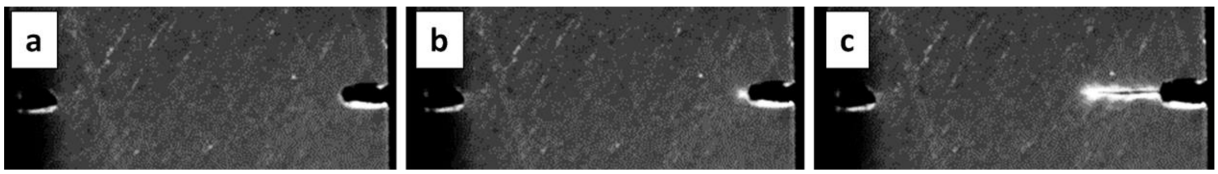

Figure 3.17 – Example of images from enhanced monitoring system: (a) test beginning, (b) early stage of crack propagation, and (c) final stage of crack propagation

The determination of the number of cycles for crack initiation was done with post-processing of the images (**Section 6.3.2**). The results of post-processing were then compared with the stiffness degradation data collected during tests to assess the possibility of correlation between them. (**Section 6.3.3**).

3.5. MEASUREMENT OF DAMAGE (STIFFNESS DEGRADATION)

In damage mechanics the concept of effective stress assumes that the initial load carrying surface A_0 decreases due to the growing of a defect surface A_{def} so that an effective load carrying surface A_{eff} can be defined as:

$$A_{eff} = A_0 - A_{def} \tag{3.1}$$

The damage *D* starts from a value of zero and increases until the value of one is reached, *i.e.* the defect surface equals to the original surface:

$$D = \frac{A_{def}}{A_0} \tag{3.2}$$

If a material is loaded, the external force (*F*) can be calculated from the nominal stress within the material as:

$$F = \sigma_{eff}\, A_{eff} = \sigma_{nom}\, A_0 \tag{3.3}$$

Here σ_{nom} denotes the applied nominal stress and σ_{eff} is the effective stress. The applied nominal stress can be calculated from this equation as:

$$\sigma_{nom} = \frac{A_{eff}}{A_0}\sigma_{eff} = \left(1 - \frac{A_{def}}{A_0}\right)\sigma_{eff} = (1 - D)\,\sigma_{eff} \tag{3.4}$$

By considering the concept of strain equivalence proposed by Lemaitre [139], the strains are assumed to be the same for the damaged and undamaged material. Thus, the effective stress can be expressed in terms of the strain and the initial stiffness as:

$$\sigma_{eff} = E_0\, \varepsilon \tag{3.5}$$

In terms of the strain and the effective stiffness as:

$$\sigma_{nom} = E_{eff}\, \varepsilon \tag{3.6}$$

Combining both equations yields:

$$E_{eff} = \frac{A_{eff}}{A_0} E_0 = (1 - D)\, E_0 \tag{3.7}$$

Finally, in terms of the stiffness:

$$D = 1 - \frac{E_{eff}}{E_0} \tag{3.8}$$

Therefore, the progression of damage could be quantified by measuring the degradation of sample stiffness. With the use of a single clip-on extensometer, it is possible to consider the sample as a spring under load.

In this regard, the damage can be correlated to a measurable parameter, *i.e.* the measured stiffness (*k*) in N/mm. By applying an external cyclic load in each cycle (ΔF_N) a variation in the displacement (Δu_N) can be measured by the clip-on extensometer.

This displacement can be divided into two components, as done by Sobieraj *et al.* [12], one due to fatigue (Δu_N^{fat}) and the other due to creep (Δu_N^{creep}) as:

$$\Delta u_N = \Delta u_N^{fat} + \Delta u_N^{creep} \tag{3.9}$$

An example of force-displacement curves considering both creep and fatigue components for a sample of the RB-T adhesive with a fatigue lifetime of 24500 cycles is shown in **Figure 3.18**.

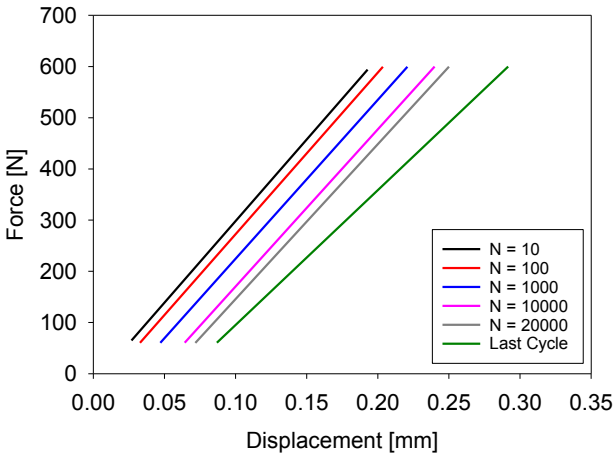

Figure 3.18 – Example of force-displacement curves for calculation of stiffness with creep and fatigue components

Stiffness as a function of each cycle (k_N) was calculated by dividing the variation of the force by the variation on the local displacement due to fatigue:

$$k_N = f(N) = \frac{\Delta F_N}{\Delta u_N^{fat}} \tag{3.10}$$

This represents the tangent on force-displacement curves. By using the same example shown in **Figure 3.18** but considering solely the effect of fatigue, the force-displacement curves become the ones shown in **Figure 3.19**.

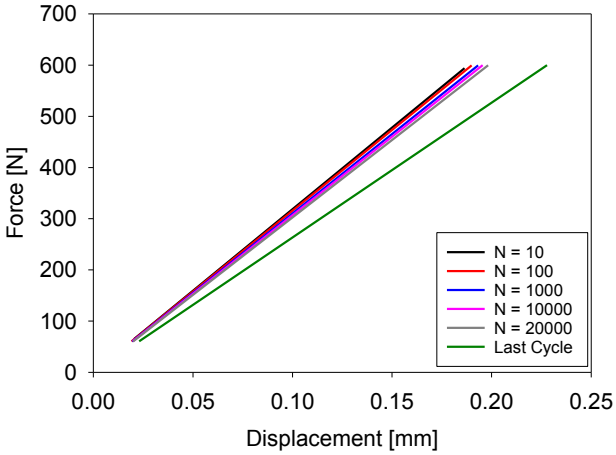

Figure 3.19 – Example of force-displacement curves for calculation of stiffness with only the fatigue component

The normalised stiffness per cycle (k_N^*) can be used in order to obtain a comparable variable for different samples. It can be calculated by dividing the stiffness per cycle by the initial stiffness as follows:

$$k_N^* = f(N) = \frac{k_N}{k_0} \tag{3.11}$$

Since the first 10 cycles were not considered, the initial stiffness was assumed to be the value of measured stiffness at the tenth cycle. Finally, the damage per cycle (D_N) was defined in terms of the stiffness degradation as:

$$D_N = f(N) = 1 - \frac{k_N}{k_0} = 1 - k_N^* \tag{3.12}$$

3.6. FRACTOGRAPHY

Fracture surface analysis (*i.e.* fractography) is a very powerful technique since it can provide insights into the fracture process such as void nucleation/cavitation, crack

initiation/propagation, localised plastic deformation (yielding), crazing, stress-whitening, damage progression and others [18,88].

Fracture surface images were taken with an optical microscopy Keyence® VHX-S50. No treatment was applied to the surface of samples under analysis. An example of fractography images is shown in **Figure 3.20**.

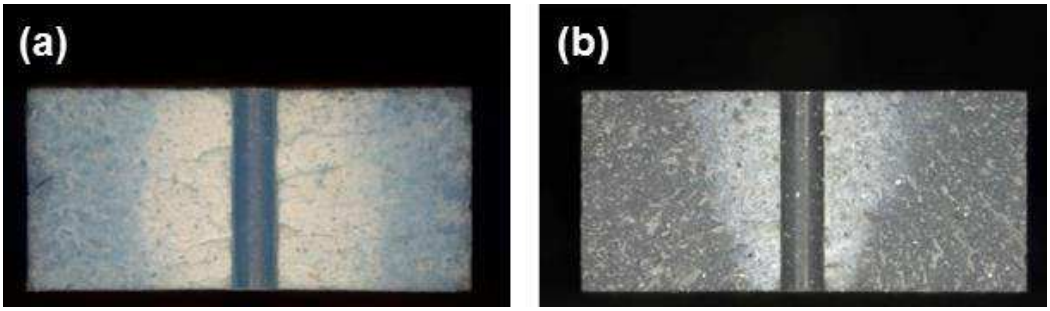

Figure 3.20 – Example of fractography image for an internally notched specimen (d10) - magnification: 30x - for both adhesives: (a) RB-T and (b) PU-T

This example illustrates some of the features which will be correlated with type of notch and adhesive properties in both quasi-static and fatigue loading; for instance, existence of stress-whitening indicating a highly damaged region around the notch, a clear presence of bevelled regions (roughness) in the RB-T adhesive (more ductile), and presence of small dots (*i.e.* voids) close to the notch root.

3.7. SUMMARY

Experimental investigations were a crucial part of this research work, especially due the complex nature of the phenomenon of fatigue, which makes it hard to produce predictive models for fatigue analysis. In order to establish models for the correlation between stress concentrations and fatigue damage behaviour, the correct planning and execution of experiments is essential for the achievement of good results. For this reason, this chapter was used to describe topics related to experimental investigations.

The selection of adhesives (**Section 3.1**) was done with the purpose of having a broad range of mechanical properties as well as industrial relevance. For this reason, two commercial structural adhesives were selected: both are single component toughened epoxies based on with hot cure. One adhesive is toughened with rubber (RB-T) and the other adhesive is toughened with polyurethane (PU-T). With respect to mechanical properties, they have

similar strength; their differences rely on the stiffness and mainly on the ductility (plastic deformation prior to failure).

The process of sample manufacturing (**Section 3.2**) was carried out with the objective of obtaining bulk specimens with the minimum amount of voids and defects, in the sense that their mechanical behaviour of samples is only affected by the presence of the notches. The quality of manufacturing was demonstrated by the values of elongation at break of un-notched specimens which surpassed the values given by data sheets of suppliers. The notches introduced to the samples were chosen to produce a wide range of stress concentrations, stress gradients, size of highly stressed region, reduction of cross section, and stress triaxialities. From this perspective, two different types of notches were used: (i) internal notches and (ii) external notches. Five different diameters of internal notches (*i.e.* holes) were used in this investigation. They allowed the evaluation of alterations in the state of stress combined with reduction of cross-section and size of highly stressed region. Three different radii of external notches were applied in this investigation, which allowed the assessment of the effect of stress concentration with a constant value of cross-section.

The experimental set-up for quasi-static and fatigue test was described in **Section 3.3**. Quasi-static tests were performed using displacement control. These tests had focus on providing input data for material models of FEA and on assessing the effect of displacement rate and different notch sizes on tensile strength. Fatigue tests were carried out using load control. They had the objective of generate data for fatigue damage modelling, capture and monitor the progression of damage and formation of cracks, and assess the effect of different stress concentrations on the fatigue behaviour of structural adhesives.

The use of bulk adhesive specimens allowed the direct monitoring of tests (**Section 3.4**). This monitoring process provided insights into the progression of damage, evolution of crazing (stress whitening) and a very good detection of crack initiation. These data can be correlated with stiffness degradation measurements, which were used as damage progression indicators (**Section 3.5**). The stiffness was assumed to be the tangent of force-displacement curves. To make different samples comparable, the normalised stiffness was used to calculate the damage. Fracture surface analysis (**Section 3.6**) was performed using optical microscopy aiming to gain understanding on fracture process such as void nucleation/cavitation, crack initiation/propagation, localised plastic deformation (yielding), stress-whitening and damage progression.

4. NUMERICAL METHODOLOGY

This chapter describes the numerical methodology employed in the present research work. Numerical investigations were carried out by means of finite element analysis (FEA) using the commercial software *Dassault® Abaqus*. FEA was performed for the modelling of both quasi-static (**Chapter 5**) and fatigue (**Chapter 6**) behaviour of the adhesives under investigation).

The process of implementation of the FEA models was divided into four steps, namely: definition of geometry (**4.1**), definition of material model (**4.2**), boundary conditions (**4.3**), as well as meshing and element choice (**4.4**).

4.1. DEFINITION OF GEOMETRY

The first procedure taken to implement a FEA model is the creation of the sample geometry. Due to the symmetry of loading and sample geometries, a quarter of the samples could be used (as deeper detailed in **Section 4.3**). The FEA sample geometries were set to reproduce the geometries of the tested samples, which are illustrated in **Figure 3.5**.

In the FEA models the sample geometry could be defined in two dimensions (2D) or three dimensions (3D) as illustrated in **Figure 4.1**. The choice of 2D or 3D models is intimately related to the complexity of implementation of the FEA model and the amount of required computational power. 2D models are always preferable due to their lower complexity and computational requirements [11,23]. Nevertheless, in some cases, 3D models are necessary, especially for complex geometries or in the case of stress singularities (*i.e.* higher stress gradients) [140]. In the next section the factors taking into account for the choice of 2D or 3D are detailed.

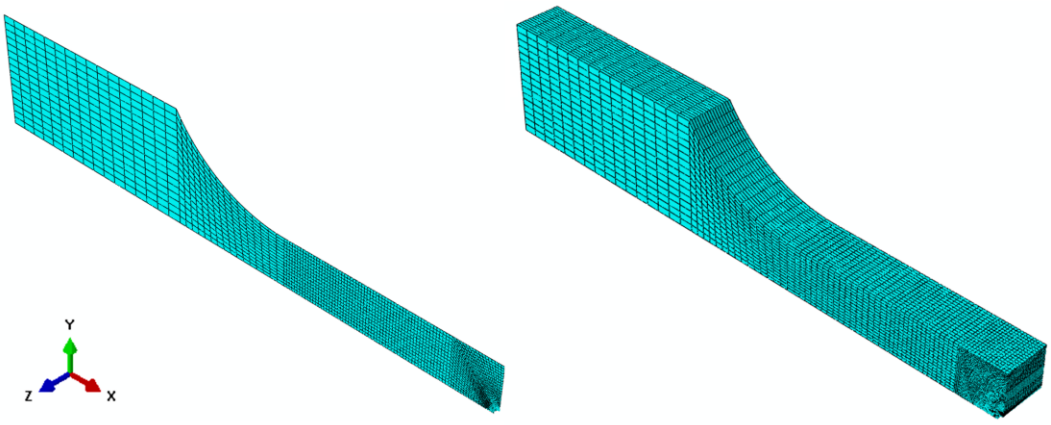

Figure 4.1 – Example of sample geometry with 2D and 3D models

4.1.1. 2D models

Several authors have shown the accuracy of 2D-finite element analysis applied for the modelling of the mechanical behaviour of adhesives [11,23,25,98,104]. Two-dimensional models allow shorter simulation times and mesh refinement at stress concentration regions. Moreover, they require relatively less modelling effort (*e.g.* pre-processing) when compared to three-dimensional analysis.

An aspect to be noticed is that samples have three dimensions (width, length and thickness) therefore an assumption must be made in order to model them as two-dimensional, namely plane stress or plane strain. In the plane stress assumption, one of the dimensions of the body is very small in relation to the others. Consequently, the stresses in the thickness direction are considered to be zero [77]. On the other hand, in a plane strain assumption the width is much larger than the thickness, which implies that the strains in the thickness direction are considered to be zero [35].

Despite the model being two-dimensional (width and length), a thickness could be specified to the third dimension in order to make values of force between experiments and simulation comparable. However, the values of stress or strain (according to chosen assumption) in thickness direction are constant. If no value is given, the software assumes a thickness of one.

Usually, plane stress conditions are assumed for bulk specimens under tensile loading [77]. However, due the presence of the notches, a tri-axial state of stress is created in the vicinity of the notch. For this reason, plane stress assumptions could not necessarily be valid. In this case a three dimensional model might be required.

4.1.2. 3D models

As mentioned earlier, there are cases in which two dimensional models are not able to provide satisfactory accuracy for design purposes. The advantage of using three dimensional FEA is that no special assumption is required to simplify the geometry and loading. Conversely, the disadvantage is that a large amount of time is required for set-up of the models and for computer processing, especially for complex geometries and in the presence of non-linear material behaviour [23].

In the present research work FE simulations were performed under plane stress, plane strain and three dimensional conditions. Simulation results were then compared to experimental data

in order to determine which geometric approach shows the best correlation with the experimentally determined mechanical behaviour of notched samples.

4.2. DEFINITION OF MATERIAL MODEL BEHAVIOUR

The definition of material model behaviour is one of the most important aspects of finite element analysis [23]. The prediction capability of FEA is strongly related to the accuracy level in which the FEA model is able to reproduce the mechanical behaviour of the material under analysis, *i.e.* the adhesive.

Many studies dealing with adhesives have identified three main classes of the mechanical behaviour of structural adhesives [141]. These classes are shown in **Figure 4.2**: linear-elastic behaviour (a-b), elasto-plastic behaviour (a-b-c) and damage behaviour (c-d). More sophisticated models could include other behaviours such as visco-plasticity, visco-elasticity or hyper-elasticity [1].

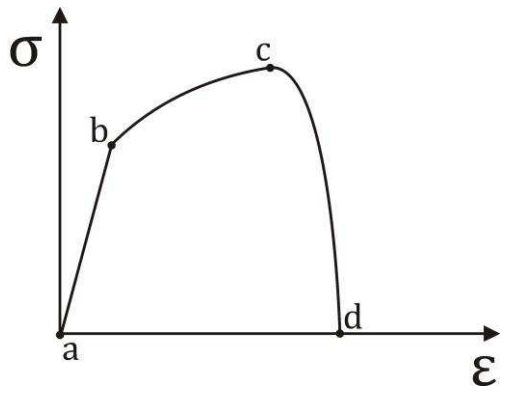

Figure 4.2 – General stress-stain material behaviour of an adhesive

As shown in **Figure 3.2** the structural adhesives under investigation presented a ductile behaviour (considerable plastic deformation prior to failure) with an extensive non-linear behaviour (b-c, in **Figure 4.2**). Taking this into account the present research work modelled the behaviour of the adhesive using an elasto-plastic model (**a-b-c**) coupled with a failure criterion to simulate the failure process (**c-d**) of the material. This combination of models has been proven suitable for characterising the mechanical behaviour of structural adhesive by several authors [65,142,143]

4.2.1. Linear-elastic behaviour

In a linear-elastic model, stress and strain have a linear relationship (Hooke's law). One of the advantages of this model is the opportunity of shorter simulation times as compared to non-

linear models. A considerable number of works have shown the validity of the use of linear-elastic models [7,11] for structural adhesives. To determine the linear-elastic response of adhesives two parameters are necessary: the Young's modulus (E) and the Poisson ratio (v). The Young's modulus is the constant that correlates stress and strain:

$$\sigma = E\varepsilon \tag{4.1}$$

The value of E was obtained from experimental data of un-notched specimens (**Section 5.1**) by performing a linear regression within the linear-elastic range of stress-strain curves. An isotropic behaviour was assumed for the adhesive. In this regard, the Poisson's ratio provides the relation between strains in the longitudinal (or axial) and in transverse directions.

Material properties of the adhesives obtained experimentally (considering nominal values) should be transformed to the so-called *true* stress-strain values. From experimental tests, values are called *engineering* (or nominal) values because they do not consider changes of the initial cross section (A_0) during the tests. The engineering stress (σ_{eng}) and the engineering strain (ε_{eng}) were transformed to true stress (σ_{true}) and true strain (ε_{true}) using the following relationships [65] :

$$\sigma_{true} = \frac{F}{A_{true}} = \frac{F}{\left(\frac{A_0}{\left(1-v\varepsilon_{eng}\right)^2}\right)} \tag{4.2}$$

$$\varepsilon_{true} = \ln(1+\varepsilon_{eng}) \tag{4.3}$$

In the present work the Poisson' ratio was obtained by measuring the strain in two directions with a bi-axial extensometer. Another approach is to obtain this parameter indirectly from shear and tensile tests. In this approach the Poisson's ratio is obtained from the Young's and the shear moduli (G):

$$v = \frac{E}{2G} - 1 \tag{4.4}$$

The liner-elastic material properties (E and v) of both adhesives are described in **Table 4.1**.

4.2.2. Elasto-plastic behaviour

Despite linear-elastic models being widely used in many applications, a non-linear behaviour is often to be expected, for instance, in low cycle fatigue (LCF) under high loads and/or in the presence of stress concentrations. As mentioned in the literature review (**Section 2.3.2**), elasto-plasticity was one of the first approaches to address the non-linear behaviour of adhesives [72]. The consideration of elasto-plastic material can influence calculated results in several ways, *e.g.* stress peak relief as demonstrated by Hua [144].

To implement the elasto-plastic behaviour of an adhesive the following data must be provided to the FEA model [141]:

a) yield criterion: to define the stress above which plastic deformation occurs;
b) hardening rule: to specify the variation of the yield surface with an increasing plastic deformation;
c) plastic flow law: to describe the evolution of plastic strain in terms of stress.

A widely used yield criterion is the von Mises criterion in which the plasticity is considered to be a function just of the deviatoric components of stress (a pure shear process). Therefore, the von Mises criterion assumes that yielding is a process independent of the hydrostatic pressure. The von Mises yield criterion defines a yield surface (f_{VM}) in which the yield stress (σ_Y) is a function of the equivalent von Mises stress (σ_{VM}) according to **Equation (4.5)**:

$$f_{VM} = \sigma_{VM} - \sigma_Y \tag{4.5}$$

Nonetheless, it is well known in literature that the yielding behaviour of polymers exhibits a hydrostatic stress dependence [66,67]. With regards to toughened epoxy adhesives the Drucker-Prager yield criterion is well accepted in the modelling of the hydrostatic stress dependence of yielding [143]. The Drucker-Prager model assumes that the fracture, as a consequence of the hydrostatic stress, is preceded by micro-void nucleation that forms thin fibrils in a phenomenon known as crazing [65]. An evidence of the suitability of the Drucker-Prager model for the adhesives under investigation is shown in **Figure 3.14**. It can be seen that the process of crazing causes stress-whitening around the notch due to the scattering of light at the crazes.

The employed FEA software (Abaqus©) offers three Drucker-Prager criteria: linear, exponential and hyperbolic. The linear Drucker-Prager was successfully applied for the

modelling of adhesives in quasi-static [142,143] and in fatigue conditions [98,104]. The linear Drucker-Prager criterion describes a yield surface (f_{DP}) in which the yield stress is a function of both equivalent von Mises stress (σ_{VM}) and hydrostatic stress (σ_H) as follows:

$$f_{DP} = \sigma_{VM} + \sigma_H \tan(\beta) - \sigma_Y \tag{4.6}$$

Here β is the friction angle, a material property that is a function of the ratio between yielding stress at tension and compression. The friction angle was measured for the RB-T adhesive (**Table 4.1**) in a previous study of our research group [57]. For the PU-T adhesive this information was not available. Since the adhesives have similar tensile strength in tension and the same value of the Poisson`s ratio, it was assumed that the value of β for both adhesives is the same. Since good correlation was obtained for both adhesives (as seen in **Section 5.3**) the assumption seems to be valid.

The influence of hydrostatic stress (σ_H) and equivalent von Mises stress (σ_{VM}) on the yielding surfaces of von Mises (f_{VM}) and linear Drucker-Prager (f_{DP}) criterion is illustrated in **Figure 4.3**.

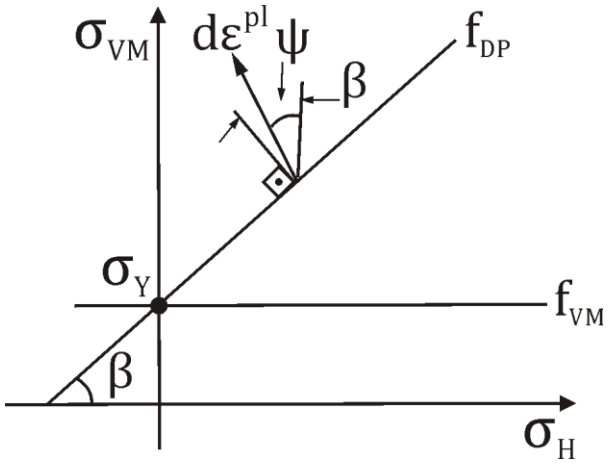

Figure 4.3 – Hydrostatic pressure dependence of yielding surfaces: von Mises criterion (f_{VM}) and linear Drucker-Prager criterion (f_{DP})

Here σ_Y is the yield stress. The dilation angle (ψ) describes the evolution of the plastic strain ($\frac{d\varepsilon^{pl}}{d\sigma}$) according to a plastic flow law. Since the assumption of associated flow was used, the dilation angle (ψ) is equal to the friction angle (β).

To determine the yield stress (σ_Y), true stress-strain curves determined in tensile tests were fitted using a polynomial regression of forth degree. Following this fitting, the yield stress was defined in terms of [145]:

$$\sigma_{true} = \sigma_Y \,,\ when \frac{d^3\sigma_{true}}{d\varepsilon_{true}^3} = 0 \tag{4.7}$$

For glassy polymers, as in the case of the adhesives under investigation, this point of the maximum second derivative is caused by molecular rearrangement and damage at both molecular and macroscopic levels [67]. A hardening rule is necessary to describe the behaviour of the adhesives (**Figure 4.4b**) after the onset of yielding, *i.e.* the plastic strain as function of the true stress:

$$\varepsilon_T^{pl} = f(\sigma_{true}) \tag{4.8}$$

The total true strain (ε_{true}) is constituted by the sum of elastic strains (ε_{true}^{el}), which are fully reversible and plastic strains (ε_{true}^{el}), which are non-reversible:

$$\varepsilon_{true} = \varepsilon_{true}^{pl} + \varepsilon_{true}^{el} \tag{4.9}$$

The plastic true deformation is calculated from experimentally obtained data with the following relation:

$$\varepsilon_{true}^{pl} = \varepsilon_{true} - \frac{\sigma_{true}}{E} \tag{4.10}$$

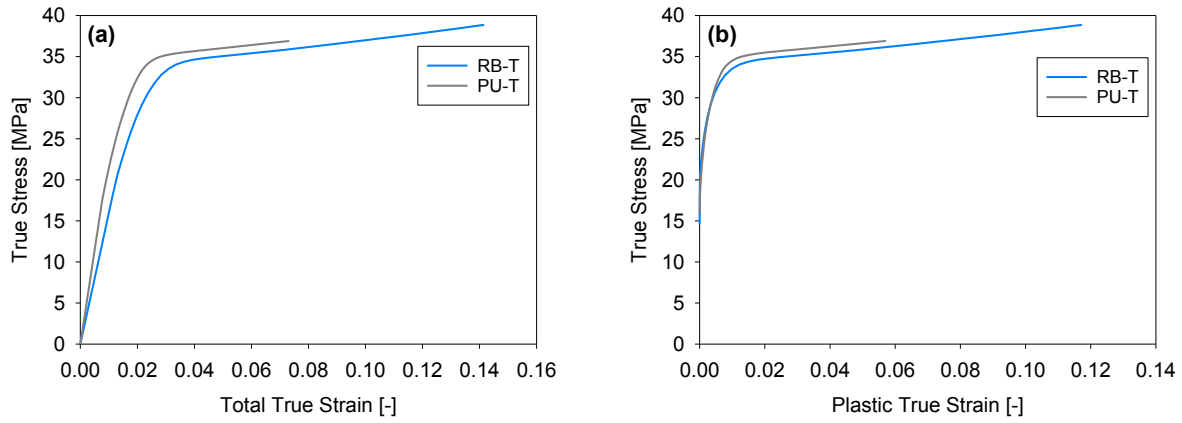

Figure 4.4 – Stress-strain behaviour of the investigated adhesives | (a) true stress-strain curve and (b) plastic hardening curve

The data which were obtained from experiments of the present work are indicated with an [*] sign. The ones obtained from the literature have the respective reference indicated. A summary of the elasto-plastic material properties is given in **Table 4.1**.

Table 4.1 – Elasto-plastic material properties of adhesives for implementation on FEA model

adhesive	***E* [MPa]**	***ν* [-]**	σ_Y **[MPa]**	$\Psi = \beta$ [°]
PU-T	2289 [*]	0.4 [*]	16 [*]	35 [57]
RB-T	1673 [*]	0.4 [*]	15 [*]	35 [57]

4.2.3. Failure criterion

To model the failure of the material under quasi-static loading a failure criterion based on the equivalent plastic strain was implemented in the FEA material model. This approach has the advantage of allowing an implementation of the failure criterion in conjunction with the Drucker-Prager elasto-plastic behaviour. To implement the failure criterion in the FEA model the following data must be provided:

a) initiation criterion: definition of when the damage starts within the material;
b) evolution criterion: definition of the evolution of damage until final failure of the material.

The criterion for the initiation of failure was defined in terms of the maximum value of plastic strain (ε_i^{pl}) obtained from tensile tests (**Figure 4.4)**. After the onset of failure it is still necessary to describe the evolution of the damage until the fully degradation of the material.

In this regard, a full plasticity consideration was used to describe the full degradation of the material. It was assumed that the material fails (under quasi-static conditions) when one of the elements of the used mesh reached full plasticity, *i.e.* the maximum value of plastic strain according to the stress-strain curve was attained. For this reason, it was required to set a characteristic length (L^D) for the elements to be degraded.

This length parameter is associated with the element geometry (*i.e.* mesh size). For the models under investigation the characteristic length was set to 0.1 mm. This value was calibrated based on the guidelines provided by Garcia *et al.* [65] for toughened epoxies. When the maximum equivalent plastic strain (ε_i^{pl}) was reached in an entire element would reach full plasticity, the simulation would be finished. The values of the above mentioned parameters are described in **Table 4.2**.

Table 4.2 – Failure criteria parameters for quasi-static failure of adhesives

adhesive	ε_i^{pl} **[-]**	L^D **[-]**
PU-T	0.1173 [*]	0.1 [*]
RB-T	0.0571 [*]	0.1[*]

The results of quasi-static modelling using the proposed failure criterion are described in **Section 5.3**.

4.3. BOUNDARY CONDITIONS

As described in the **Section 2.3.2**, when using FEA one of the most important steps is the correct definition of boundary conditions. This is due to the fact that the definition of boundary conditions requires a full understanding of the mechanics of the problem.

They should be defined in a way to correctly reproduce the conditions of experimental testing. Furthermore, when possible, they can be used to simplify the analysis, reducing the complexity or the size of the model without losing details and crucial information [23].

The boundary conditions (**Figure 4.5**) were similar for 2D and 3D models. They were set so as to reproduce the experimental conditions of tensile loading. The samples (notched and un-notched) and loading (tension) were symmetric. For this reason, just a quarter of the model was analysed using symmetry criteria. Moreover, it was assumed that elements of the samples which were clamped in the testing machine do not deform (*i.e.* rigid body behaviour).

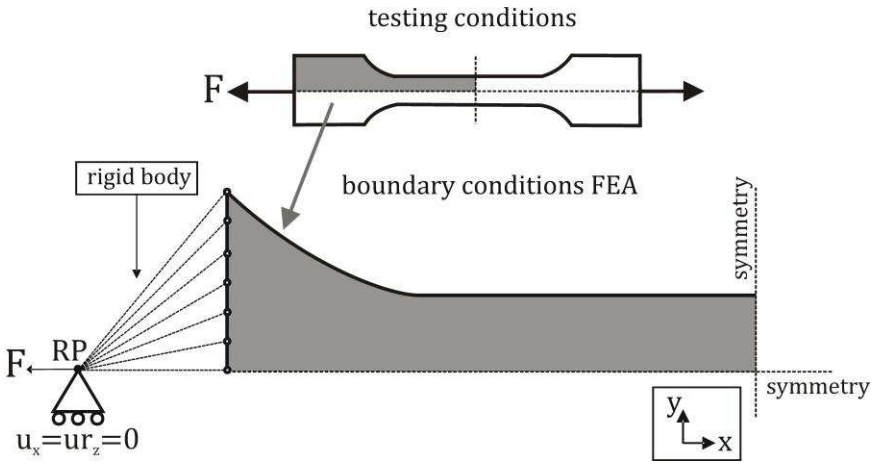

Figure 4.5 – Boundary conditions of FEA models for uniaxial tensile loading

A reference point (*RP*) was created in order to represent the force applied by the testing machine. The *RP* had a constraining with sliding condition, *i.e.* the *RP* could move only in

one direction as in a uniaxial test. Finally, the *RP* was connected to the model using a rigid body constraint.

4.4. MESHING AND ELEMENT CHOICE

The occurrence of stress concentrations requires finer meshing to correctly describe peak stress and stress gradients [23]. However, the size of the mesh should not be so small that the simulation takes too much time. As shown in **Figure 4.6**, an approach to optimise meshing is to divide the mesh in three regions: coarse mesh, transition mesh and fine mesh.

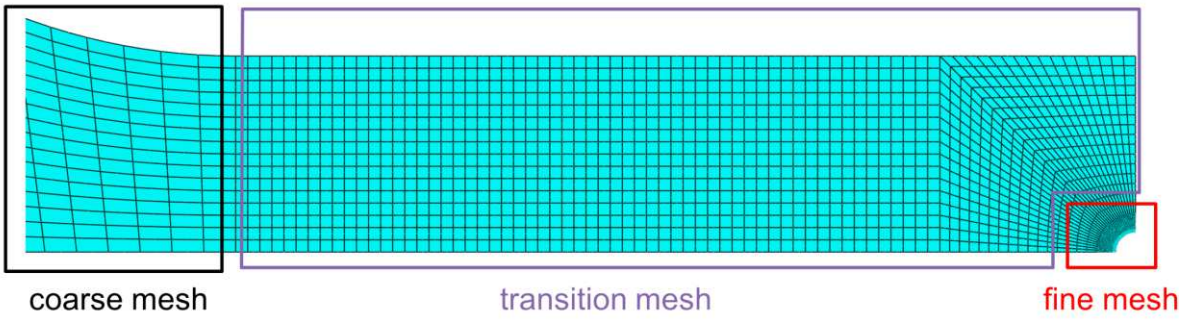

Figure 4.6 – Regions of meshing in an internally notched sample

When the mesh is refined properly, the results should ideally converge to an exact solution. Therefore, care must be taken to ensure that the mesh contains enough elements to provide results of sufficient accuracy whist avoiding an excessive number of elements that will cause large files and long process times [23]. The creation of efficient meshes becomes increasingly important in three-dimensional models and/or in the presence of material non-linearity.

In accordance with the previously mentioned aspects, the meshing of the models was performed based on the following guidelines:

a) three regions of meshing: coarse, transition and fine;
b) mesh refinement close to notch regions;
c) same mesh size for both adhesives;
d) same mesh size for 2D and 3D models (width and length directions) since in the thickness direction the 2D models do not require mesh.

Since values of stress concentrations at the notch root have an analytical solution for the two-dimensional and linear-elastic case [136], the mesh refinement was performed in a FEA 2D-linear elastic model. The definition of mesh size was performed using an iterative process of mesh refinement until the results of FEA matched the analytical values. This procedure

allowed a mesh fine enough to provide accurate results. The same mesh size was used for all models (as stated in the guidelines provided above).

The choice of element type is a key aspect in the implementation of an FEA model. This choice is closely related to the geometry (2D or 3D) in which the FEA model is defined. For instance, a 2D model requires surface elements (*e.g.* plane stress/plane strain) whereas 3D models require solid elements (*e.g.* brick, tetrahedron) [23]. The element order is another relevant aspect in the choice of element type. Linear elements are simpler whilst higher order elements (*e.g* quadratic, cubic) may provide more accuracy at the cost of more computational demand [23]. Bearing this in mind, the chosen types of elements and respective geometries used in the present research are detailed in **Table 4.3.**

Table 4.3 – Element type according to geometry model

model geometry	element type	characteristics
2D-plane stress	CPS8	8-node, biquadratic, reduced integration
2D-plane strain	CPE8	8-node, biquadratic, reduced integration
3D	C3D20R	20-node, quadratic brick, reduced integration

4.5. SUMMARY

In the present research work the numerical investigations were carried out by means of Finite Element Analysis (FEA) using a commercial software (Dassault© Abaqus). FEA is a useful, powerful and precise technique for modelling the mechanical behaviour of structural adhesives providing very detailed analysis of stress under several loading conditions, different geometries and material behaviours. In order to ensure a suitable implementation of an FEA model for the adhesive the following procedures were taken: (i) mechanical characterisation of the adhesive through experimental testing, (ii) calibration of material model parameters, (iii) implementation of FEA models, and (iv) validation of FEA models, including experimental and numerical investigations.

The definition of model geometry (**Section 4.1**) can be performed using 2D or 3D models. A 2D model is less complex to implement and allows faster simulation times. However, some simplifications must be assumed (plane strain or plane stress) which can lead in some cases to non-accurate results. 3D models do not require simplifications. On the other hand, they might require excessive computational time, especially for complex geometries and/or for non-linear material behaviour. In order to define the most suitable geometric model, FEA was performed

both in 2D (plane stress and plane strain) and in 3D and then correlated to experimental results.

The set-up of the material model (**Section 4.2**) is one of the key aspects of FEA. In the present research work the mechanical response of adhesives was defined by an elasto-plastic behaviour combined with a failure criterion. The elastic behaviour of the adhesive was determined by the Young's modulus and the Poisson's ratio. The plastic behaviour was assumed to be hydrostatic stress dependent expressed by a linear Drucker-Prager model. Finally, the failure was defined for the quasi-static case by a criterion based on the equivalent plastic strain (**Section 5.3**).

The boundary conditions (**Section 4.3**) were set to reproduce uniaxial tensile loading. They were defined in order to optimise simulation time by assuming some simplifications without losing accuracy. Since symmetry conditions were assumed, only a quarter of the geometry was modelled. Elements clamped by the machine were considered un-deformable. The force was applied in a reference point connected to the sample using a rigid body conditions.

The meshing of the models (**Section 4.4**) was performed based on the following guidelines: (i) mesh refinement close to notch regions, (ii) same mesh size for both adhesives, (iii) same mesh size for 2D and 3D models. The definition of mesh was performed using an iterative process of mesh refinement by calibrating FEA results with 2D-linear elastic analytical solution of stress. Finally, the element choice was determined as a function of the chosen geometry (2D-plane stress, 2D-plane and 3D) using surface and solid elements with quadratic order.

5. QUASI-STATIC BEHAVIOUR OF STRUCTURAL ADHESIVES

The focus of this chapter lies on the investigations regarding the quasi-static behaviour of structural adhesives under the effect of stress concentration due to the presence of notches.

The first section (**5.1**) presents results of quasi-static tensile testing for un-notched specimens. Tests for un-notched specimens were performed to establish a base for comparison with notched specimens and to provide material input data for FEA models. Two different displacement rates were used for the tests (2 mm/min and 10 mm/min) aiming to evaluate the strain-rate dependence of the mechanical behaviour of the investigated adhesives.

The second section (**5.2**) is related to the results of quasi-static testing of notched specimens (internal and external). The effect of stress concentration was assessed in terms of stress-strain curves, tensile strength, elongation at break, and fracture behaviour. Findings were then correlated to distributions of stress concentration factor and stress triaxiality, and mechanical properties of the adhesives.

The third section (**5.3**) deals with the modelling of the quasi-static behaviour of the adhesives. The aim of this section is twofold: (i) to validate the FEA models by comparing simulation results with experimental data (stress-strain curves), and (ii) to predict the failure stress under quasi-static conditions.

5.1. QUASI-STATIC BEHAVIOUR OF UN-NOTCHED SPECIMENS

The quasi-static characterisation of the adhesives was performed initially on un-notched specimens. Under load the cross-section of these specimens experience a homogeneous state of stress. They were used in order to establish a base for comparison with notched specimens (*i.e.* inhomogeneous state of stress) and obtain input material data for the FEA models.

As shown in **Section 5.2**, it is expected that the presence of notches will cause a local increase of strain rate near the notch [13]. For this reason, quasi-static tensile tests were carried out on un-notched specimens at two different displacement rates (2 mm/min and 10 mm/min) aiming to evaluate the influence of an increasing displacement rate (*i.e.* strain rate) on the tensile behaviour of the adhesives.

The stress-strain curves related to the quasi-static tests are shown in **Figure 5.1** for RB-T and PU-T adhesives. Four tests were performed for each adhesive and displacement rate. The engineering (or nominal) stress was calculated dividing the applied force (given by the testing

machine) by the initial cross-section of the sample. The cross-section was measured before the beginning of the test. The engineering strain was obtained directly from the testing machine using a clip-on extensometer (see **Section 3.3**).

Both adhesives showed similar engineering stress-strain curve behaviour with nearly linear-elastic behaviour for low levels of engineering strain followed by yielding and the beginning of a non-linear behaviour with a considerable amount of plastic deformation at higher stresses. The RB-T adhesive exhibited a more ductile behaviour with larger values of plastic deformation prior to failure. With regards to strain rate sensitivity, the variation of displacement rate had no clear effect on the Young's modulus (*i.e.* tangent of the linear-elastic region).

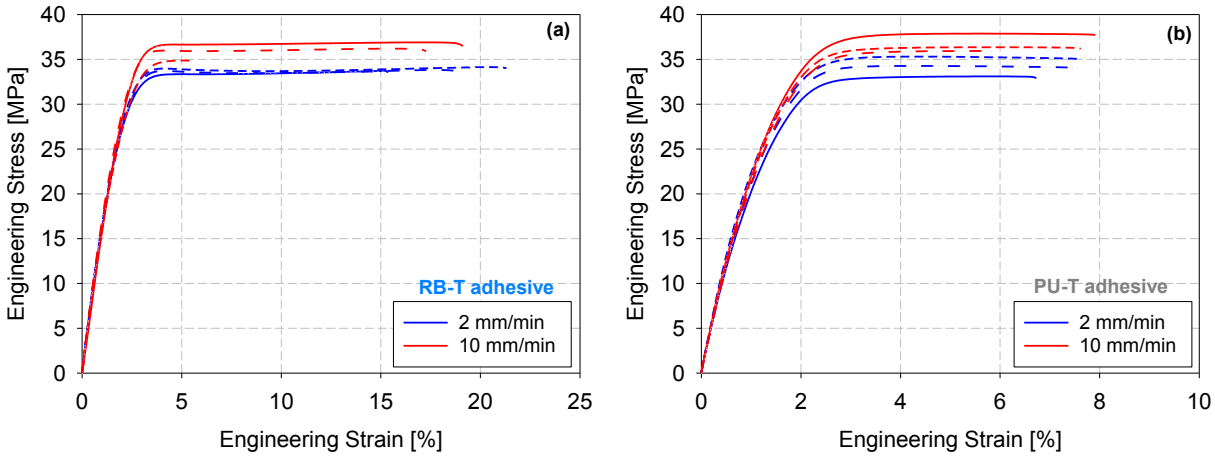

Figure 5.1 – Effect of displacement rate on stress-strain behaviour: RB-T adhesive (left) and PU-T adhesive (right)

The effect of displacement rate on the mean values of tensile strength and strain at break is presented with standard deviation in **Figure 5.2**.

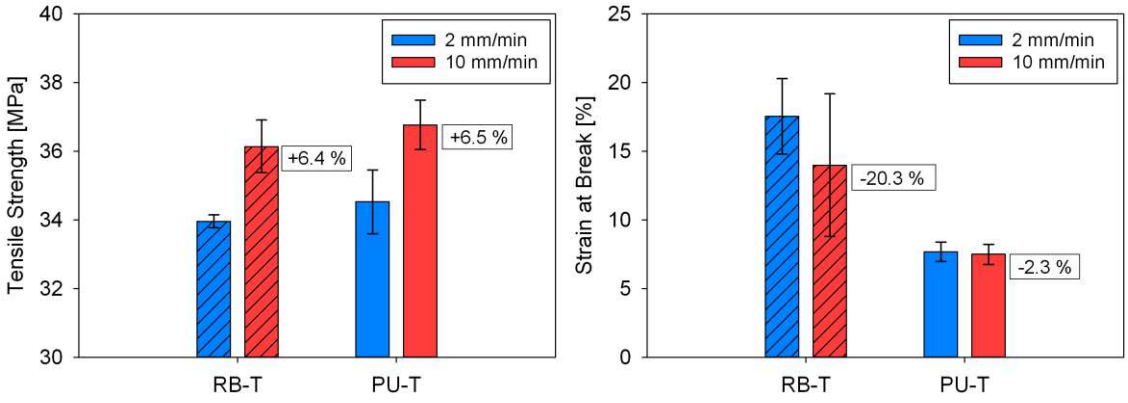

Figure 5.2 – Effect of displacement rate on tensile strength and strain at break

Both adhesives presented an increase of tensile strength (more than 6%) with an increasing strain rate. This strengthening behaviour for higher strain rates is common for adhesives [23]. At the same time, the effect of displacement rate on the elongation at break is not well defined due to the high values of deviation, which make the elongation at break results statistically not distinct.

5.1.1. Fractography – un-notched samples

Representative fractography images of the cross-section of samples were selected to demonstrate the fracture behaviour of the un-notched specimens of both adhesives at different displacement rates. A magnification of 30x was used for the images showed in the present section (**Figures 5.3** and **5.4**).

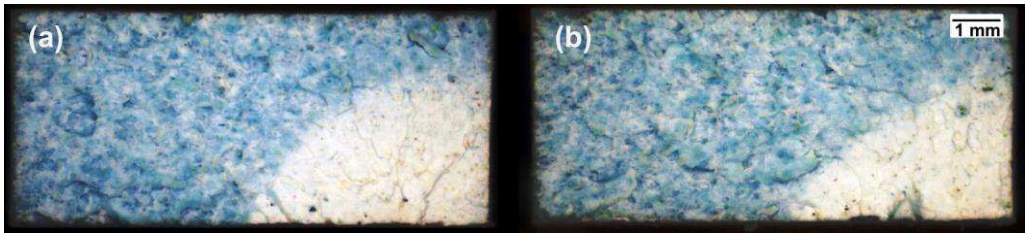

Figure 5.3 – Adhesive RB-T - fracture surface of quasi-static test of un-notched specimen: (a) 2 mm/min, (b) 10 mm/min

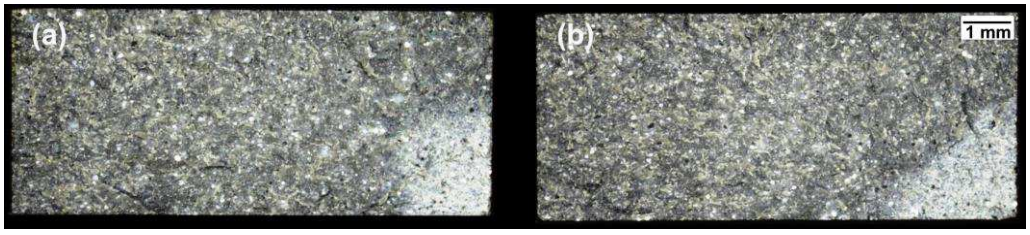

Figure 5.4 – Adhesive PU-T - fracture surface un-notched specimen quasi-static: (a) 2 mm/min, (b) 10 mm/min

Some patterns were common for all images: (i) the crack started on the surface in one of the corners ("corner crack") and (ii) near the region where the crack nucleates a "stress-whitening" region occurs, which is typical for failure of toughened adhesives as cited in detail in **Section 2.1.3**. Furthermore, it is interesting to highlight the differences in the crack propagation pattern of both adhesives with a more "textured" surface for the RB-T adhesive (**Figure 5.3**), whereas for the PU-T (**Figure 5.4**) the failure surface is much more "flat". This is likely related to the ductility (plastic deformation prior to failure) of the adhesives since less ductile polymers are related to more brittle (*i.e.* flat) fracture as it is the case of the PU-T

adhesive [13,23]. On the other hand, when comparing the effect of displacement rate on the fracture pattern of adhesives, none remarkable effect could be observed with regards to size or intensity of the whitening region.

5.2. QUASI-STATIC BEHAVIOUR OF NOTCHED SPECIMENS

Quasi-static tests were carried out on notched specimens in order to assess the influence of stress concentrations on the stress-strain behaviour and on the tensile properties, *e.g.* tensile strength and elongation at break. This influence was then correlated to the mechanical properties of the adhesives.

When dealing with notched samples it is important to define two terms: the net stress and the gross stress. As can be seen in **Figure 5.5,** the gross stress is associated with the entire cross-section of the sample (A^{gr}), *i.e.* width multiplied by thickness. On the other hand, the net stress is related to the net cross-sectional area (A^{net}), *i.e.* disregarding the notch area.

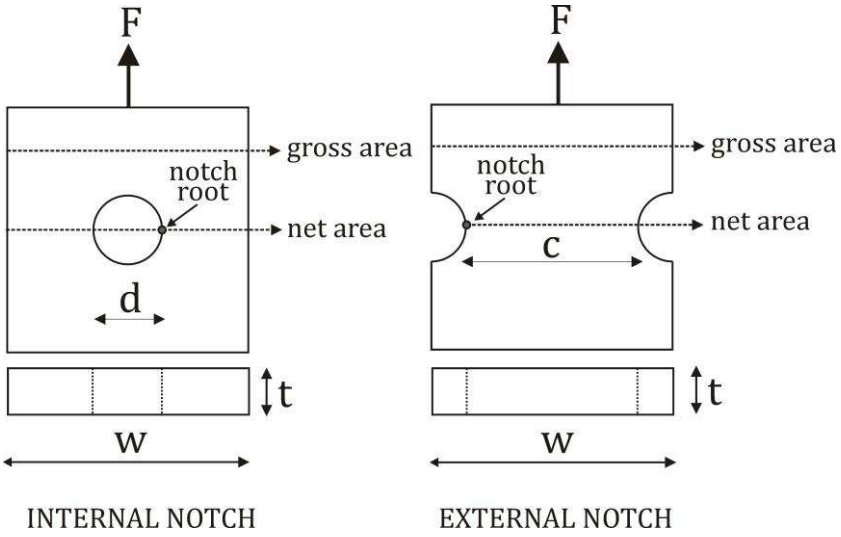

Figure 5.5 – Definition of net and gross stress and position of notch root

The engineering gross stress is calculated from:

$$\sigma_{eng}^{gr} = \frac{F}{A_0^{gr}} = \frac{F}{tw} \tag{5.1}$$

The net stress for an internal notch is obtained from:

$$\sigma_{eng}^{net} = \frac{F}{A_0^{net}} = \frac{F}{t(w-d)} \tag{5.2}$$

While the net stress for an external notch from:

$$\sigma_{eng}^{net} = \frac{F}{A_0^{net}} = \frac{F}{tc} \tag{5.3}$$

Here A_0 is the initial cross-section; the values of *t, c, d* and *w* are defined in **Figure 5.5**.

5.2.1. Tensile behaviour – stress-strain curves

Tensile experiments were performed on notched specimens at a constant displacement rate of 2 mm/min. For each notch size three different tests were conducted. In order to facilitate the understanding of the stress-strain plots, just one sample for each notch type is shown in **Figures 5.6** and **5.7**. A very important property of the adhesive is the stiffness, which depends on the area considered for calculation of stress. Notched specimens had different net areas but the same gross area. Therefore, to ensure comparability of stress-strain curves the engineering gross stress was plotted against the engineering strain.

Representative stress-strain curves of internally and externally notched specimens of the adhesive RB-T are shown in **Figure 5.6** for different sizes of internal (d02, d06, d10, d15 and d20) and external (r03, r05 and r10) notches. One curve of an un-notched sample is also included for comparative reasons. Dashed lines are related to internal notches and full lines are related to external notches.

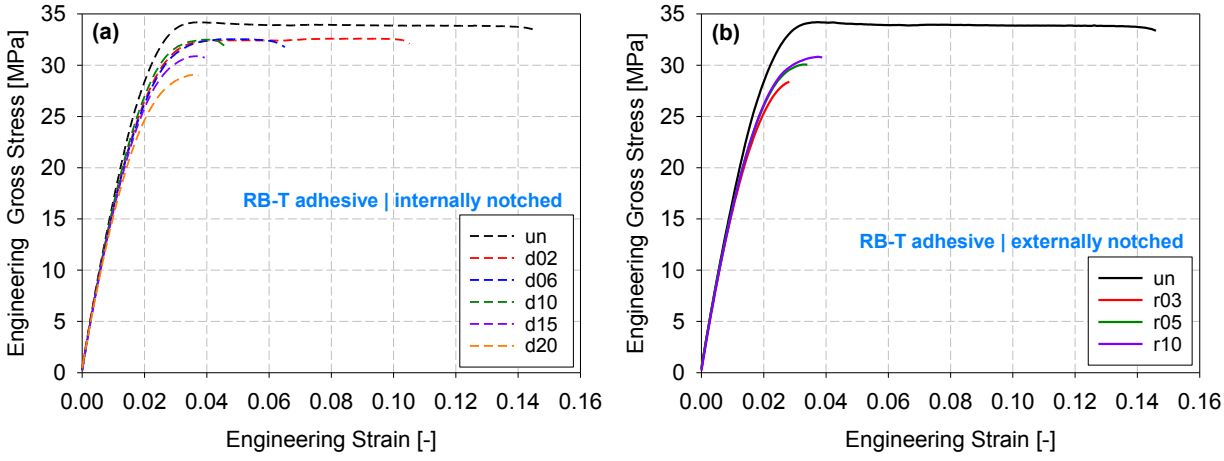

Figure 5.6 – Representative stress-strain curves of notched specimens (Adhesive RB-T): (a) internally notched and (b) externally notched

The samples had similar stiffness within the elastic range, which is an indication of the homogeneity on the production of the samples. Above the stress of about 20 MPa the stiffness

of samples started to change. This could be related to the damage, which is stronger for notched specimens (see **Section 5.2.3**). With regards to the maximum gross stress the unnotched samples had the highest value followed by the d02 sample and decreasing with an increasing notch size for the other samples. Moreover, the reduction in strain at break is substantial for samples with bigger notches.

Typical stress-strain curves for internally and externally notched specimens of the adhesive PU-T are shown in **Figure 5.7**. Samples r03 and r10 had practically the same behaviour. For this reason, their curves overlap in the chart. Some features on the stress-strain behaviour of the PU-T adhesive are similar to the RB-T adhesive, namely the similar stiffness within the elastic range (until approximately 15 MPa), strong reduction of strain at break and higher value of maximum gross stress for the un-notched sample.

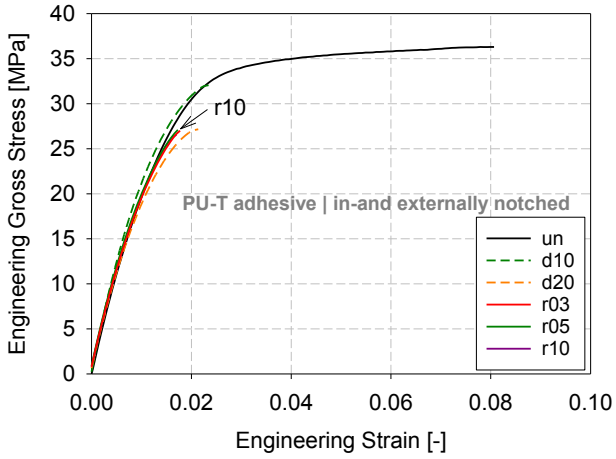

Figure 5.7 – Representative stress-strain curves of notched specimens (Adhesive PU-T)

To further discuss the effect of notches on the tensile behaviour of the adhesives. Mean values and standard deviations of maximum values of net stress and strain break were taken from the three tests of each notch size (internal and external). For the RB-T adhesive, these results are shown in **Figure 5.8** for internally notched samples and in **Figure 5.9** for externally notched ones. It is worth to emphasise that regarding maximum net stress, the values obtained for notched specimens were higher than the ones for un-notched specimens. This means that the RB-T adhesive exhibited notch strengthening, a phenomenon already reported for toughened epoxies in the literature [88]. Moreover, as reported above on the stress-strain curves (**Figure 5.6**), the notched specimens showed a considerable reduction of strain break between 20 and 80% with a reduction on the scatter of the mean values as compared to un-notched samples. This effect of strain at break reduction due to notches was also observed by Takano and Nielsen [14].

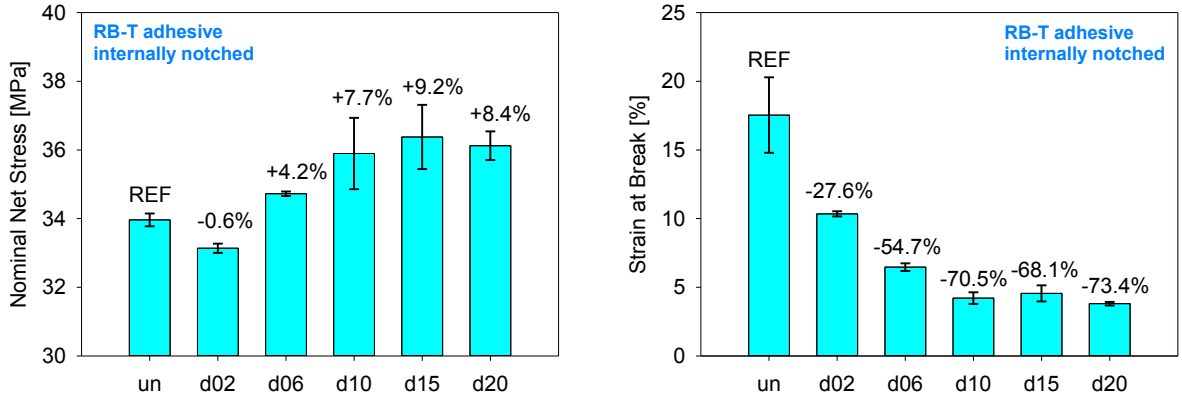

Figure 5.8 – Tensile behaviour | Adhesive RB-T: internally notched

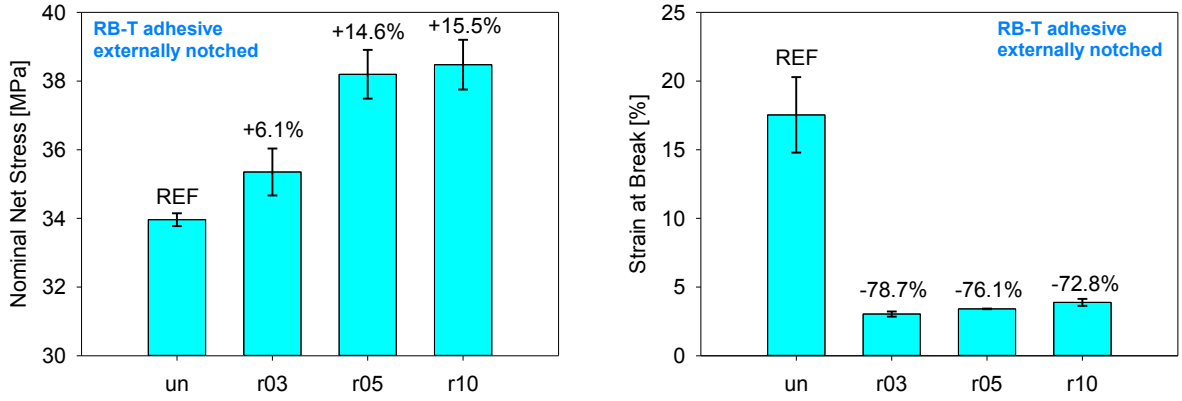

Figure 5.9 – Tensile behaviour | Adhesive RB-T: externally notched

For the internally notched specimens this behaviour (*i.e.* stress strengthening and reduction of strain at break) could be related to the reduction of cross-sectional area caused by the notch [146] as illustrated in **Figure 5.10**. The reduction of strain at break (*SBR*) was defined as:

$$SBR = \frac{\varepsilon_{un}^{break} - \varepsilon_{n}^{break}}{\varepsilon_{un}^{break}} x\ 100 \tag{5.4}$$

Here $\varepsilon_{n}^{\max}$ is the strain at break of the notched specimens, and $\varepsilon_{un}^{\max}$ is the strain at break of the un-notched specimens. The increase of maximum net stress (*IMS*) was defined similarly (difference between notched and un-notched values) but using the maximum net stress as variable:

$$IMS = \frac{\sigma_{\max,n}^{net} - \sigma_{\max,u}^{net}}{\sigma_{\max,u}^{net}} x100 \tag{5.5}$$

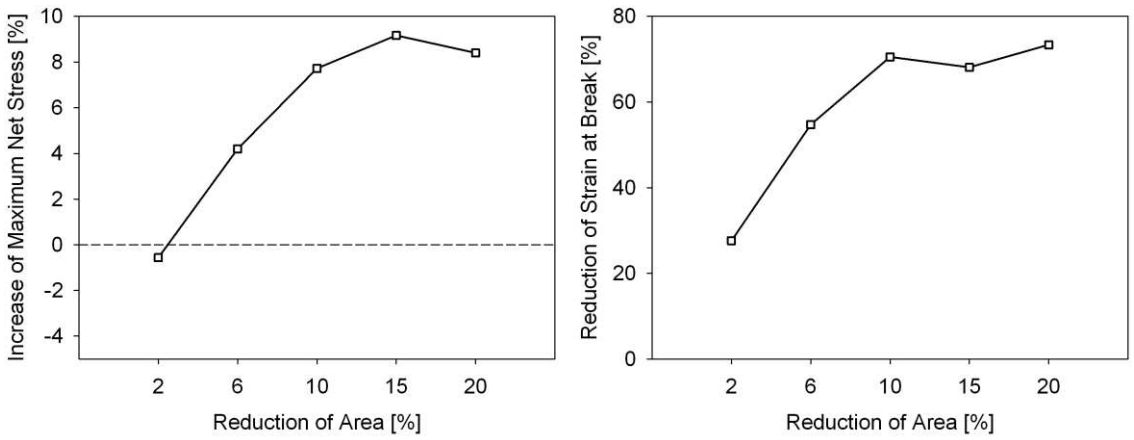

Figure 5.10 - Effect of reduction of area on the tensile behaviour | Adhesive RB-T: internally notched

These results indicate that for the RB-T adhesive the reduction of area due to notches caused an increase of maximum net stress and a reduction of strain at break. This effect occurs even at low values of area reduction, since a reduction of area of only 2% can already cause a reduction of strain at break of more than 20%.

The notched tensile behaviour of the PU-T adhesive can be seen in **Figure 5.11**. Regarding strain at break the PU-T showed the same behaviour as the RB-T adhesive with a strong reduction of strain at break (more than 60%) for the notched specimens with a reduction of scatter of results. Nevertheless, the maximum net stress was reduced for the notched specimens of the PU-T adhesive, which contrasts to the behaviour of the RB-T adhesive. This could be attributed to constraining effects regarding the different ductility of both adhesives. When notched, a more ductile adhesive (*e.g.* RB-T adhesive) is constrained due to plastic deformation under higher stress levels causing notch strengthening (*i.e.* higher maximum net stress for a notched specimen) as explained by Hertzberg *et al.* [52]

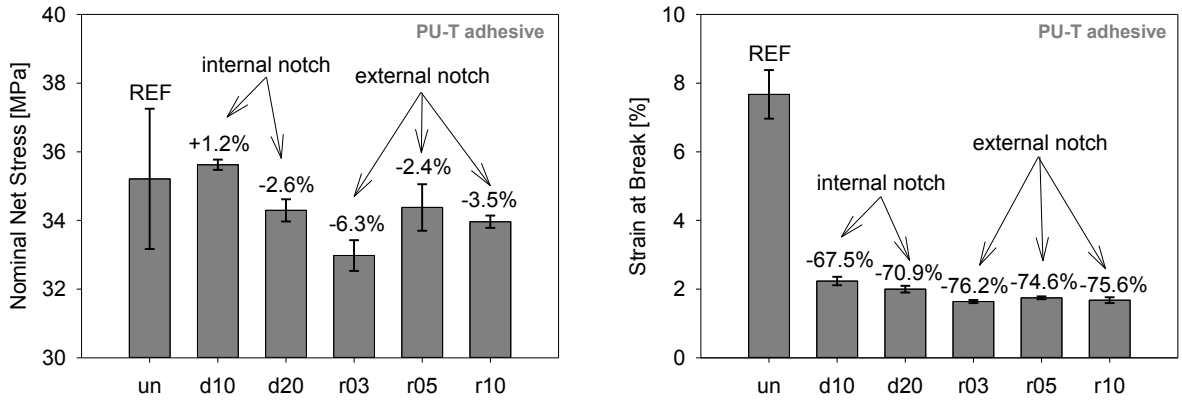

Figure 5.11 – Tensile behaviour | Adhesive PU-T

To correlate previous findings to the mechanical properties of the adhesives the results which were common for both adhesives were plotted together in **Figure 5.12**. By comparing the values of maximum net stress it is possible to observe that for the *un-notched* and the *d10-notch* specimens (small internal notch) the adhesives showed quite similar values. However, with an increasing notch size the maximum net stress difference between un-notched and notched specimens grew to more than 10%: This is an evidence that adhesives react differently according to their ductility and that, under quasi-static conditions, a more ductile adhesive is less notch sensitive than a more brittle one [14,52]. In addition, it is interesting to highlight that RB-T adhesive still remained with higher values of strain at break also when notched.

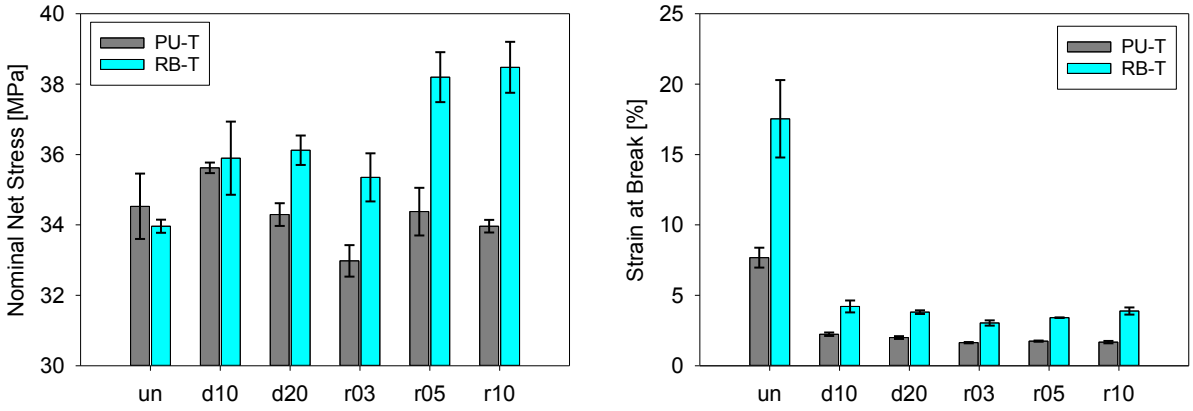

Figure 5.12 – Comparison of tensile behaviour | PU-T vs RB-T adhesives

5.2.2. Monitoring of testing

The monitoring of tests using cameras (**Section 3.4**) provided more evidences of the dissimilar behaviour of the adhesives according to type of notch (*i.e.* stress concentration). As mentioned earlier, the adhesives had different levels of ductility with the RB-T adhesive showing considerably more plastic deformation prior to failure than the PU-T adhesive. These differences were reflected on how the adhesives reacted under an increasing load

In **Figure 5.13**, the images of test monitoring for the RB-T adhesive with internal notches are shown. Starting from an unloaded state (leftmost image) no whitening is observed, by increasing the load the whitening initiates until a crack is formed and the sample fails. This stress-induced whitening is an indication of damage. This phenomenon is called *crazing*, which is associated with regions of stress concentration. It occurs due to the onset of micro-voids followed by the formation of thin fibrils [65].

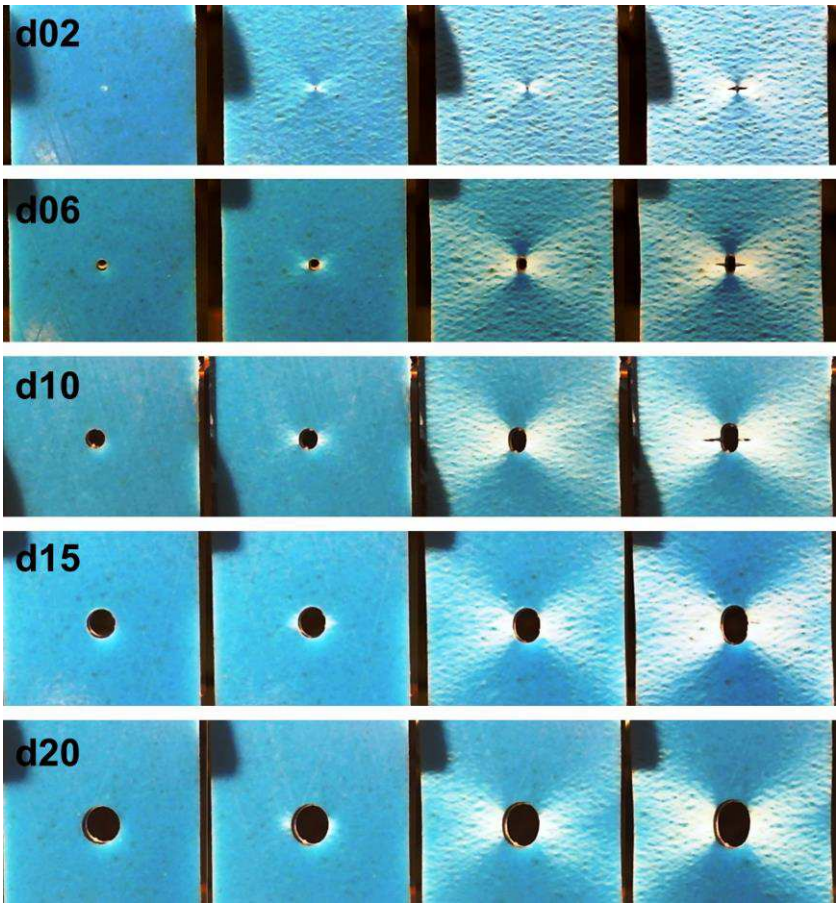

Figure 5.13 – Test monitoring - Quasi-static testing | Adhesive RB-T: internally notched

For very small notches (d02), there is widespread stress whitening in the whole cross-section; with an increase of the notch size (*i.e.* d10) this behaviour becomes more localized. As mentioned in **Section 3.3** the monitoring system for externally notched specimens was different than the internally notched specimens.

The images of test monitoring for the RB-T adhesive with external notches are depicted in **Figure 5.14**. These images revealed the same aspects as observed for the internally notched samples: presence stress-whitening with an increasing load. The differences are related to type of notch with the r10-notch showing more widespread stress whitening than the r05 and then the r03 samples.

On the other hand, the stress-whitening was far less present in the PU-T than in the RB-T samples as shown for the internally notched specimens in **Figure 5.15** and for the externally ones in **Figure 5.16**. Since the PU-T adhesive is significantly less ductile, this pattern could be an indication of the fact that the damage behaviour under increasing load is dependent not only on the type of the notch but also on the mechanical properties of the adhesives.

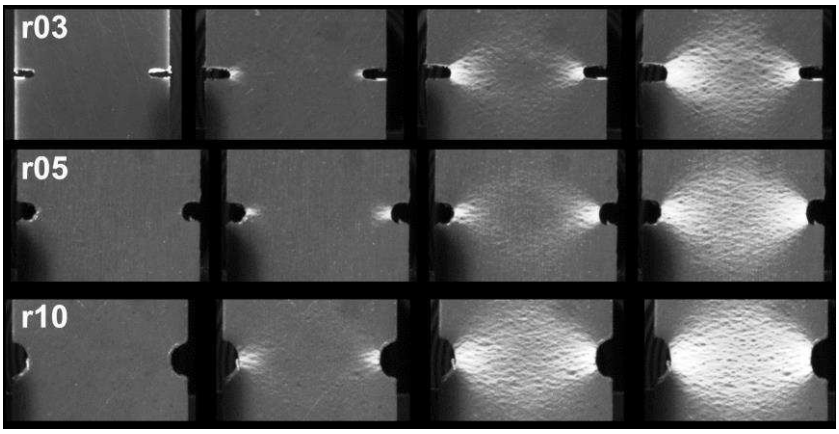

Figure 5.14 – Test monitoring - Quasi-static testing | Adhesive RB-T: externally notched

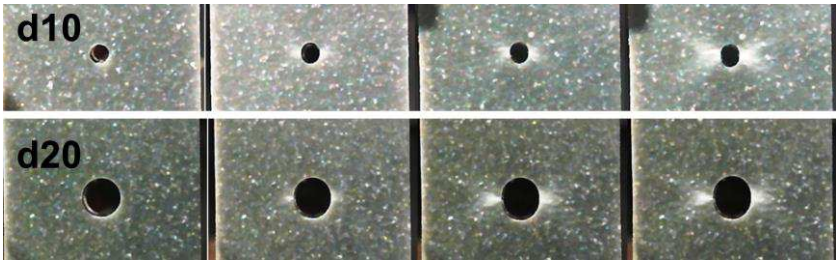

Figure 5.15 – Test monitoring - Quasi-static testing | Adhesive PU-T: internally notched

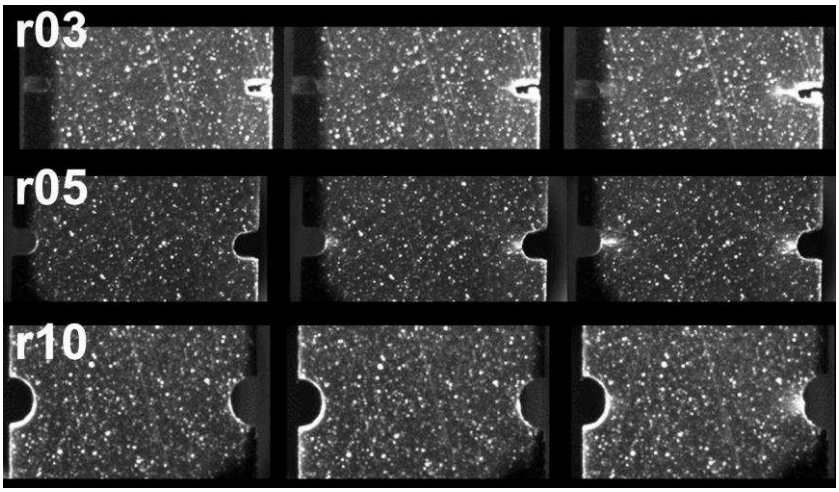

Figure 5.16 – Test monitoring - Quasi-static testing | Adhesive PU-T: externally notched

5.2.3. Fractography – notched specimens

To understand the influence of notches on the fracture mechanisms of adhesives, fracture surface images with a magnification of 30x were taken from the notched specimens. In **Figure 5.17** fracture surfaces of the internally notched specimens of the RB-T adhesive are shown. Red arrows with same size were added to the images to provide a basis for comparison. Stress-whitening is very clear close to the notch root. These white regions were

more textured (rough) in contrast to the blue regions (flatter). Furthermore, the red arrows indicate the fact that the whitening regions have about the same size. This suggests that when a critical damage size is reached the notched samples fail.

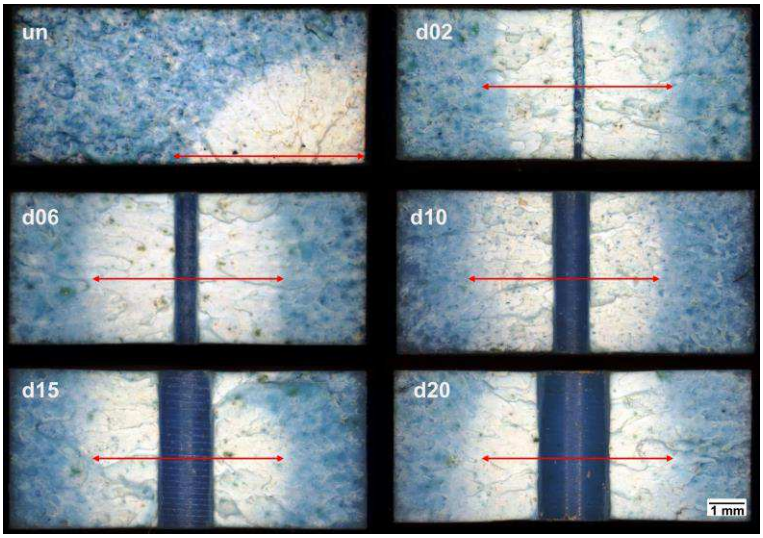

Figure 5.17 - Fracture surface internal notch - Quasi-static testing | RB-T adhesive

By comparing the specimens with internal notches of different adhesives (**Figure 5.18**), the red arrows show that the size of stress whitening region is bigger for the RB-T adhesive (more ductile).

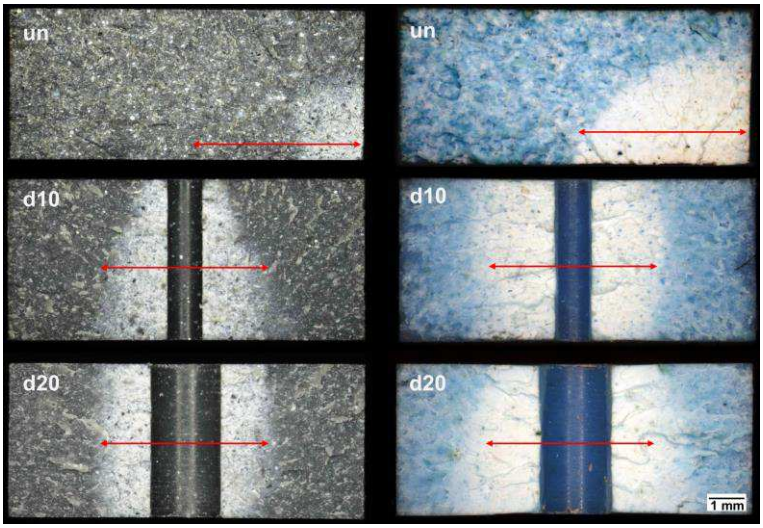

Figure 5.18 – Comparison of fracture surface internal notch | PU-T and RB-T adhesives

To gain insights into the influence of stress concentrations and stress triaxiality in the previously described experimental findings, a 2D-FEA was carried out considering linear-elastic behaviour (as done by Katnam *et al.* [88]) under plane-stress conditions. Linear-elastic properties of the adhesive are described in **Table 4.1**.

The distribution of stress concentration factor ($k_T(x)$) was calculated by dividing the values of the maximum principal stress (σ_{MP}) by the nominal net stress (σ_{eng}^{net})[88]:

$$k_T(x) = \frac{\sigma_{MP}(x)}{\sigma_{eng}^{net}} \tag{5.6}$$

The distribution of the stress triaxiality ($\eta(x)$) was defined by dividing the hydrostatic stress by the von Mises equivalent stress:

$$\eta(x) = \frac{\sigma_H(x)}{\sigma_{VM}(x)} \tag{5.7}$$

The distributions of stress concentration factor and stress triaxiality are shown in **Figure 5.19** (internal notch) and **Figure 5.20** (external notch).

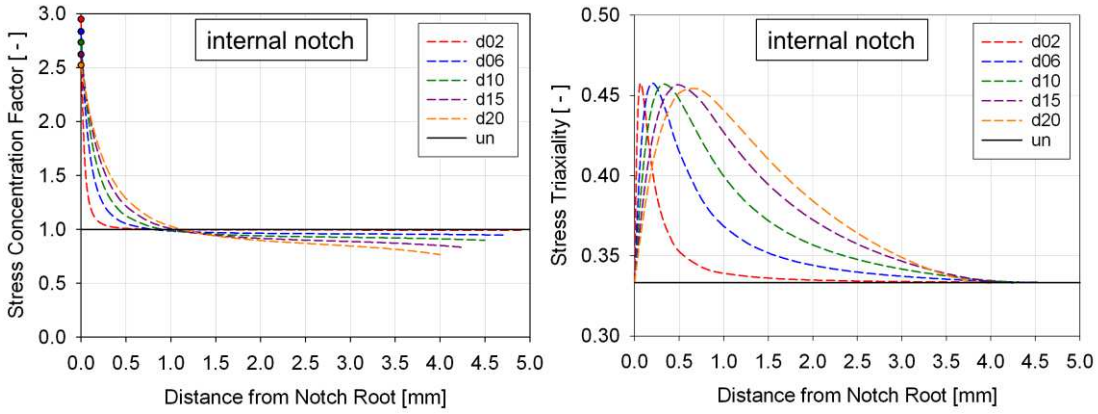

Figure 5.19 – Distributions of stress concentration and stress triaxiality | Internal notch

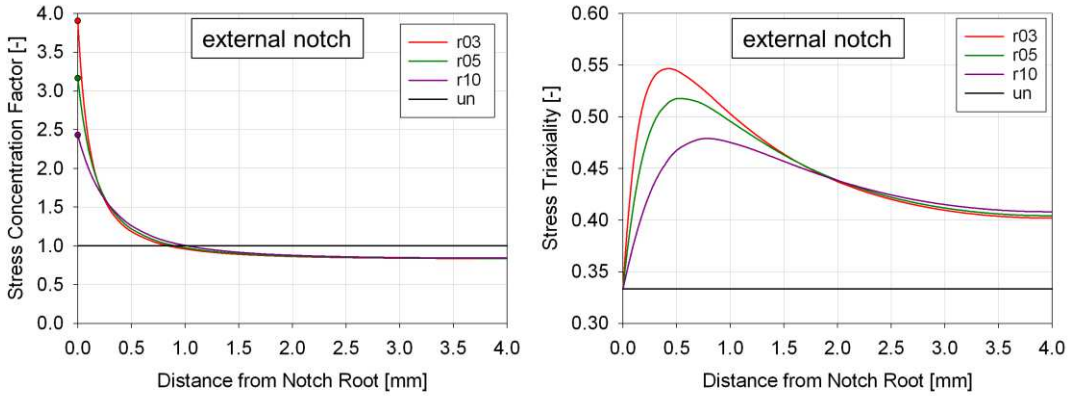

Figure 5.20 – Distributions of stress concentration and stress triaxiality | External notch

These simulation results indicate that the highest values of stress concentration and stress triaxiality occur close to the notch root (less than 1 mm). This region with higher values of

stress concentration and stress triaxiality coincide with stress whitening regions. For internally notched specimens, the maximum value of stress triaxiality is the same but the position of the maximum changes according to the notch size. On the other hand, the values of stress triaxiality are higher for externally notched specimens and change both in maximum value and in location.

For the externally notched specimens (**Figure 5.21**) the same fracture pattern was observed: stress-whitening close to the notch root (region with higher stress concentration and higher stress triaxiality) and larger whitening for the RB-T adhesive. Furthermore, it is possible to observe a flatter surface for the PU-T adhesive.

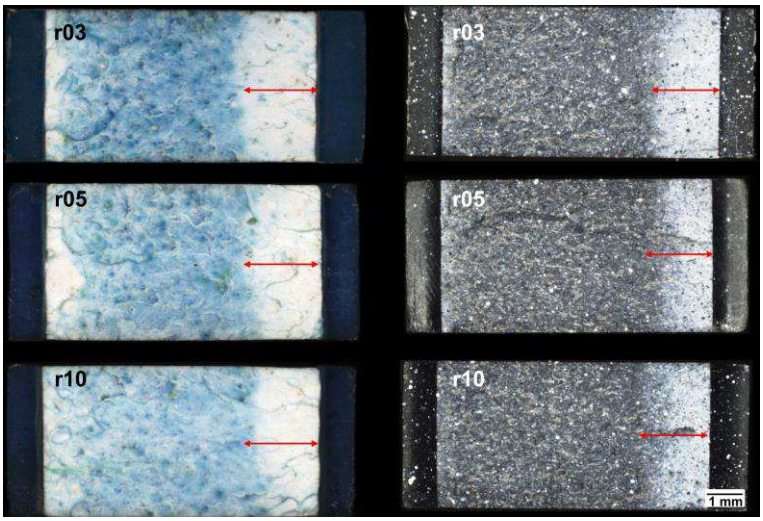

Figure 5.21 – Comparison of fracture surface - external notch | RB-T (left) and PU-T (right)

By zooming in (magnification of 50x) at the stress-whitening region close to the notch, the presence of a flatter surface for the PU-T could be seen even more clearly (**Figure 5.20**).

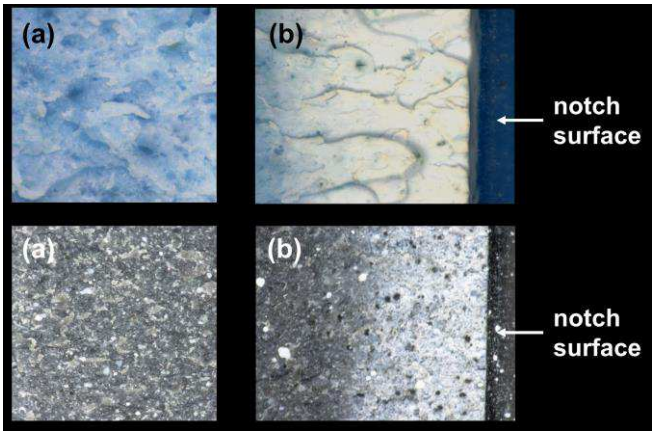

Figure 5.22 – Comparison of fracture surface for an external notch (magnification 50x) | RB-T (top) and PU-T (bottom) – (a) far from notch and (b) close to notch

In this image the existence of dark circular dots is visible within the whitening region. They might be an indication of void coalescence, a typical feature on the fracture of toughened epoxies [15,88]. The voids are more numerous close to the notch root, where the stress triaxiality is higher. This correlation between void formation and stress triaxiality has been extensively reported in the literature by several authors (*e.g.* Lemaitre [147], Morin *et al.* [18] and Katnam et al. [88]).

5.3. MODELLING OF QUASI-STATIC BEHAVIOUR OF STRUCTURAL ADHESIVES

The modelling of quasi-static behaviour was carried out aiming to:

a) validate the assumptions made for the FEA models (**Chapter 4**) by comparing numerical simulations with experimental data (stress-strain curves);
b) predict the value of failure stress of notched specimens under quasi-static conditions .

The aspects to be evaluated with regards to the numerical models were: (i) geometric model (2D-plane stress, 2D-plane strain and 3D), (ii) material model (linear Drucker-Prager), and (iii) failure criterion (equivalent plastic strain).

5.3.1. Set-up of the model

The validations of the modelling of quasi-static behaviour were conducted by comparing numerical simulations with experimental results (engineering stress-strain curves) from tensile testing of un-notched and notched samples.

To ensure that results between simulations and experiments were comparable. A reference point was created in the numerical model at the same position where the extensometer was placed on the experimentally tested specimen. The displacement of this reference point was used to calculate the strain on the numerical model. Finally, the engineering net stress on the numerical models was calculated dividing the applied stress by the initial net area (see **Figure 5.5**). For un-notched specimens, it is possible to calculate the true stress and true strain using **Equations (4.2)** and **(4.3)**.

5.3.2. Comparison of stress-strain curves

Firstly, un-notched specimens were compared. The simulations (3D, 2D-plane stress and 2D-plane strain) and experimental results for both adhesives are shown in **Figure 5.23**. The 3D and the 2D-plane stress simulations presented excellent agreement with experimental results,

whereas the 2D-plane strain results showed high discrepancies (especially in the plastic region). Since the 2D-plane strain model was not able to reproduce the behaviour even for the simplest case of un-notched, the simulations for notched specimens were performed only for the 3D and 2D-plane stress models.

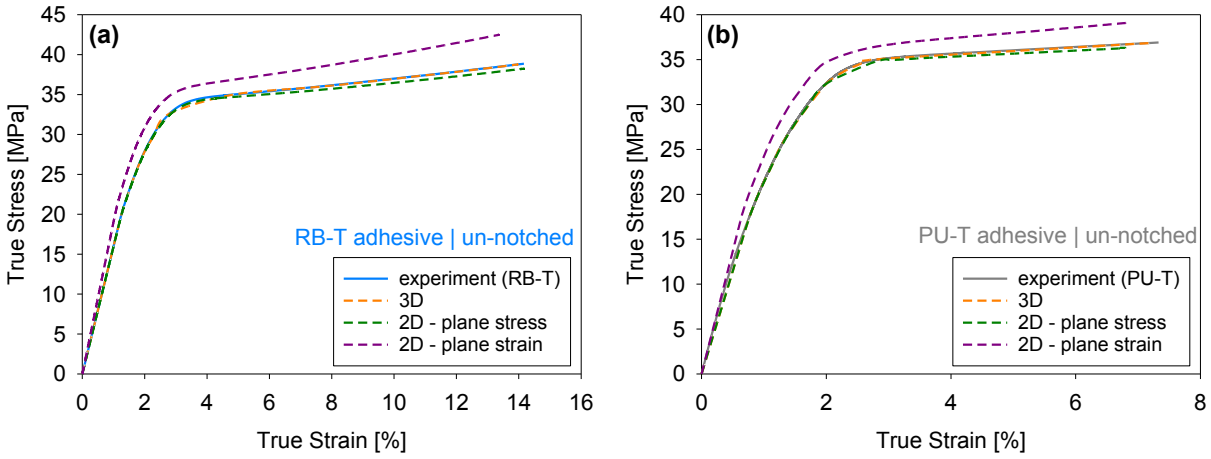

Figure 5.23 – Comparison of stress-strain curves of un-notched specimens | FEA simulation and experiments: (a) RB-T adhesive and (b) PU-T adhesive

For notched specimens, one representative stress-strain curve for each notch type was chosen from experimental results in order to ease visualisation of the different curves. Therefore, it is important to highlight that some differences are to be expected between simulations and experiments due to the scatter associated with the experiments. The results from simulations of internally and externally notched specimens of the RB-T adhesives are shown in **Figure 5.24**.

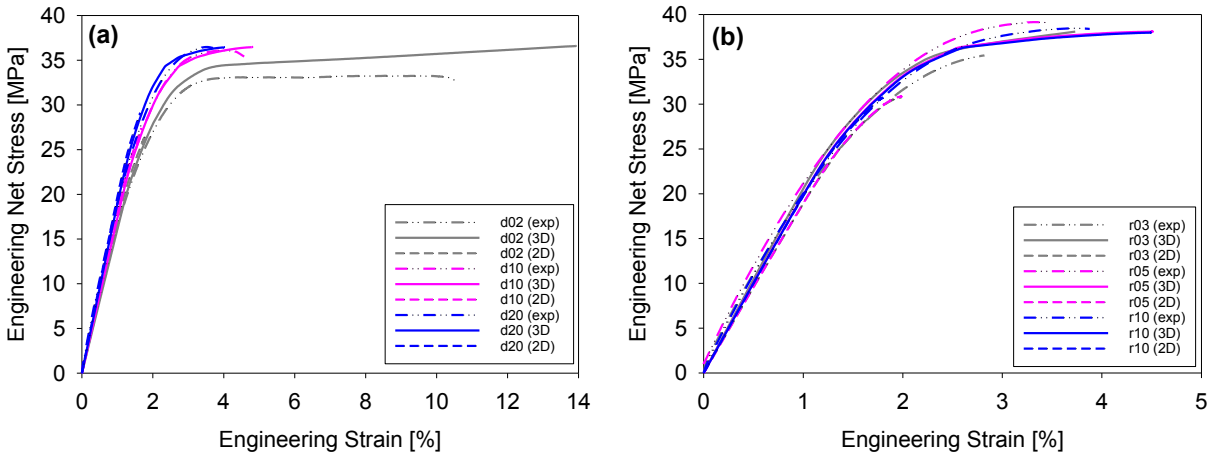

Figure 5.24 – Comparison of stress-strain curves (RB-T adhesive): (a) internal notch and (b) external notch

Regarding internal notches (**Figure 5.24a**) for values under 25 MPa the trend of simulations (2D and 3D) was very similar to the experimental curves. Above this value of stress the curves related to the 2D simulation were prematurely terminated because the failure criterion is reached (see **Section 4.2.3**). This could suggest that the simplifications of plane stress conditions are not necessarily suitable for very high levels of stress (close to the failure stress). In 3D models the agreement was very good up to 30 MPa with an excellent agreement for bigger notches (d10 and d20). For external notches (**Figure 5.24b**) 2D models underestimated the maximum stress. On the other hand, 3D models followed the trend of experimental results even for higher values of stress, but slightly overestimated the maximum stress.

The stress-strain curves of internally and externally notched specimens of the PU-T adhesive are illustrated in **Figure 5.25**. For internally notched samples (**Figure 5.25a**) the agreement was very good for 3D models until approximately 20MPa for the d10 samples and until 30MPa for the d20 samples. The correlation for external notches was very good in the entire range of stresses with a slight overestimation of maximum stress (**Figure 5.25 b**). Regarding 2D models, the same observations could be made for the PU-T adhesive, *i.e.* good agreement up to 25 MPa with premature reaching of failure criteria.

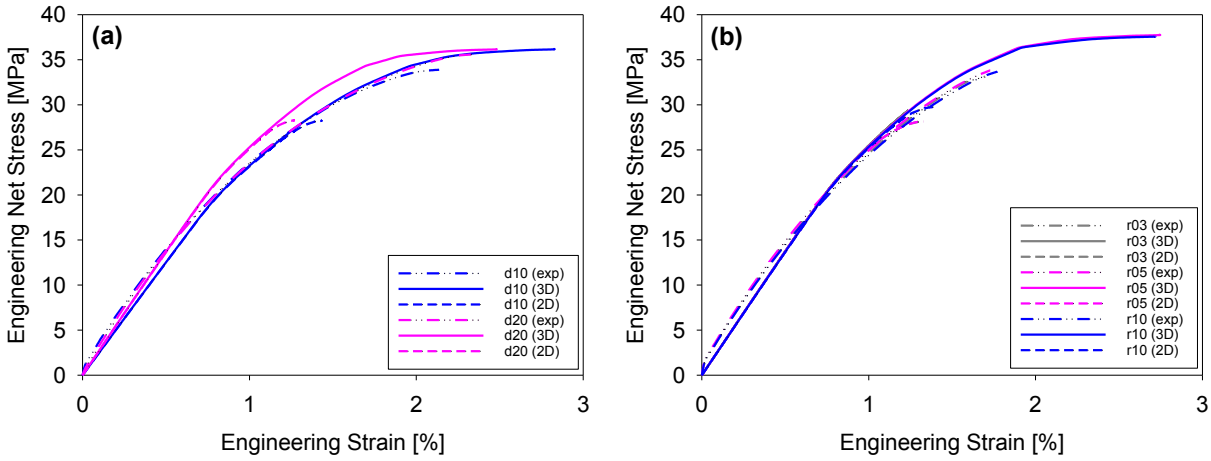

Figure 5.25 – Comparison of stress-curves (PU-T adhesive): (a) internal notch and (b) external notch

The simulation results for both adhesives indicate that the 3D models are suitable for high quality modelling of the quasi-static behaviour of the adhesives including very high levels of stress. On the other hand, stress-strain curves related to 2D-plane stress models displayed premature failure compared to experiments. Nevertheless, 2D-plane stress models showed good agreement for stresses associated with some fatigue conditions (stresses lower than 25

MPa). This suggests that 2D-plane stress models are likely suitable for modelling the fatigue of the adhesives under stresses that not reach values close the quasi-static strength of adhesives.

5.3.3. *Prediction of failure stress*

The prediction of failure stress was performed based on the simulations of stress-strain curves of the adhesives. The predicted failure stress (σ_{fail}^{pred}) was considered to be the maximum value of stress obtained from stress-strain curves. In order to quantify the accuracy of predictions, the predicted values were compared to the measured values taken from experiments (σ_{fail}^{meas}). The relative error (RE_{pred}) was chosen as an indicator of accuracy:

$$RE_{pred} = \frac{(\sigma_{fail}^{pred} - \sigma_{fail}^{meas})}{\sigma_{fail}^{meas}} x100 \tag{5.8}$$

The predictions of failure stress (RB-T adhesive) for both models (3D and 2D), experimental values, and respective relative errors are summarised in **Table 5.1**.

Table 5.1 – Failure stress (RB-T adhesive): measured/predicted values and relative error for 2D-plane stress and 3D models

sample type	σ_{fail}^{meas} **[MPa]**	σ_{fail}^{pred} **(3D) [MPa]**	RE_{pred} **(3D) [%]**	σ_{fail}^{pred} **(2D) [MPa]**	RE_{pred} **(2D) [%]**
un	34.0	36.2	6.6	33.7	-0.7
d02	33.1	36.6	10.5	26.6	-19.8
d10	35.9	36.5	1.7	27.3	-24.0
d20	36.1	36.5	1.0	29.1	-19.4
r03	35.4	38.1	7.8	30.8	-13.0
r05	38.2	38.1	-0.2	30.9	-19.2
r10	38.5	38.0	-1.2	30.7	-20.1
Average error (notched samples)			**3.7**		**19.3**

As previously observed in the stress-strain curves, the 2D model underestimated the values of failure stress of notched samples between 13% and 24%. On the other hand, the predictions with the 3D model showed very good agreement regarding experimental results with an average error of 3.7% and a maximum error of less than 11% for all types of notches.

For the PU-T adhesive, predicted and experimental values of failure stress, as well as relative errors are given in **Table 5.2**.

Table 5.2 – Failure stress (PU-T adhesive): measured/predicted values and relative error for 2D-plane stress and 3D models

sample type	σ_{fail}^{meas} **[MPa]**	σ_{fail}^{pred} **(3D) [MPa]**	RE_{pred} **(3D) [%]**	σ_{fail}^{pred} **(2D) [MPa]**	RE_{pred} **(2D) [%]**
un	35.2	36.8	4.6	34.3	-2.5
d10	35.6	36.2	1.6	28.3	-20.7
d20	34.3	36.2	5.5	28.3	-17.4
r03	33.0	29.4	-10.8	27.4	-16.9
r05	34.4	37.8	9.9	28.2	-18.1
r10	34.0	37.6	10.7	29.8	-12.4
Average error (notched samples)			**7.7**		**17.1**

With respect to accuracy of predictions, the same trend is observed for the PU-T adhesive: (i) underestimation of failure stress of notched specimens for 2D models (between 12.4 and 20.7%), and (ii) very good accuracy for the 3D model (average of error 7.7% and maximum error of 10.8%). By considering 3D models of the notched specimens for both adhesives combined, the overall average error was of 5.5%.

Regarding the accuracy of predictions, no other work dealing with failure stress prediction of notched bulk adhesive specimens has been found in the literature. However, for the sake of comparison the average error related to the failure stress prediction of notched specimens of some other engineering materials are listed below:

- Taylor *et al.* [148] obtained an average error of 11.3% and a maximum error of 19% in the prediction of failure stress for notched specimens of PMMA with stress concentration factor of samples varying between 2.1 and 14;
- Gomez *et al.* [149] used the local strain energy to assess the static strength of U-notched specimens of PMMA with an error of less than 13% for most of the cases;
- Susmel and Taylor [150] obtained an average error of less than 15% in the prediction of the failure stress of low carbon steel. The notched specimens showed large plastic deformation at the notch root (similar to the adhesives under investigation).

Compared to these results from the literature (for other materials), the values of overall average error of 5.5% (with 3D models) for both adhesives obtained in the present research work are very promising. This value of accuracy suggests the suitability of the proposed failure criterion (equivalent plastic strain) to predict the failure stress of notched specimens of the adhesives under investigation.

5.4. SUMMARY

Under working conditions structural adhesives are often subjected to high levels of stress, which makes the understanding of the quasi-static behaviour a key aspect on the technological application of this type of engineering material. In this scenario the present chapter is focused on the investigation of the quasi-static behaviour of structural adhesives under the effect of stress concentration due to the presence of notches.

Experiments were performed with un-notched specimens (**Section 5.1**) to establish a base for comparison with notched specimens and to provide material input data for FEA models. Two different displacement rates were used for the tests (2 mm/min and 10 mm/min) aiming to evaluate whether mechanical properties of adhesives were sensitive to displacement rate variation. The adhesives under investigation showed strain rate sensitivity with an increase on tensile strength around 6% for a higher strain rate. However, no clear effect of displacement rate was observed on the fracture surface. Moreover, adhesives presented great differences with regards to plastic deformation prior to failure. This is reflected on the strain at break with RB-T (~15%) and PU-T (~8%).

Experiments on internally and externally notched specimens (**Section 5.2**) revealed that the tensile behaviour of the adhesives changed due to the presence of notches. A strong reduction of elongation at break was observed for both adhesives. Regarding maximum net stress one adhesive has shown notch strengthening (RB-T) and the other notch weakening (PU-T). This distinct behaviour could be associated to the so-called *constraining effect* that occurs under higher levels of stress and plastic deformation, which is more present in more ductile materials (*e.g.* RB-T adhesive).

This difference in behaviour was also observed in the images from monitoring of the tests that revealed that the RB-T adhesive underwent widespread stress whitening (crazing) prior to failure, whereas in the PU-T adhesive this whitening was far more localised. Fracture surface analysis demonstrated the presence of highly damaged regions with voids close to the notch regions. These regions of whitening were larger for the RB-T adhesive as compared to the

PU-T adhesive. These findings were correlated to 2D-linear elastic FEA calculations that indicated that the stress whitening (*i.e.* high damage) and voids occur within regions with higher values of stress concentration and stress triaxiality.

The numerical modelling of the quasi-static behaviour (**Section 5.3**) of the adhesives aimed to validate FEA models and predict the failure stress under quasi-static conditions. The validation was done by comparing experimental stress-strain curves with curves generated from simulations. Regarding un-notched samples 2D-plane stress and 3D models showed excellent agreement with experimental results in the entire stress range. For internally and externally notched specimens simulation results for both adhesives indicate that the 3D models are suitable for modelling the quasi-static behaviour of the adhesives including very high levels of stress. On the other hand, stress-strain curves related to 2D-plane stress models displayed slightly premature failure with regards to experiments. Nevertheless, 2D-plane stress models are still suitable for modelling the fatigue of the adhesives under stresses that not reach values close the quasi-static strength of adhesives.

The predictions considering 2D-plane stress models underestimated the values of failure stress between 13% and 25%. At the same time, predictions with 3D models showed excellent agreement regarding experimental results with an overall average error of 5.5% for all notch types of both adhesives. The accuracy level obtained in the present research work compared to the accuracy of other works in the literature (for other notched materials) indicate the suitability of the proposed failure criterion (equivalent plastic strain) in predicting the failure stress of notched specimens of the adhesives under investigation.

6. FATIGUE BEHAVIOUR OF STRUCTURAL ADHESIVES

This chapter is concerned with the understanding of the fatigue behaviour of adhesives under the effect of stress concentrations caused by notches. Un-notched, internally notched, and externally notched specimens were tested under cyclic tension-tension load with constant amplitude and a stress ratio of R = 0.1. Experimental results were analysed in terms of SN curves (total lifetime and crack initiation phase), damage evolution curves (*i.e.* stiffness degradation), and fractography. Findings were correlated to numerical simulations of stress concentration factor and stress triaxiality.

Section 6.1 is focused on the fatigue behaviour of un-notched specimens. This investigation was performed aiming to establish a base for comparison with notched specimens and to understand the influence of mechanical properties on the fatigue strength of adhesives. **Section 6.2** deals with the fatigue behaviour of internally notched specimens. This type of specimens had different (**Table 3.3**): (i) cross-section areas and (ii) stress concentration factors. The analysis was focused on the effect of these different aspects, and on the determination of which effect is dominant on fatigue strength, damage evolution and/or fracture behaviour of samples. **Section 6.3** the effect of external notches on the fatigue behaviour of structural adhesives is described. Since samples had the same cross-section (**Table 3.4**), it was possible to assess the isolated effect of stress concentrations on the fatigue strength, crack initiation lifetime, damage behaviour, and fracture pattern of specimens.

The findings obtained in the present chapter will be used to set-up modelling approaches used for the prediction of fatigue lifetime in **Chapter 7**.

6.1. FATIGUE BEHAVIOUR OF UN-NOTCHED SPECIMENS

The experiments with un-notched specimens were aimed to:

a) establish a base for comparison with notched specimens;
b) understand the influence of mechanical properties on the fatigue strength of adhesives;

6.1.1. SN curve (un-notched specimens)

The experimental fatigue data points were fitted using the Basquin's law:

$$\log \sigma_{a,nom} = \log S_0 - \frac{1}{B} \log N_f \tag{6.1}$$

Where $\sigma_{a,nom}$ is the nominal stress amplitude and N_f is the number of cycles to failure. The SN curves of both structural adhesives are shown in **Figure 6.1** with a 95% confidence interval (dashed lines) and a 50% probability of failure (solid lines).

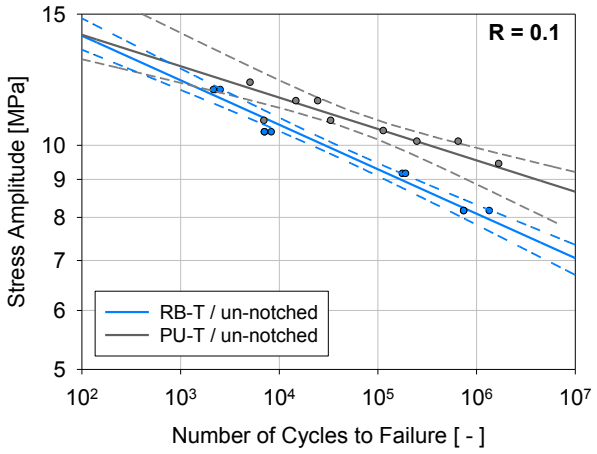

Figure 6.1 – SN curves (un-notched): RB-T (blue) and PU-T (gray)

The parameters of the SN curves are given in **Table 6.1**, where *n* is number of tested samples, *FSL* is the fatigue strength loss, *B* is the inverse negative slope of the SN curve, S_0 is the y-intercept of the SN curves and *rsq* is the r-squared of the linear regressions.

Table 6.1 – Parameters of SN curves (un-notched) | RB-T and PU-T adhesives

adhesive	***n* [-]**	***FSL* [%]**	***B* [-]**	**S_0 [MPa]**	***rsq* [-]**
RB-T	11.0	12.9	16.7	18.5	0.97
PU-T	9.0	10.5	20.7	17.9	0.84

The values of *rsq* (higher than 0.8) indicate a good correlation of the fitting using the Basquin's law with experimental data. The fatigue strength loss is an indicator of the severity of the process of fatigue [50]. It defines the percentage of fatigue strength decay per decade of cycles (a factor of 10 in the lifetime). Based on these results, it is possible to assume that the process of fatigue for the RB-T adhesive is slightly more severe. In the next sections it will be evaluated whether this behaviour is extended to the case of notched specimens.

When comparing both adhesives, the PU-T adhesive presents higher fatigue strength in the whole fatigue range. In **Table 6.2** the relation between fatigue strength and ultimate quasi-static tensile strength (σ_{UTS}) of adhesives is presented. These results suggest that for low cycle fatigue (N_f= 10^3), where stresses are higher, the fatigue strength for both adhesives was nearly the same percentage of the ultimate tensile strength (~80%). By moving towards high cycle

fatigue ($N_f = 10^6$), where stresses are lower, the percentage of fatigue strength with regards to ultimate strength changes to 50% (RB-T) and 56.6% (PU-T).

Table 6.2 – Relation between fatigue strength and ultimate tensile strength for fatigue lifetimes of 10^3 and 10^6

adhesive	σ_{UTS} [MPa]	σ_{max} @10^3 [MPa]	σ_{max} / σ_{UTS} @10^3 [%]	σ_a @10^6 [MPa]	σ_{max} / σ_{UTS} @10^6 [%]
RB-T	34.0	27.1	80.0	18.0	50.0
PU-T	35.2	28.7	81.1	20.4	56.0

6.1.2. Damage evolution (stiffness degradation)

The cyclic loading caused continuous damage to the specimena throughout the duration of tests. This damage due to fatigue was defined in terms of the degradation of stiffness as described in **Section 3.5**. The damage evolution curves for both adhesives are shown in **Figure 6.2**. The values of nominal stress amplitude related to each curve are listed in the upper left side of charts. Curves with the same colour were tested at the same level of nominal stress amplitude.

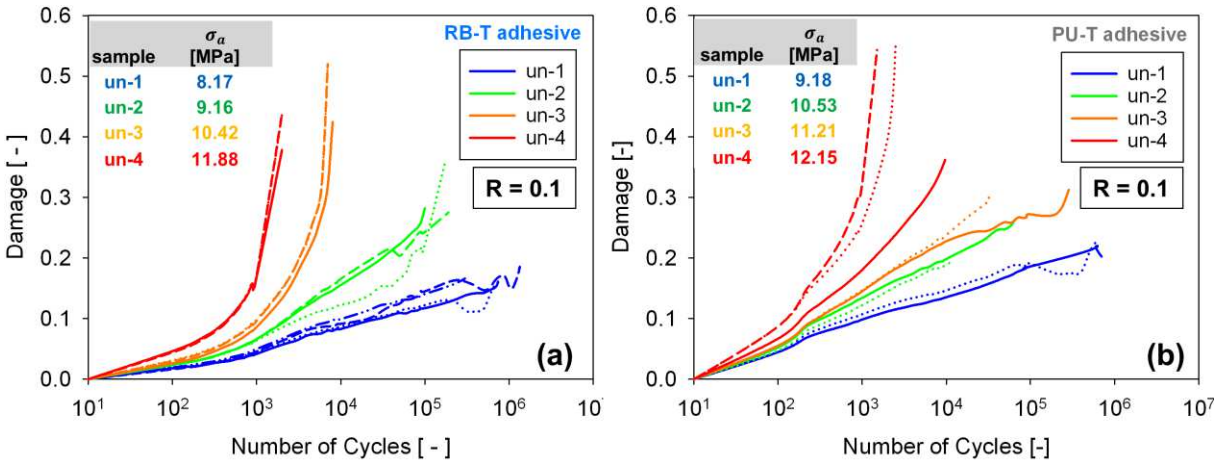

Figure 6.2 – Fatigue damage curves (un-notched): (a) RB-T and (b) PU-T

Higher values of stress amplitude caused faster damage evolution for both adhesives. This was reflected on the number of cycles to failure which were lower for higher stress amplitude levels [19,110,112]. Furthermore, the maximum amount of bearable damage prior to failure was higher with an increase of stress amplitude. Nevertheless, the maximum damage has not surpassed 0.6 in none of the cases.

6.1.3. Fractography (un-notched specimens)

Representative fracture surface images of both adhesives are shown in **Figure 6.3**. The images were selected for samples at the low cycle fatigue (LCF, high stress) range and the high cycle fatigue range (HCF, low stress). In these images it is possible to observe the presence of stress whitening (an indicator of damage processes) and dark spots (voids) at the regions where the crack started (corners) in a similar behaviour observed for quasi-static tests (**Section 5.1.1**).

Regarding the differences between adhesives, the fatigue fracture surface revealed that the RB-T adhesive (more ductile, blue colour) had larger regions of stress whitening as compared to PU-T adhesive [13,23]. This trend was also observed for quasi-static conditions (**Section 5.1.1**).

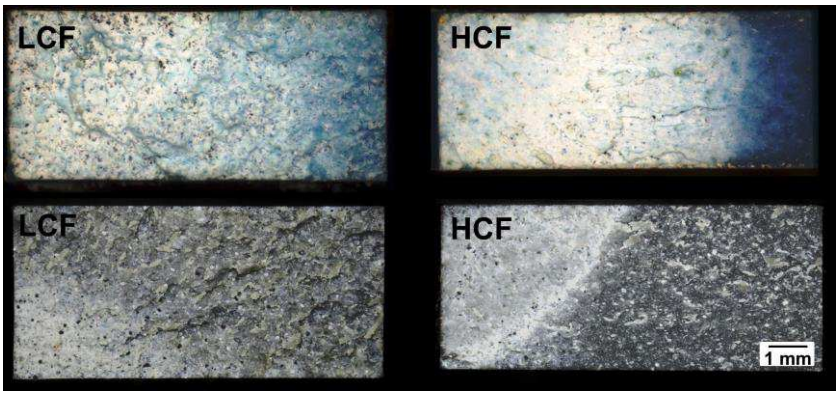

Figure 6.3 – Fatigue fracture surfaces: (a) RB-T (LCF), (b) RB-T (HCF), (c) PU-T (LCF) and (d) PU-T (HCF)

The effect of the stress amplitude level (LCF x HCF) can be noticed on the topography of the samples [112,125]. For high levels of stress (LCF, left side) the fracture images showed a more "rough" surface. On the other hand, for low levels of stress (HCF, right side) the fracture surfaces were more "flat", especially for the PU-T adhesive which is more brittle. This fracture behaviour suggests that the process of fatigue is affected by mechanical properties (ductility and brittleness) and by the level of applied stress.

6.2. FATIGUE BEHAVIOUR - INTERNAL NOTCHES

As mentioned in the beginning of the present chapter, internally notched specimens had different: (i) cross-section areas and (ii) stress concentrations factors. In this regard, the aim of the investigation with internally notched specimens was to evaluate how these aspects would

affect the fatigue behaviour of structural adhesives and to determine which factor (cross-section area or stress concentration factor) would have the prevailing effect on the fatigue response of the adhesives.

6.2.1. SN curve (internally notched specimens)

The SN curves related to the fatigue experiments with internally notched specimens of the RB-T adhesive are shown **Figure 6.4** with a 95% confidence interval (dashed line) and a 50% probability of failure (solid line). The values of stress amplitude are related to the net area of samples (excluding the notch area, see **Section 5.2**). For comparative reasons, the SN curve related to the un-notched tests was included in the chart.

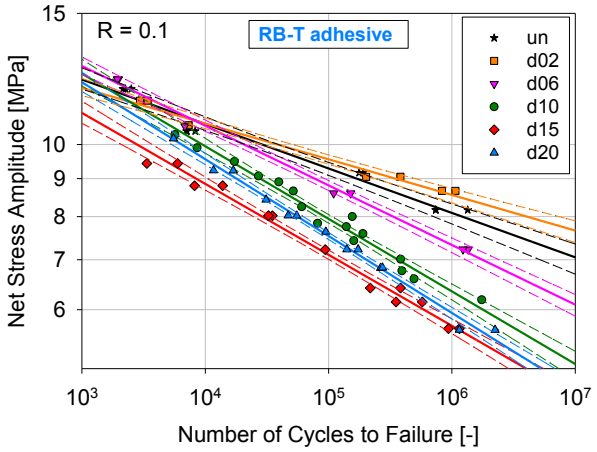

Figure 6.4 – SN curve (RB-T adhesive) | Internal Notch

These results evidence the effect of notches on the reduction of the strength of the RB-T adhesive since notched specimens exhibited lower fatigue strength in the entire fatigue lifetime range as compared to un-notched (black curve) ones. This indicates that under fatigue loading the RB-T adhesive is weakened by notches. Moreover, the reduction of fatigue performance has stronger effects at the high cycle fatigue range. This behaviour has been seen in other polymers as mentioned in the introduction [91,99]. The only exception to this behaviour was shown by the d02-sample, whose fatigue strength was similar to that of un-notched samples. It is likely that the size of highly stressed region was not large enough to cause a substantial change of the fatigue strength [99].

In **Table 6.3**, k_T is the stress concentration factor, n is the number of tested samples, *FSL* is the fatigue strength loss, and B and S_0 are Basquin's parameters. The parameters of the SN curves indicate a good correlation of linear regressions ($rsq > 0.95$). The slope of the SN curve (B) is clearly affected by the size of the notch. Moreover, it is possible to assume that an

increasing notch size (higher stressed region) cause a more severe process of fatigue [91,99]. This is evidenced by higher values of the fatigue strength loss (*FSL*) for bigger notches (*e.g.* d06, d10, d15 and d20).

Table 6.3 – Parameters of SN curves | RB-T adhesive (internally notched)

sample	k_T [-]	*n* [-]	*FSL* [%]	*B* [-]	S_0 [MPa]	*rsq* [-]
un	1.00	11.0	12.8	16.7	18.5	0.97
d02	2.92	8.0	10.4	20.9	16.6	0.98
d06	2.83	8.0	16.8	12.5	22.2	0.99
d10	2.73	16.0	20.1	10.3	24.4	0.97
d15	2.62	13.0	19.7	10.5	21.3	0.99
d20	2.52	13.0	21.2	9.7	24.8	0.99

From the SN curves of the PU-T adhesive with internal notches given in **Figure 6.5**, the same trend could be observed (as for the RB-T adhesive): (i) alteration of slope of the SN curve and (ii) reduction of fatigue strength compared to un-notched (un, black curve) with stronger effects at the high cycle fatigue.

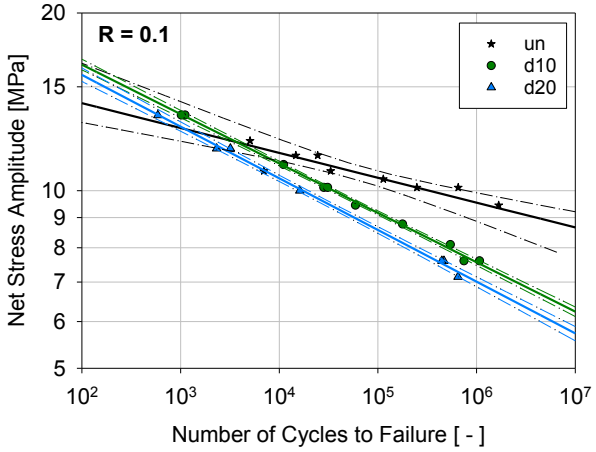

Figure 6.5 – SN curve (PU-T adhesive) | Internal Notch

From the SN curve parameters (**Table 6.4),** once more the severity of the process of fatigue is increased for bigger notches with higher values of the FSL for the notched specimens (d10 and d20). From the literature, it is expected that higher stress concentration factors would cause a more severe fatigue process [27,52]. However, by looking at the fatigue strength of notched specimens at a lifetime of 10^6 cycles (where strain are predominantly elastic) (**Figure 6.4**) and the values of the stress concentration factor (k_T) in **Table 6.3**, the results seem counter-intuitive. With this regard, it is important to reiterate the concept of highly stressed

volume [83–85]. It states that not only the peak maximum stress affects the fatigue process, but that the fatigue strength is inversely proportional to size of the highly stressed volume.

Table 6.4 – Parameters of SN curves | PU-T adhesive (internally notched)

sample	k_T [-]	n [-]	FSL [%]	B [-]	S_0 [MPa]	rsq [-]
un	1.00	9.00	10.52	20.72	17.94	0.84
d10	2.73	10.00	17.53	11.94	24.04	1.00
d20	2.52	7.00	18.27	11.41	23.52	1.00

For this reason, a 3D-FEA simulation was performed using linear-elastic models in order to calculate the distribution of stress concentration factor on the cross-section of three types of internal notches (d02, d10 and d20). These results are plotted in **Figure 6.6**. The dark blue colour indicates regions without stress concentration. As could be seen from these plots despite the maximum stress for d02 sample being higher, the size of the highly stressed region is very small as compared to the d10 and the d20.

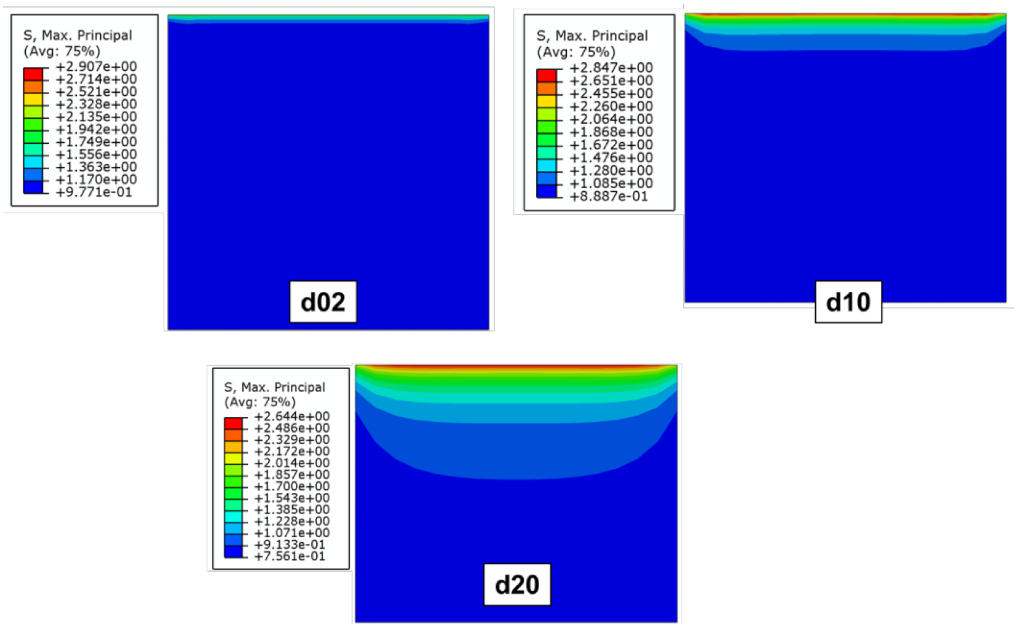

Figure 6.6 – Highly stressed region – internal notch: d02, d10 and d20

For the internally notched specimens, by comparing the effect caused by the peak stress (stress concentration factor) and by the size of the highly stressed region (**Figure 6.7**) it is revealed that the highly stressed volume had a prevailing influence on the reduction of fatigue strength. Because with an increasing stress concentration factor (but decreasing highly stressed region) the fatigue strength was increased. On the other hand, with an increasing highly stressed region the fatigue strength was reduced.

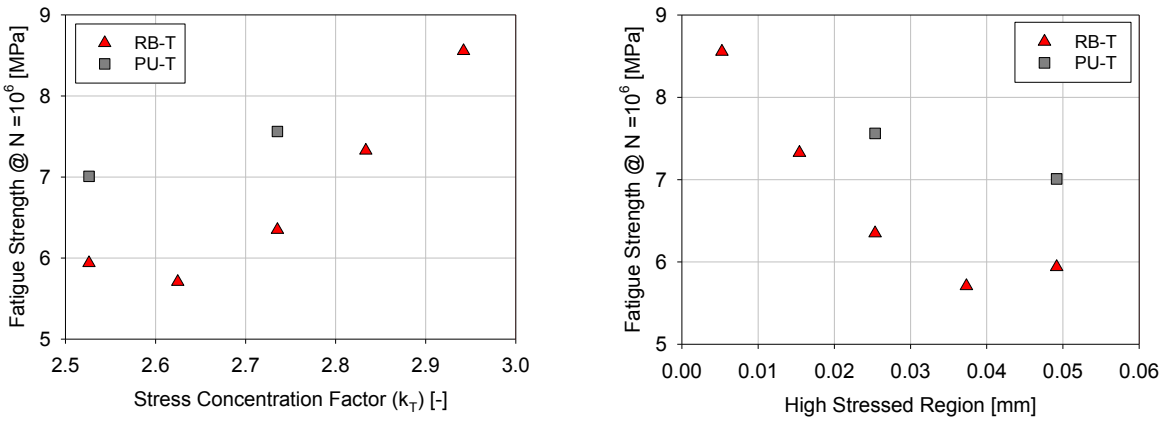

Figure 6.7 – Fatigue strength of internally notched specimens: (a) effect of stress concentration factor and (b) effect of highly stressed region

6.2.2. Damage evolution (stiffness degradation)

Four representative curves of each notch type were selected for the analysis of the damage evolution. In each plot the values of net stress amplitude and respective fatigue lifetime are shown. For all curves a common behaviour is observed: (i) in the beginning the damage increases gradually, (ii) then, the slope of the damage curve starts to increase with increasing number of cycles, and (iii) the damage variable increases rapidly near the critical number of cycles corresponding to the fatigue lifetime [110]. For every type of notch, an increase of net stress amplitude was accompanied by faster damage evolution and a reduction of fatigue lifetime. It can be seen from **Figure 6.8** that un-notched (un) and samples with a small notch size (d02) had a similar damage evolution behaviour with higher values of maximum damage prior to (damage > 0.3) obtained at higher stress amplitudes.

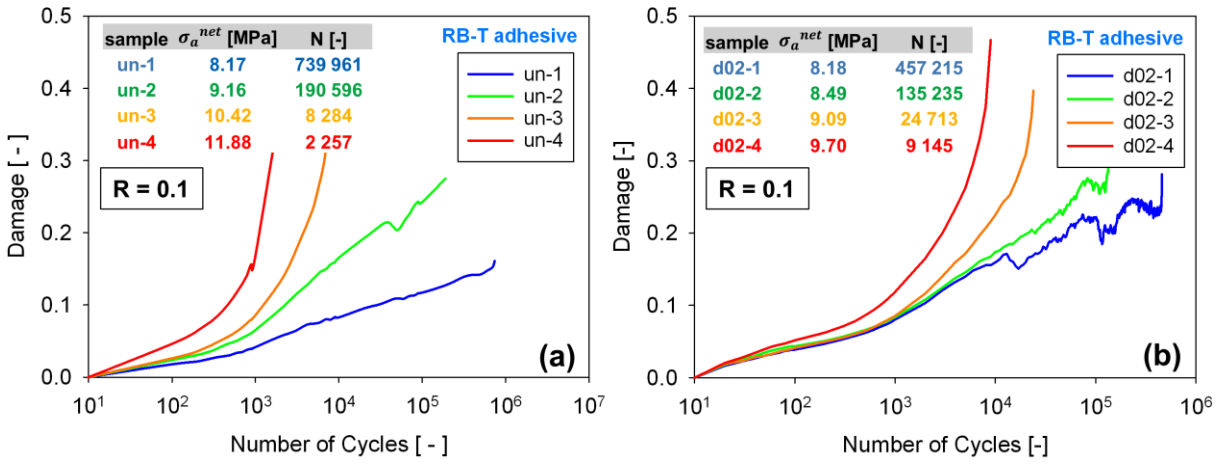

Figure 6.8 – Damage evolution - RB-T (internally notched): (a) un and (b) d02

In **Figure 6.9,** by increasing the notch size (d06 and d10) the maximum damage prior to failure is reduced to less than 0.3 for the d06 sample and to less than 0.2 for the d10 sample.

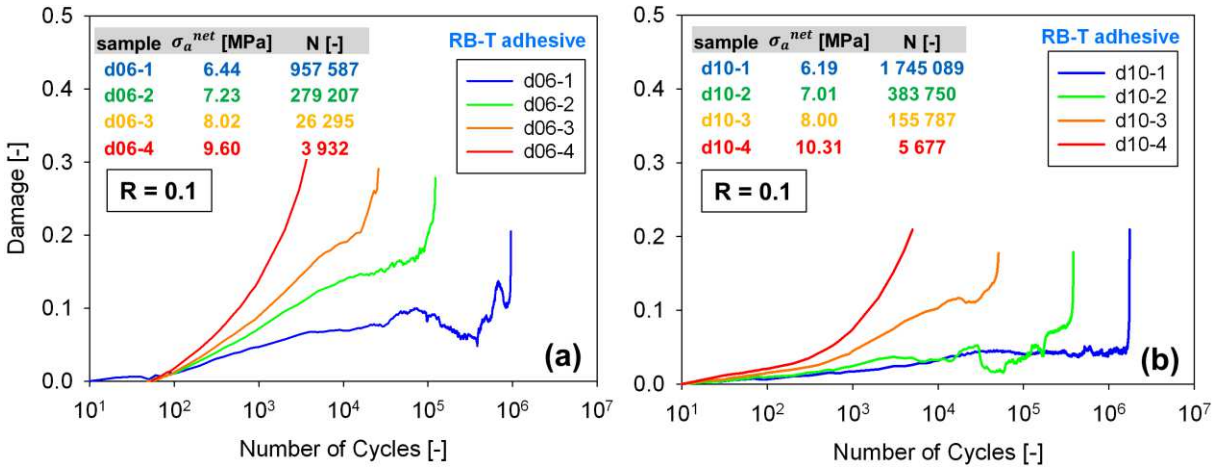

Figure 6.9 – Damage evolution - RB-T (internally notched): (a) d06 and (b) d10

Finally, for the notches d15 and d20, the values of maximum damage do not surpass 0.3 (**Figure 6.10**). These results provide evidence that an increase in the notch size (highly stressed region) cause a reduction on the maximum damage prior to failure. Therefore, it is possible that the reduction of maximum bearable damage could be reflected on the reduction of the fatigue strength which is seen in the SN curve results (**Figure 6.4**).

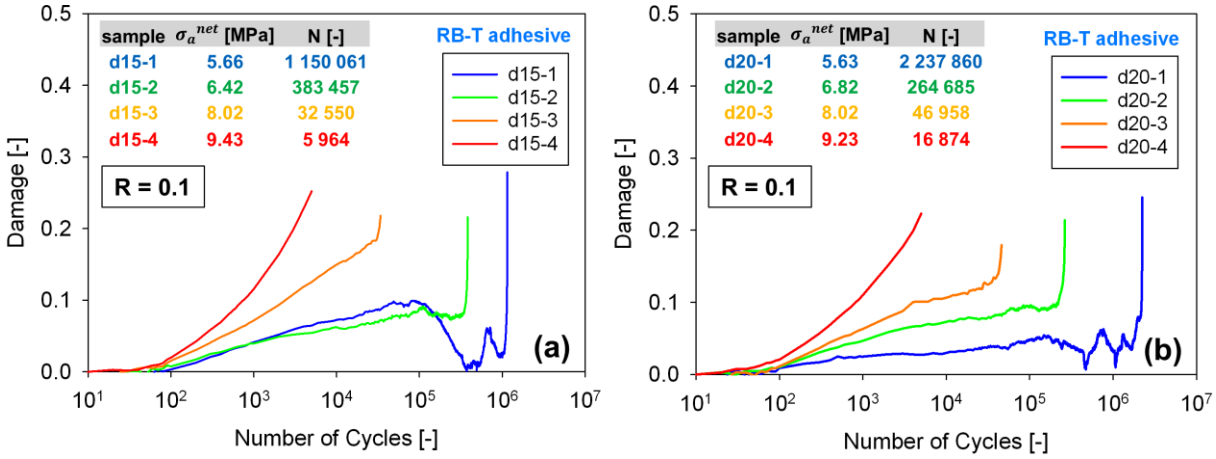

Figure 6.10 – Damage evolution - RB-T (internally notched): (a) d15 and (b) d20

For the PU-T adhesive (**Figure 6.11**), which is more brittle, the reduction on the maximum damage prior to failure is even stronger with the damage values inferior to 0.2 for all types of notches. Moreover, the slope of the damage curves increased with an increasing stress amplitude.

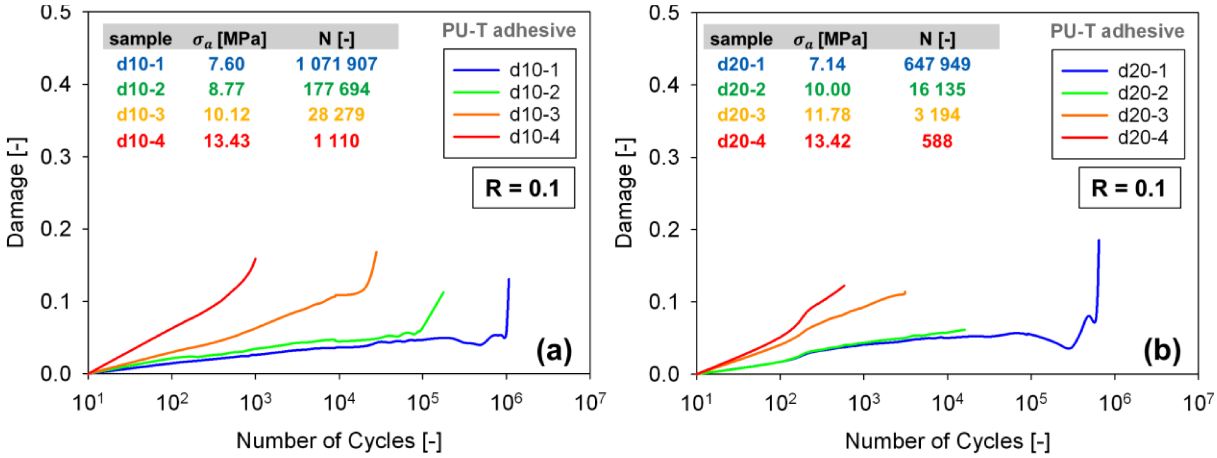

Figure 6.11 – Damage evolution - PU-T (internally notched): (a) d10 and (b) d20

6.2.3. Test monitoring

The monitoring of tests for internally notched specimens was carried out with the first monitoring system (**Section 3.4.1**), in which image recording and loading were not synchronised. For this reason, the test monitoring provided qualitative information on the behaviour of the adhesives, especially with regards to the fracture behaviour of the samples. Images from a test monitoring of internally notched samples with lifetime in the high cycle fatigue range (low stress amplitude) are shown in **Figure 6.12**.

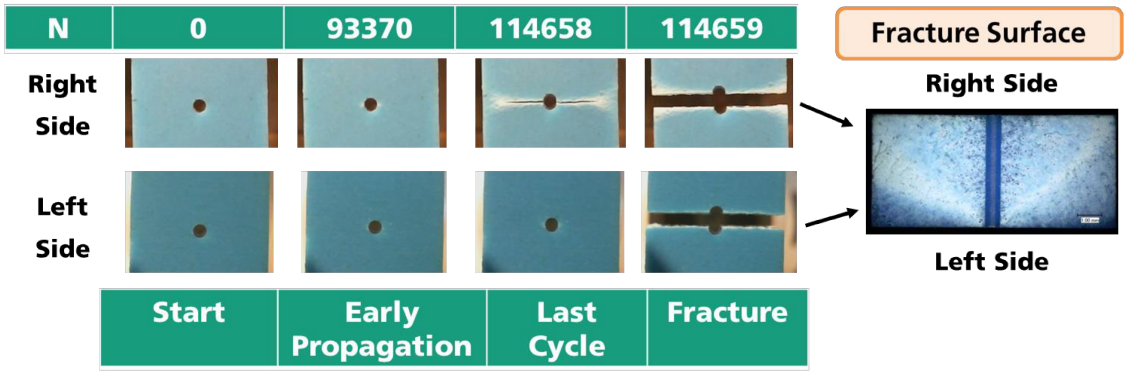

Figure 6.12 – Test monitoring | RB-T adhesive: high cycle fatigue (low stress amplitude)

These images make clear that the process of crack propagation of the samples was not entirely symmetric. In the example given in **Figure 6.12** the crack nucleated on one side of the sample (right side) and propagated. The left side was under pressure due to the opening of the crack on the other side. For this reason, prior to failure (last cycle) the crack was widely propagated in the right side and still very small on the left side. These differences are reverberated on the fracture surfaces that exhibit a "V-like" pattern due to the un-symmetric propagation of crack.

Conversely, for a sample with lifetime in the low cycle fatigue range (high stress amplitude) the crack propagation behaviour was more symmetric (**Figure 6.13).** Cracks nucleated on both sides of the sample nearly at the same time. Then, crack propagation occurred in parallel on both sides until the final fracture of the sample.

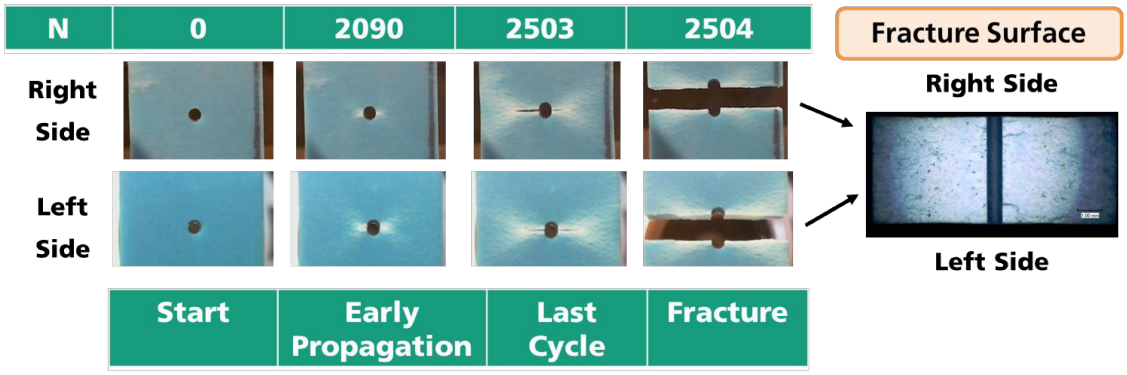

Figure 6.13 – Test monitoring | RB-T adhesive (internally notched): low cycle fatigue (high stress amplitude)

6.2.4. Fractography

Fracture surface images in this section were taken with a magnification of 30x. In **Section 6.2.3** it was highlighted that the fracture behaviour of internally notched specimens is affected by the applied stress amplitude. At low stress amplitudes (high cycle fatigue) a "V-like" shape is observed. By increasing the stress amplitude, the fracture pattern becomes more "symmetric". These features can be seen in **Figure 6.14**, where the fracture surface images of the d02-notch are shown for four different levels of stress. These images also reveal the presence of stress whitening (an indicator of damage) and small dark spots (*i.e.* void formation) close to the notch root [15,30]. These voids are more visible at low levels of stress (**Figure 6.14a-b**).

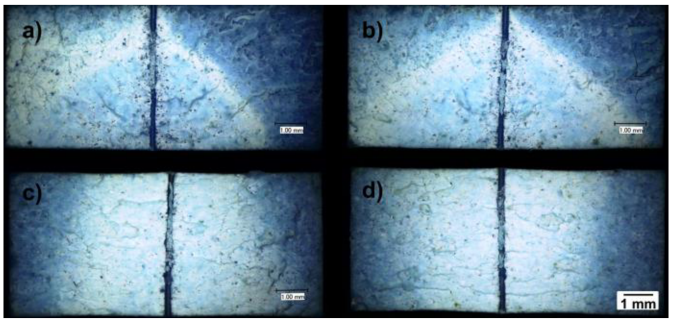

Figure 6.14 – Fatigue fracture surface of fatigue tests | Adhesive RB-T (d02)

σ_a^{net} : (a) 8.2 MPa, b) 8.5 MPa, c) 9.1 MPa, d) 9.7 MPa

It is widely accepted that the formation of voids (small dark spots) is related to the stress triaxiality, especially in notched specimens [18,88,147]. Bearing this in mind, 3D-FEA simulation (linear-elastic material behaviour) was carried out aiming to calculate the distribution of stress triaxiality in the cross-section of internally notched specimens. These distributions are plotted in **Figure 6.15**. They show that for a small notch size (d02) high values of stress triaxiality are confined to a very small region close to the notch region; it is possible to imply that this region with higher stress triaxiality matches the regions with a higher amount of voids in **Figure 6.14a-b**

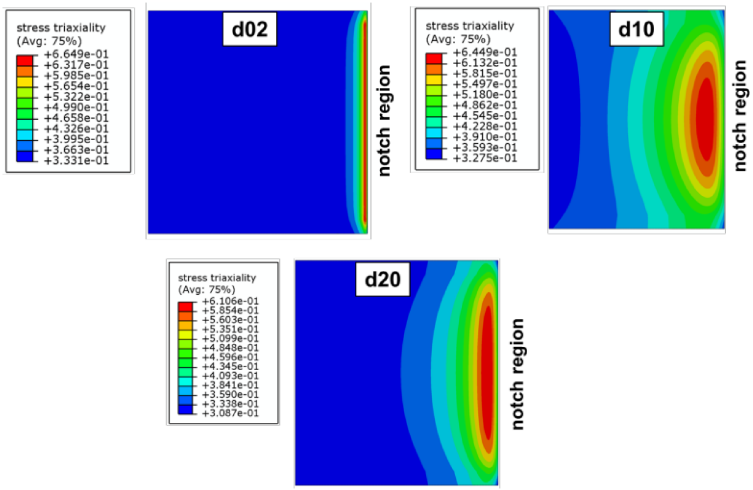

Figure 6.15 – Stress triaxiality distribution (internal notches) – d02, d10 and d20

With an increase in the notch size, the regions with higher stress triaxiality become larger. By examining the fracture surface images of notches with larger diameters (**Figure 6.14-19**), the presence of stress whitening close to the notch is also present. Furthermore, the size of the regions with a higher amount of voids is larger. These results are an indication of the association between higher stress triaxiality and void formation.

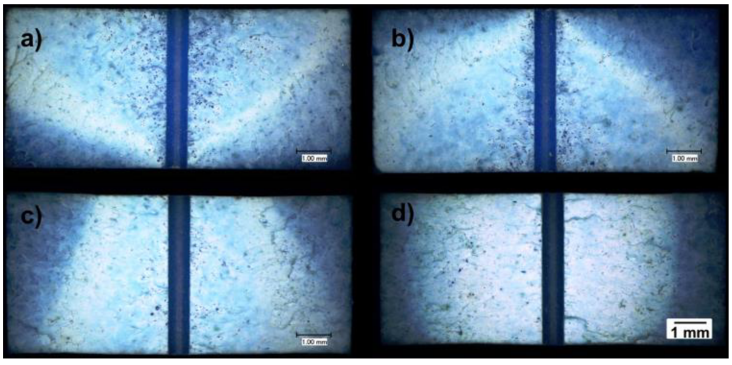

Figure 6.16 – Fatigue fracture surface | Adhesive RB-T (d06) -
σ_a^{net} : a) 6.5 MPa, b) 7.2 MPa, c) 8.0 MPa, d) 9.6 MPa

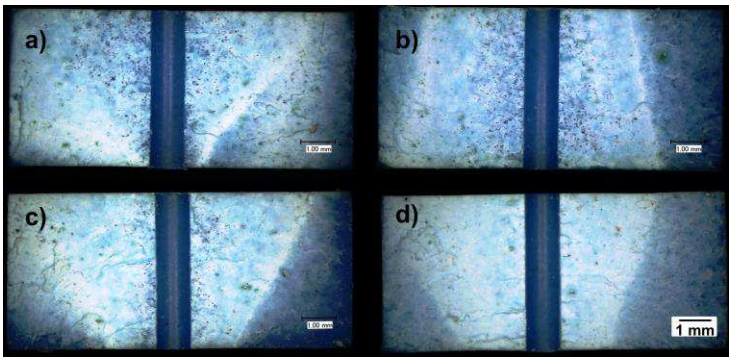

Figure 6.17 – Fatigue fracture surface | Adhesive RB-T (d10) - σ_a^{net} *: a) 6.2 MPa, b) 7.0 MPa, c) 8.0 MPa, d) 10.3 MPa*

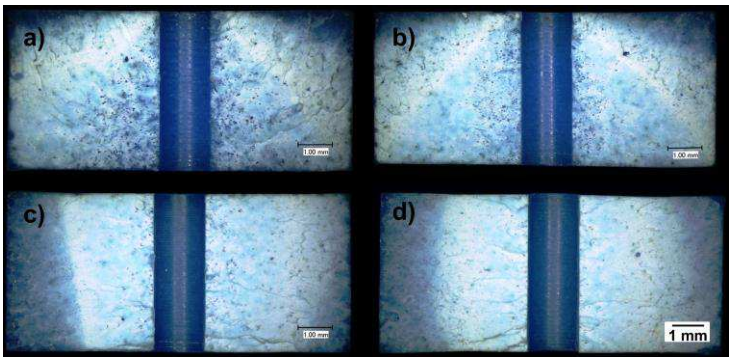

Figure 6.18 – Fatigue fracture surface | Adhesive RB-T (d15) - σ_a^{net} *: a) 5.6 MPa, b) 6.4 MPa, c) 8.0 MPa, d) 9.4 MPa*

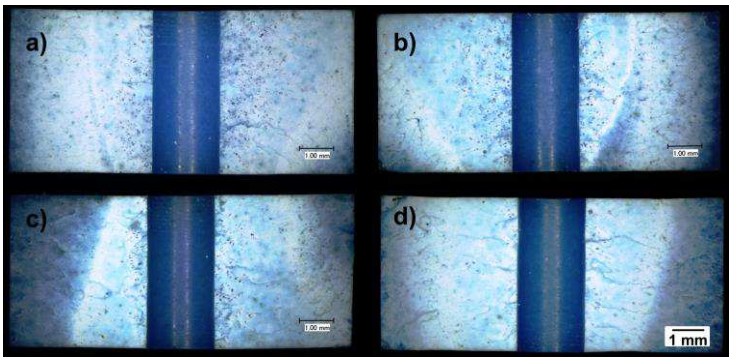

Figure 6.19 – Fatigue fracture surface | Adhesive RB-T (d20) - σ_a^{net} *a) 5.6 MPa, b) 6.8 MPa, c) 8.0 MPa, d) 9.2 MPa*

For the PU-T adhesive, stress whitening also took place around the notch region (**Figure 6.20** and **Figure 6.21**). However, the amount of voids was smaller as compared to the RB-T adhesive. This could be explained by the different ductility of the adhesives. The PU-T is more brittle; therefore, the effect of the stress triaxiality on void formation, which is related to plastic deformation, is less pronounced [52].

All fracture images of the PU-T adhesive showed a "V-like" pattern. Therefore, it could be inferred that the effect of stress amplitude on the fracture was not so strong as compared to the RB-T adhesive.

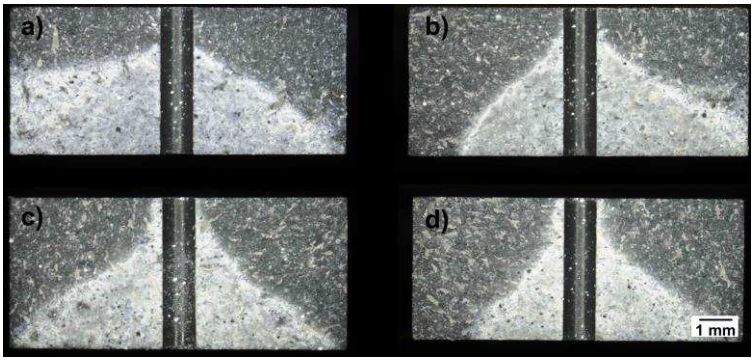

Figure 6.20 – Fatigue fracture surface | Adhesive PU-T (d10) - σ_a^{net} *: a) 7.2 MPa, b) 10.0 MPa, c) 11.8 MPa, d) 13.4 MPa*

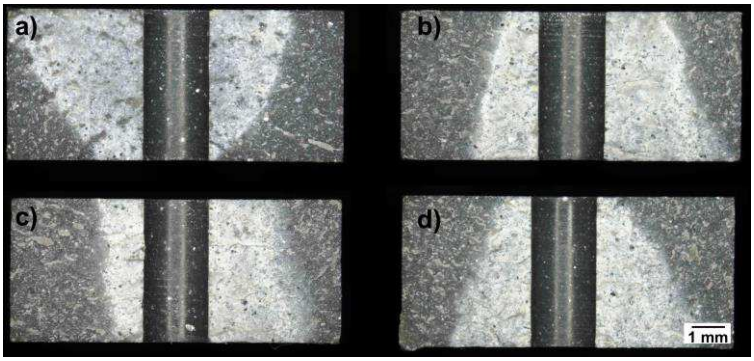

Figure 6.21 – Fatigue fracture surface | Adhesive PU-T (d20) - σ_a^{net} *: a) 7.6 MPa, b) 9.5 MPa, c) 11.1 MPa, d) 13.4 MPa*

6.3. FATIGUE BEHAVIOUR - EXTERNAL NOTCHES

The investigations with internally notched specimens revealed that an increasing size of the highly stressed region could reduce the fatigue strength of structural adhesives. In order to analyse the sole effect of stress concentrations caused by different notches it was necessary to perform tests with specimens having the same cross-section area.

Therefore, experiments with externally notched specimens (**Table 3.4**) were carried out aiming to assess the effect of stress concentrations on: (i) fatigue strength, (ii) crack initiation lifetime, (iii) damage behaviour, and (iv) fracture behaviour. These findings were then correlated to the mechanical properties of the structural adhesives.

In order to ease the process of comparison between different externally notched specimens and different adhesives, fatigue experiments were carried at four defined stress amplitude levels, which are described in **Table 6.5**. The net maximum stress is calculated as follows:

$$\sigma_{\max}^{net} = 2\frac{\sigma_a^{net}}{(1-R)} \tag{6.2}$$

Here R is the stress ratio, which in the present investigation was set to be 0.1. The superscript *net* indicate that the stress were calculated considering the net area (disregarding the notch).

Table 6.5 – Selected stress levels for fatigue experiments with externally notched specimens

	Level 1	**Level 2**	**Level 3**	**Level 4**
σ_a^{net} [MPa]	6.3	7.9	9.8	11.5
$\sigma_{\max}^{net}$ [MPa]	14.0	17.5	21.8	25.5

Therefore, plastic deformation in the notch root expected even for the lowest level of stress amplitude based on the values of maximum net stress, stress concentration factor and the yield stress of the adhesives (**Table 4.1**).

6.3.1. SN curve

The SN curves related to the fatigue experiments with externally notched specimens of both adhesives are shown in **Figure 6.22** with a 95% confidence interval (dashed line) and a 50% probability of failure (solid line).

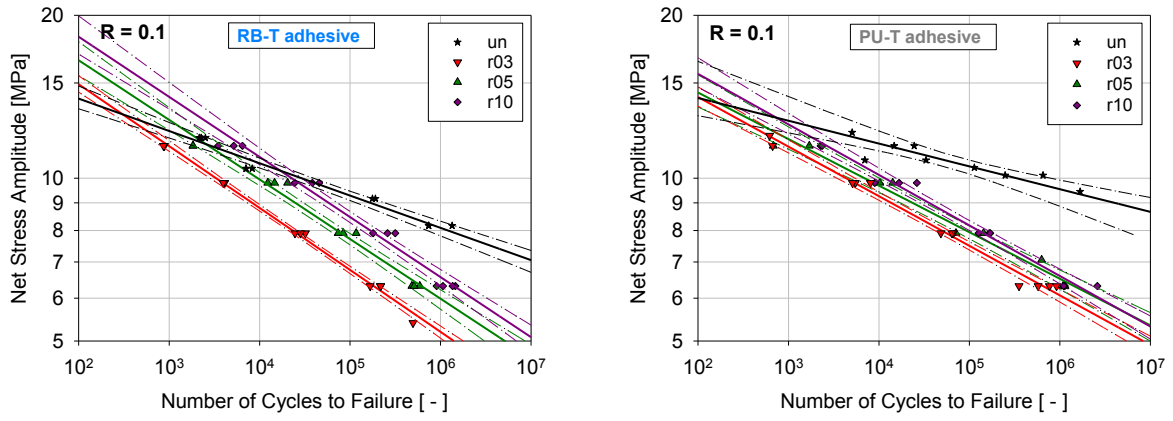

Figure 6.22 – SN curve | External Notch: RB-T adhesive (left) and PU-T adhesive (right)

For both adhesives there was a reduction in fatigue strength due to the notches, especially at the high cycle fatigue range (lower stress amplitudes) [91]. The reduction of fatigue strength

was proportional to the stress concentration factors (k_T) of the notches, *i.e.* higher values of k_T caused higher fatigue strength reduction [12]. The values of k_T are listed in **Table 6.6** and **6.7** along with the parameters of the SN curves for both adhesives (explanation of the meaning parameters is shown in **Section 6.2.1**). The values of *rsq* close to the one indicate a good correlation of linear regressions.

The SN curves of externally notched specimens of the RB-T adhesive are more separated from each other as compared to the PU-T adhesive. This observation might indicate that the RB-T adhesive (more ductile) is more sensitive to the effects caused by different values of stress concentration.

Table 6.6 – Parameters of SN curves | RB-T adhesive (externally notched)

sample	k_T [-]	*n* [-]	*FSL* [%]	*B* [-]	S_0 [MPa]	*rsq* [-]
un	1.00	11.0	12.9	16.7	18.5	0.97
r03	3.90	11.0	23.2	8.7	25.3	0.99
r05	3.16	11.0	22.4	9.1	27.4	0.98
r10	2.42	13.0	22.6	9.0	30.4	0.97

The slope of the SN curves (*B*) has not changed significantly. Therefore, it is possible to assume that the differences in the SN curves are related to the S_0 parameter, which translates (*i.e.* shifts) the SN curves. In order to ensure that these effects were caused solely by the different values of stress concentration, a 3D-FEA with linear-elastic material model was carried out. The objective was to calculate the distributions of stress concentration (related to the maximum principal stress) in the cross-section to determine the size of the highly stressed region of the externally notched specimens. The results of simulations are plotted in **Figure 6.23**.

Table 6.7 – Parameters of SN curves | PU-T adhesive (externally notched)

sample	k_T [-]	*n* [-]	*FSL* [%]	*B* [-]	S_0 [MPa]	*rsq* [-]
un	1.00	9.0	10.5	20.7	17.9	0.84
r03	3.90	12.0	19.0	10.9	14.5	0.99
r05	3.16	9.0	18.0	11.6	15.5	0.98
r10	2.42	11.0	19.4	10.7	14.8	0.98

The maximum value of the FEA-calculated stress concentration factor between different type of notch is not the same (r03 = 4.20, r05 = 3.38 and r10 = 2.58). However, the size of the

regions without stress concentration (dark blue region) is very similar. These findings support the idea that the effect of external notches on the fatigue strength is caused mainly by the values of stress concentration factor.

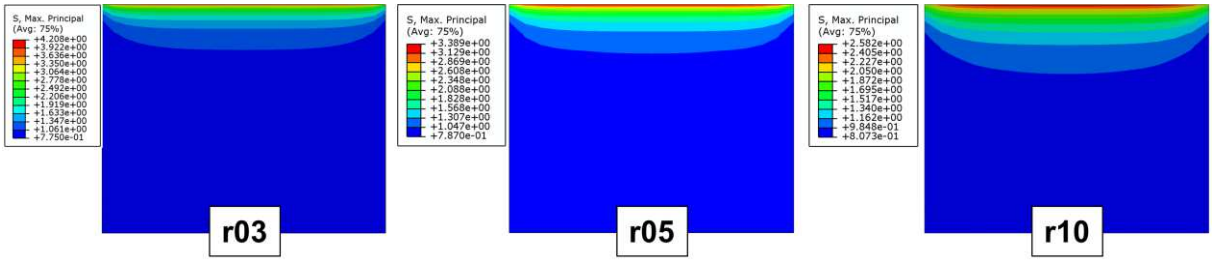

Figure 6.23 – Highly stressed region - external notch: r03, r05 and r10

Comparing results of internally and externally notched specimens with regards to SN curve, highly stressed region and stress concentration factors it is possible to suggest that: (i) the slope of SN curve is altered due the size of the highly stressed region and (ii) the SN curve is translated (*i.e.* shifted up or down) due the value of stress concentration factor. This is an important finding with regard to lifetime prediction using the stress-life approach.

Experimental results indicate that the relation between the strength of adhesives and stress concentration depends on the level of applied stress. Under quasi-static conditions (very high stress) (**Section 5.2**) the RB-T adhesive had higher tensile strength as compared to the PU-T adhesive. However, under fatigue conditions, the relative strength between adhesives was dependent on the stress concentration factor and the level of stress (**Figure 6.24**). By comparing the strength of different externally notched samples of the RB-adhesive and the PU-T adhesive, the following relation could be drawn:

a) for the r03-notch (k_T = 3.9): RB-T adhesive (i) was stronger at quasi-static conditions, (ii) had the same strength at low cycle fatigue (LCF) and (iii) was weaker at the high cycle fatigue (HCF);
b) for the r05-notch (k_T = 3.16): RB-T adhesive (i) was stronger at quasi-static conditions, (ii) was stronger at low cycle fatigue (LCF) and (iii) was weaker at the high cycle fatigue (HCF);
c) for the r10-notch (k_T = 2.42): RB-T adhesive (i) was stronger at quasi-static conditions, (ii) was stronger at low cycle fatigue (LCF) and (iii) has the same strength at the high cycle fatigue (HCF);

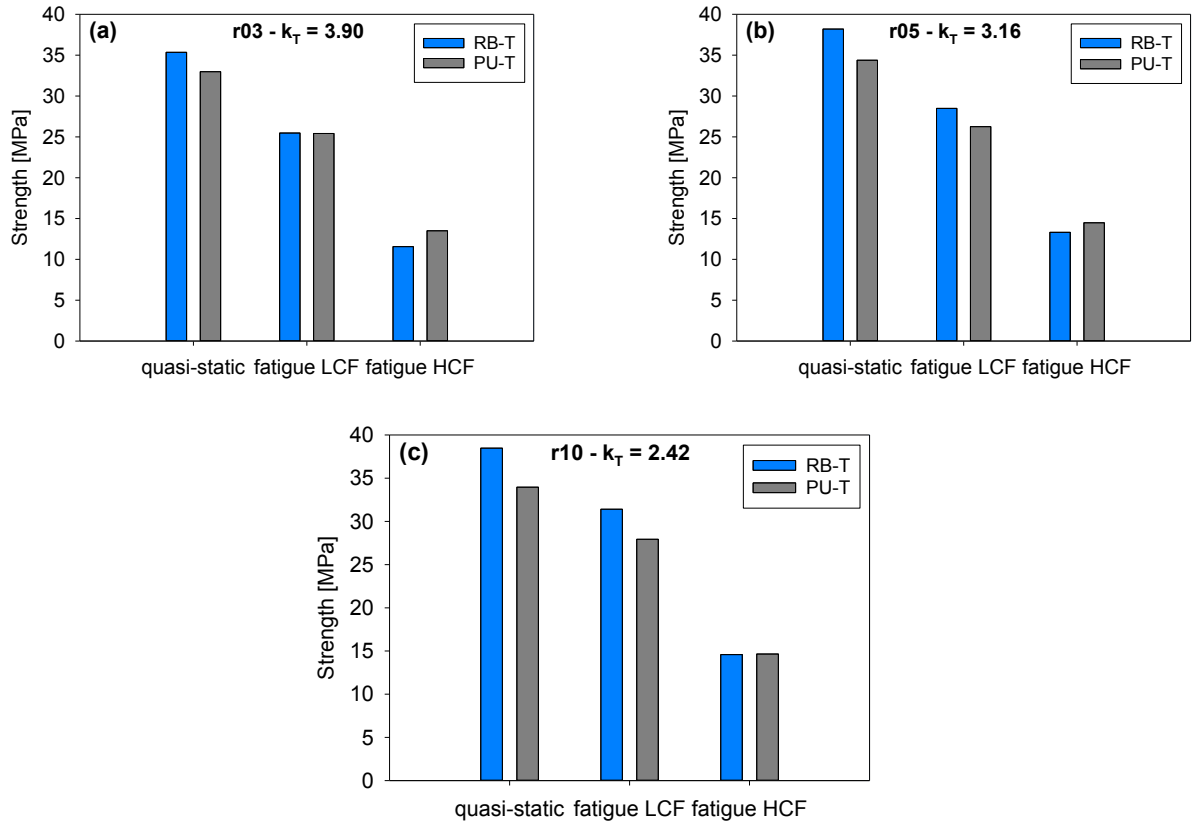

Figure 6.24 – Effect of stress concentration on the quasi-static and fatigue (LCF, HCF) strength of externally notched samples of the RB-T and the PU-T adhesives | (a) r03, (b) r05 and (c) r10

Another indicator of the effect of stress concentrations on the fatigue response of materials is the notch sensitivity (q) calculated from **Equation (2.24)**. The notch sensitivity (see **Section 2.4**) varies between 0 (no sensitivity) to 1 (full sensitivity). The values of notch sensitivity based on the fatigue strength for a lifetime of 10^6 are depicted in **Figure 6.25**.

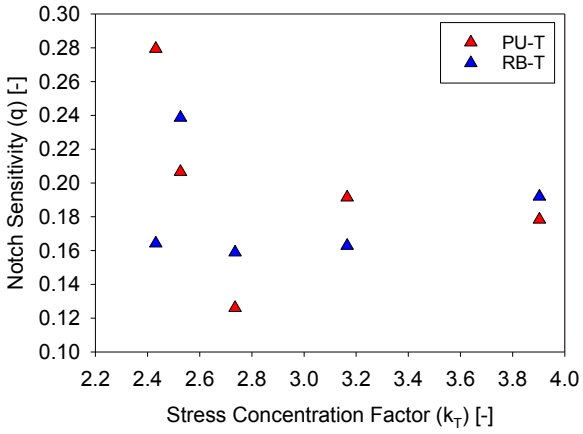

Figure 6.25 – Notch sensitivity at a fatigue lifetime of 10^6 cycles | RB-T and PU-T adhesives

The values of notch sensitivity for the PU-T adhesive varied between 0.12 and 0.28. For the RB-T adhesive, these values varied between 0.16 and 0.24. In both cases, the values of notch sensitivity were lower than typical values of metals [151], which indicates that the investigated adhesives are less sensitive to notches than metallic materials.

6.3.2. Crack initiation

The monitoring system for externally notched specimens allowed a synchronisation between the acquisition of images and the loading of samples. Therefore, an accurate assessment of the number of cycles for crack initiation was possible. The SN curves for crack initiation for both adhesives are shown in **Figure 6.26**.

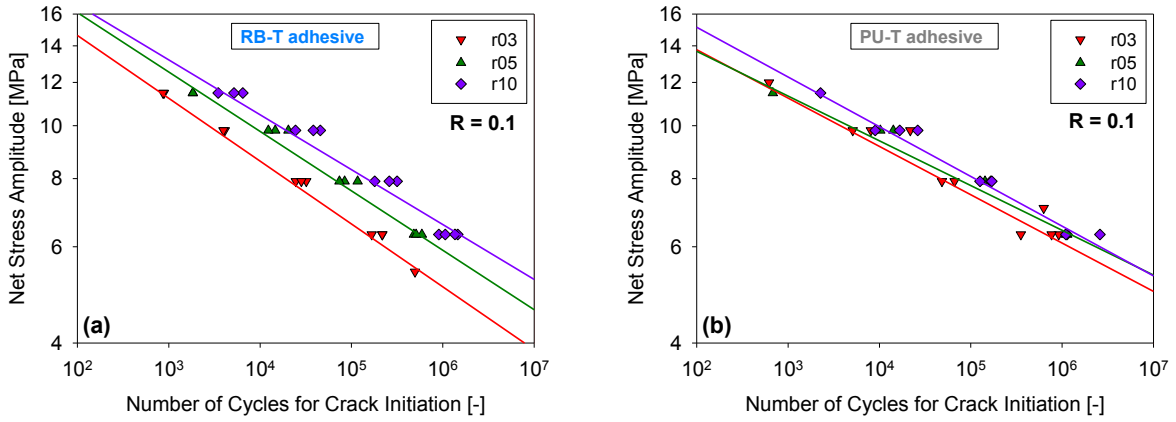

Figure 6.26 – SN curves for crack initiation | (a) RB-T adhesive and (b) PU-T adhesive

By comparing samples tested at the same stress level, it is possible to observe that lifetime for crack initiation for the r03-notch samples was shorter as compared to the r05 and r10 notches. The r10-notch samples had the longest crack initiation lifetime regardless of applied stress. For the RB-T adhesive, the SN curves appear to have the same slope with a shift depending on the type of notch. Moreover, differences between crack initiation lifetimes of different notched samples seem to be stronger for the RB-T adhesive.

Another important key aspect of the present investigation was to evaluate whether the crack initiation or the crack propagation was the dominant phase on the process of fatigue, and to correlate this dominance with the stress concentration and the mechanical properties of the adhesives. In this regard, the percentage of fatigue lifetime spent on crack initiation for both adhesives (along with scatter bars) is presented in **Figure 6.27**. This figure reveals that for both adhesives most of the fatigue lifetime is spent on crack initiation. For lower stress

concentrations (r10-notch) this value could be higher than 80%. With an increase in stress concentration factor (r03-notch) the percentage of lifetime spent on crack initiation is reduced.

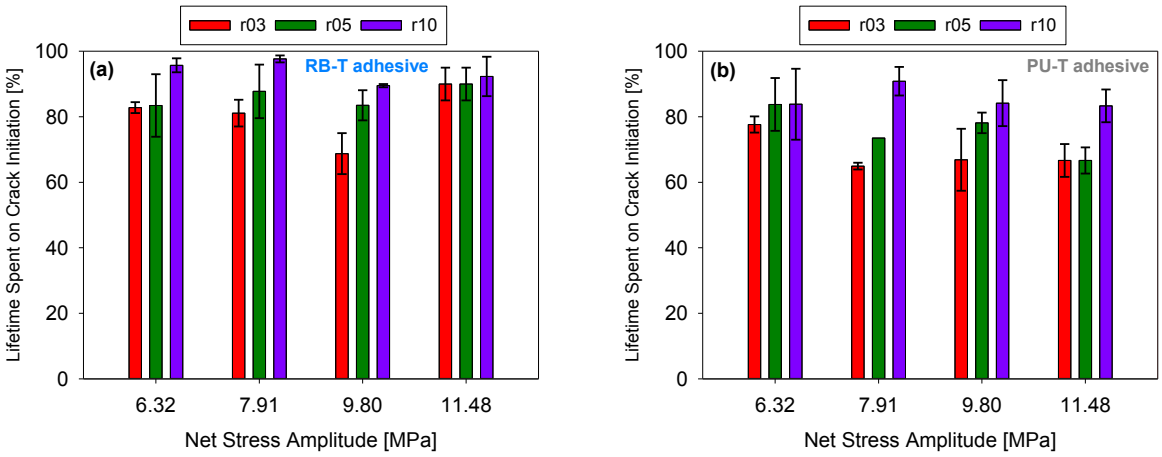

Figure 6.27 - Lifetime spent on crack initiation: (a) RB-T adhesive and (b) PU-T adhesive

These results indicate that crack initiation phase is shortened by an increasing stress concentrations factor. The comparison between SN curves for crack initiation of different adhesives is presented in **Figure 6.28**.

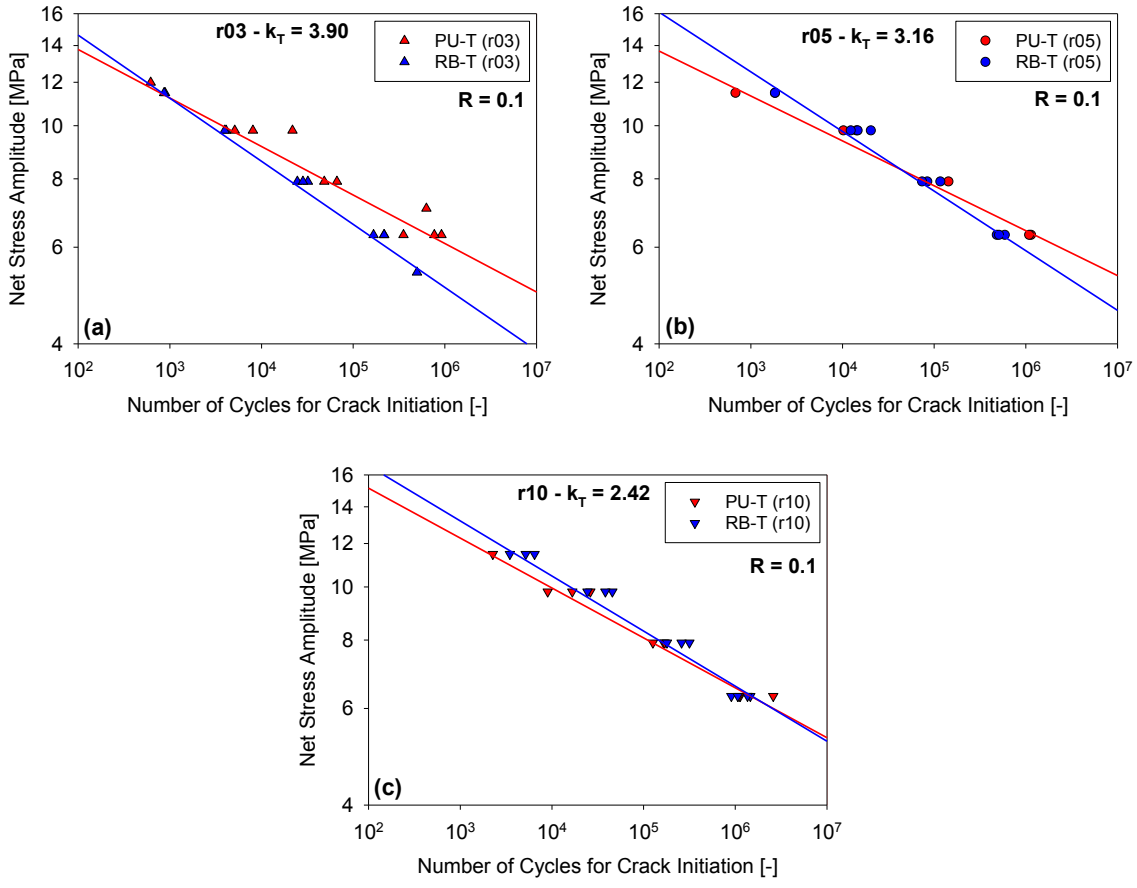

Figure 6.28 – SN curves for crack initiation | comparison between RB-T and PU-T adhesives

The results of SN curves provide support for understanding the effect of stress concentrations and its relationship with the mechanical properties of the adhesives. For samples with high stress concentration (r03-notch / **Figure 6.28a**), the lifetime for crack initiation was longer for the PU-T adhesive (more brittle). For a medium stress concentration (r05, **Figure 6.28b)**, the lifetime for crack initiation was longer for the PU-T adhesive in the high cycle fatigue and for RB-T adhesive in the low cycle fatigue. Finally, for a low stress concentration (r10, **Figure 6.28c**), the lifetime for crack initiation was longer for the RB-T adhesive.

Therefore, the crack initiation lifetime is influenced by the level of stress concentration, by the level of applied stress, and by the mechanical properties of the adhesives (the most ductile adhesive was more sensitive) [12]. The parameters of the SN curves for crack initiation are given in **Table 6.8**. They indicated a good correlation of the Basquin's law with experimental data ($rsq > 0.95$).

Table 6.8 – Parameters of SN curves for crack initiation | RB-T and PU-T adhesives

adhesive	notch type	*n [-]*	*FSL [%]*	*B [-]*	*S_0 [MPa]*	*rsq [-]*
RB-T	r03	11.0	23.3	8.7	24.8	0.99
RB-T	r05	11.0	22.2	9.2	26.6	0.98
RB-T	r10	12.0	20.7	10.0	26.4	0.95
PU-T	r03	10.0	18.4	11.3	20.7	0.95
PU-T	r05	6.0	17.2	12.2	20.0	0.97
PU-T	r10	10.0	18.9	11.0	23.0	0.97

6.3.3. Damage evolution (stiffness degradation)

The damage curves for the externally notched specimens (r03, r05 and r10) at four levels of stress, and for both adhesives are shown in **Figure 6.29**. One representative damage curve for each level of stress amplitude was selected for the plots. In each damage curve the point of crack initiation was signed with a triangle. These results indicate that the crack initiation causes a sudden increase of damage (*i*.e. reduction of stiffness) in the samples. As expected, an increase of net stress amplitude was accompanied by faster damage evolution and a reduction of fatigue lifetime.

The maximum damage prior to failure was less than 0.2 for the majority of samples. Some similarities in the damage behaviour are shared for every notched specimen: (i) in the beginning the damage increases gradually proportional to applied stress, (ii) then the slope of

the damage curve starts to increase with increasing number of cycles and (iii) finally, the damage variable increases rapidly near the number of cycles corresponding to the failure of the material.

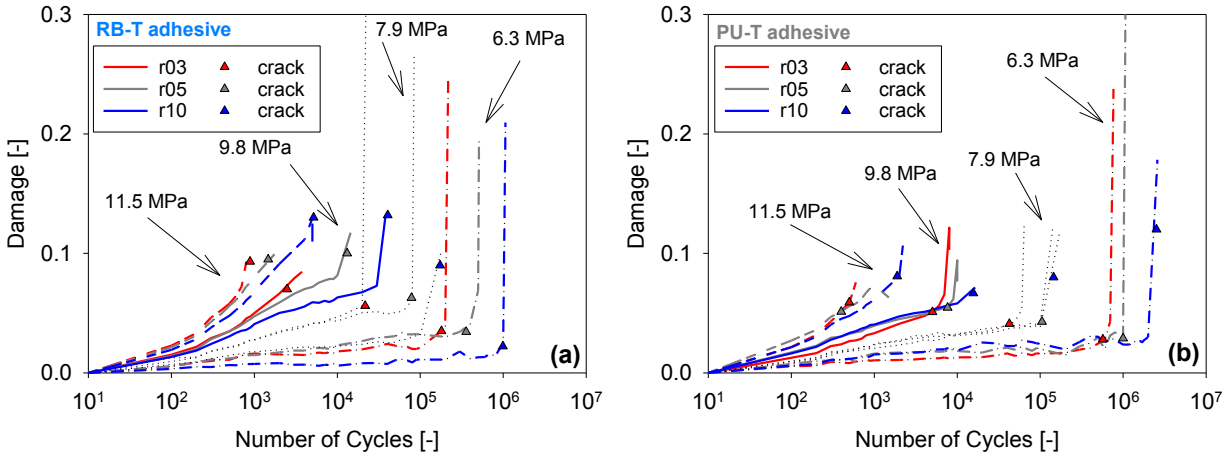

Figure 6.29 – Damage curves | External notches: (a) RB-T adhesive and (b) PU-T adhesive

This trend of smooth increase followed by a sudden increase near the point of failure was also observed by other researchers [12,19].

By analysing the damage curves of the PU-T adhesive, it is possible to observe that for samples under the same level of stress (*e.g.* 6.3 MPa) the evolution of damage follows the same trend (same slope). The only difference is that for samples with higher stress concentration factor (r03-notch) the crack initiation takes place earlier.

This analysis provides additional evidence that stress concentrations make the process of crack initiation shorter (see also **Figure 6.27**). Since the crack initiation causes a sudden increase of damage, the fatigue strength of samples with higher stress concentration is reduced.

6.3.4. Fractography

Fracture surface images were taken with a magnification of 30x. One representative image for each level of stress amplitude was selected. The fracture images for the r03-notch at four levels of stress are shown in **Figure 6.30** for both adhesives. Red arrows with the same length were added to the images in order to ease the process of comparison. It can be seen that fracture surfaces are non-symmetric. Based on the test monitoring images (**Figure 3.14**), the crack starts at one side and propagates towards the other side. Stress whitening close to the notch root takes place in all samples.

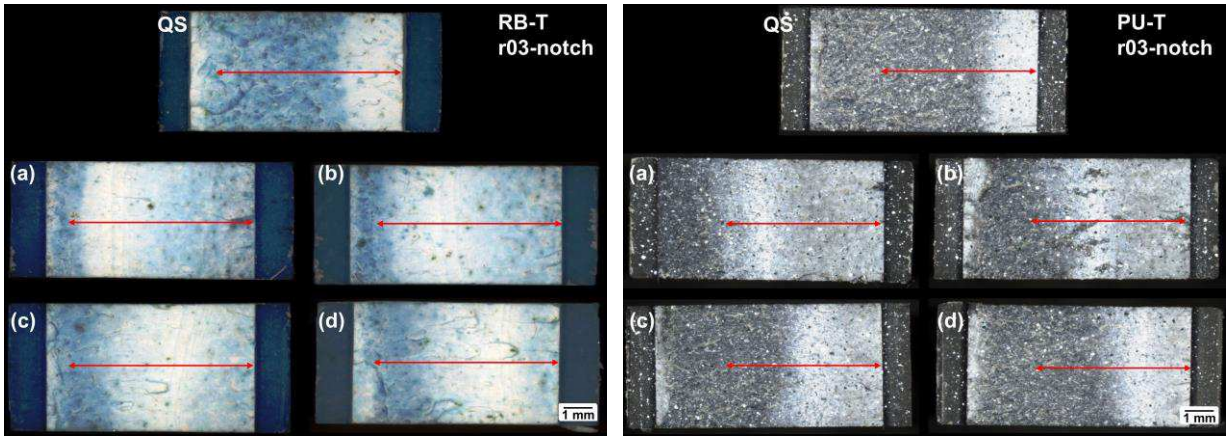

Figure 6.30 – Fatigue fracture surface | External notch (r03) - RB-T (left) and PU-T (right)
σ_a^{net} : a) 6.3 MPa, b) 7.9 MPa, c) 9.8 MPa and d) 11.5 MPa

However, the size of the stress whitening region is larger for tests under lower stress amplitude (**Figure 6.30a**). This could be explained by the fact that the propagation of cracks reduces the size of the effective area bearing the load. For lower values of stress the size of this effective area could be smaller as compared to higher values of stress.

By comparing the adhesives, the RB-T adhesive (more ductile) exhibited a larger stress-whitening region as compared to PU-T adhesive. This trend was observed also for externally notched specimens under quasi-static conditions (**Section 5.2.3**). The observations regarding the r03-notch are also useful to explain the behaviour of the r05-notch (**Figure 6.31**) and the r10-notch (**Figure 6.32**).

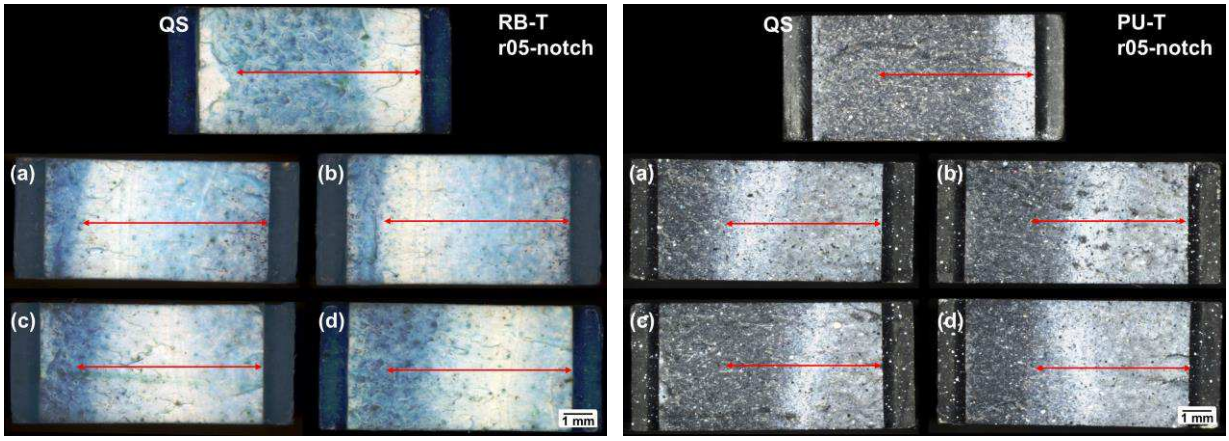

Figure 6.31 – Fatigue fracture surface – External notch (r05) – RB-T (left) and PU-T (right)
σ_a^{net} : a) 6.3 MPa, b) 7.9 MPa, c) 9.8 MPa and d) 11.5 MPa

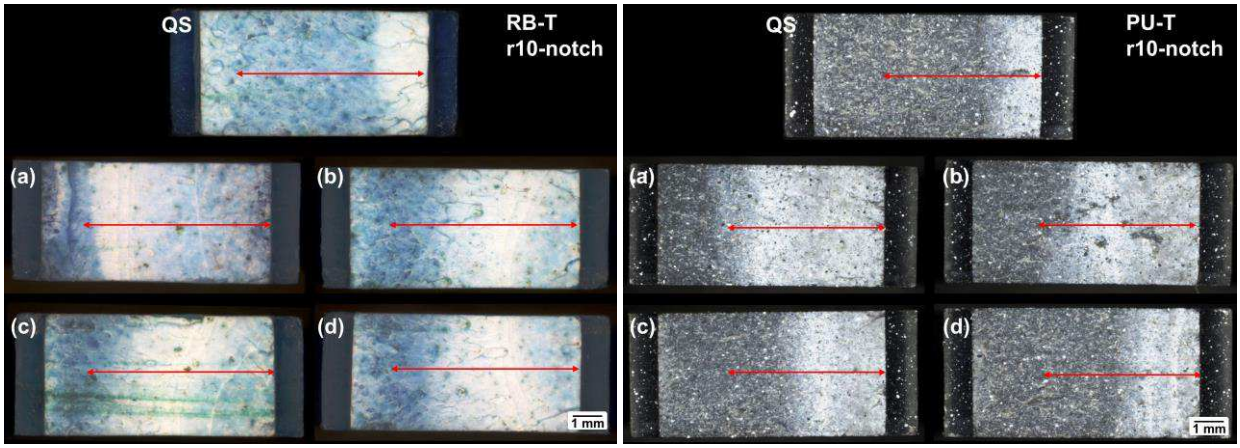

Figure 6.32 – Fatigue fracture surface – External notch (r05) – RB-T (left) and PU-T (right) σ_a^{net} *: a) 6.3 MPa, b) 7.9 MPa, c) 9.8 MPa and d) 11.5 MPa*

As mentioned in the fractography analysis of internally notched specimens, the distribution of stress triaxiality has a strong influence on the formation of voids [15,110]. For this reason, 3D-FEA (linear-elastic material behaviour) was performed to calculate the distribution of stress triaxiality in the cross-section of the externally notched specimens (**Figure 6.33**).

These results support the idea that stress triaxiality are related to the formation of voids since the regions with a higher amount of dark spots (close to the notch root / **Figures 6.30-32**) correspond to the regions with higher values of stress triaxiality (red regions).

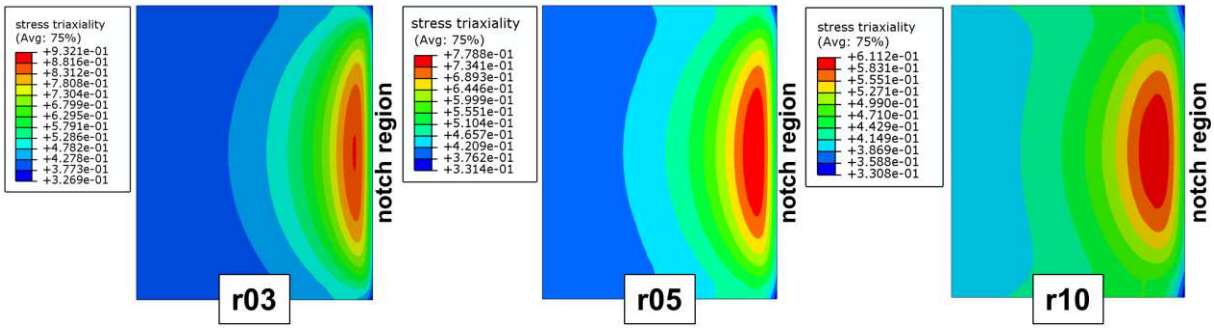

Figure 6.33 – Distribution of stress triaxiality on the cross-section of externally notched specimens | r03, r05 and r10

6.4. SUMMARY

Structural adhesives are frequently working under cyclic loading conditions (*e.g.* rotating blades, engine vibration) which can lead to failure due to fatigue [8]. The phenomenon of fatigue, which involves the phases of crack initiation and crack propagation, is very complex.

Therefore, the present chapter investigates the fatigue behaviour of structural adhesives with focus on the effect of stress concentrations due to notches. In this regard, un-notched, internally notched and externally notched specimens were tested under a sinusoidal cyclic tension-tension load with a stress ratio of 0.1.

The experiments with un-notched specimens (**Section 6.1**) were carried out in order to create a base for comparison with notched specimens and to understand the influence of mechanical properties on the fatigue strength of structural adhesives. SN curve results revealed higher fatigue strength of the PU-T adhesive in the entire fatigue range. The fatigue strength of adhesives was correlated with the quasi-static strength. Results showed that at 10^3 cycles the fatigue strength was approximately 80% of the quasi-static strength and at 10^6 cycles the fatigue strength is reduced to approximately 50% of the quasi-static strength.

Regarding damage evolution curves of un-notched specimens, higher values of stress amplitude caused faster damage evolution for both adhesives. This was reflected on the number of cycles to failure which were shorter at higher stress amplitudes. Fracture surface analysis revealed that the RB-T adhesive (more ductile) had larger regions of stress whitening (indicator of damage) as compared to PU-T adhesive. Furthermore, fracture images are more "rough" at high levels of stress. On the other hand, for low levels of stress the fracture surface is more "flat", especially for the PU-T adhesive (more brittle).

The fatigue experiments with internally notched specimens (**Section 6.2**) demonstrated a reduction of fatigue strength with an increasing notch size. The reduction of fatigue performance was stronger at the high cycle fatigue range. Fatigue results revealed that under stress concentration conditions not only the value of the maximum peak stress (stress concentration factor) affects the fatigue strength; the size of the highly stress volume has a key role in the reduction of fatigue strength and on the change of the slope of the SN curves.

Damage curves of internally notched specimens showed gradual increase of damage in the first cycles of loading. Then, the slope of the damage curve starts to increase with increasing number of cycles until the damage variable increases rapidly close to the critical number of cycles corresponding to the fatigue lifetime. Moreover, there was a reduction of maximum damage prior to failure with an increasing notch size. Fracture surface analysis revealed the presence of stress whitening (*i.e.* damage) close to the notch root, which combined with 3D-FEA investigation suggest that the nucleation of voids is more present at regions with higher stress triaxiality ratios.

The fatigue experiments with externally notched specimens (**Section 6.3**) revealed that the reduction of fatigue strength was proportional to the stress concentration factors of the notches, *i.e.* higher values of stress concentration factor caused stronger fatigue strength reduction. The SN curves of different externally notched specimens had nearly the same slope. However, the curves were translated (*i.e.* shifted) according to the value of stress concentration factor of the samples.

Damage curves of specimens with external notches showed that the crack initiation causes sudden increase of damage (*i.e.* reduction of stiffness) in the samples. For samples under the same level of stress the evolution of damage follows the same trend (same slope). However, for samples with higher stress concentration factor the crack initiation takes place earlier.

Regarding fracture surface analysis, the size of the stress whitening region is larger for tests under lower stress amplitude. This could be explained by the fact that the propagation of cracks reduces the size of the effective area bearing the load. For lower values of stress the size of this effective area could be smaller as compared to higher values of stress. By comparing the adhesives, the RB-T adhesive exhibited a larger stress-whitening region (damage) as compared to PU-T adhesive.

The SN curves for crack initiation lifetime of both adhesives indicated that for both adhesives most of the fatigue lifetime was spent on the crack initiation phase (60 to 95%) with higher percentage values obtained for lower stress concentration factors. Moreover, it was found that crack initiation phase is shortened by an increasing stress concentration factor. The severity of this effect is influenced by the mechanical properties of the adhesives (the most ductile adhesive was more sensitive) and by the level of applied stress.

7. FATIGUE LIFETIME PREDICTION OF NOTCHED SPECIMENS

The present chapter presents the process of setting-up of a fatigue modelling method for predicting the fatigue lifetime of notched specimens of the structural adhesives under investigation. The setting-up of the method was made taking into account the findings regarding the effect of stress concentrations on the fatigue behaviour of structural adhesives discussed in **Chapter 6**.

In **Section 7.1** the process of setting-up of the method for lifetime prediction is detailed. The proposed method was based on the stress-life method using the theory of critical distances to address the effect of stress concentration on the lifetime predictions.

The process of lifetime prediction using the proposed method is described in **Section 7.2** including the choice of reference SN curve, the choice of equivalent stress, the definition of critical distance parameters and the choice of geometrical model.

In **Section 7.3** the validation of the method was performed using linear-elastic material models by comparing predicted fatigue lifetimes (ranging from 10^3 to 10^6 cycles) with experimental results of notched specimens with different levels of stress concentration.

In **Section 7.4** the predictions of fatigue lifetime were extended considering elasto-plastic materials behaviour. Predicted results were then compared to results where linear-elastic material behaviour was assumed. Moreover, the advantages, limitations, and potential improvements for the proposed method of prediction are discussed.

7.1. DEFINITION OF METHOD FOR PREDICTION OF FATIGUE LIFETIME

The definition of a suitable method for the lifetime prediction of notched components requires a deep understanding of the factors influencing the fatigue behaviour under stress concentration conditions. These factors were investigated in **Chapter 6**, which include: effect of stress triaxiality, effect of highly stressed region and effect of the stress concentration factor (peak stress).

Besides that, for notched adhesive specimens, it was found that the crack initiation phase was the dominant phase in the process of fatigue. Therefore, it is expected that solely fracture mechanics methods would not provide accurate predictions since they do not consider the crack initiation lifetime.

In this regard some requirements were established in the process of definition of the method for lifetime prediction. The prediction method should be:

a) efficient and straightforward;
b) suitable for both adhesives (PU-T and RB-T);
c) suitable for different levels of stress concentration and highly stressed regions;
d) able to predict the whole fatigue range including low and high cycle fatigue;
e) able to predict the total fatigue including crack initiation and crack propagation.

Based on these guidelines it was considered that the most suitable method for lifetime prediction of the notched specimens is the stress-life approach. The theoretical framework of this approach is described in details in **Section 2.5.1**.

The theory of critical distances (TCD) was implemented in the prediction method to account for the effects of stress concentrations on the fatigue lifetime. The TCD has been proven a valid approach for dealing with adhesives under quasi-static [101,102] and fatigue conditions [22] including the influence of material elasto-plasticity [98] and stress multiaxiality [104].

The stress-life method combined with TCD requires a reference SN curve (obtained experimentally) considering the total lifetime (crack initiation and propagation) to provide a relationship between stress amplitude (*i.e.* fatigue strength) and fatigue lifetime. As stated in **Chapter 1**, the present work intended to overcome the limitations related to the "transferability" of SN curve between different samples. Therefore, the same reference SN curve was used to predict samples with different levels of stress concentration.

After the definition of a reference SN curve, a stress analysis should be carried out in order to obtain the information of the equivalent stress as a function of the distance from the notch root. Moreover, the stresses on the reference SN curve should be transformed from nominal stresses to equivalent stresses (see **Section 7.2**). In this step, FEA can be very helpful allowing an easy calculation of stress even for complex geometries. Finally, the fatigue lifetime is obtained by correlating the results of stress calculations with the "transformed" reference SN curve.

The entire process of fatigue lifetime prediction including choice of a reference SN curve, choice of equivalent stress, definition of critical distance and definition of a geometric model are described in detail in the next section.

7.2. PROCESS OF FATIGUE LIFETIME PREDICTION

The process of fatigue lifetime prediction using the stress-life method in combination with the theory of critical distances is shown in **Figure 7.1**

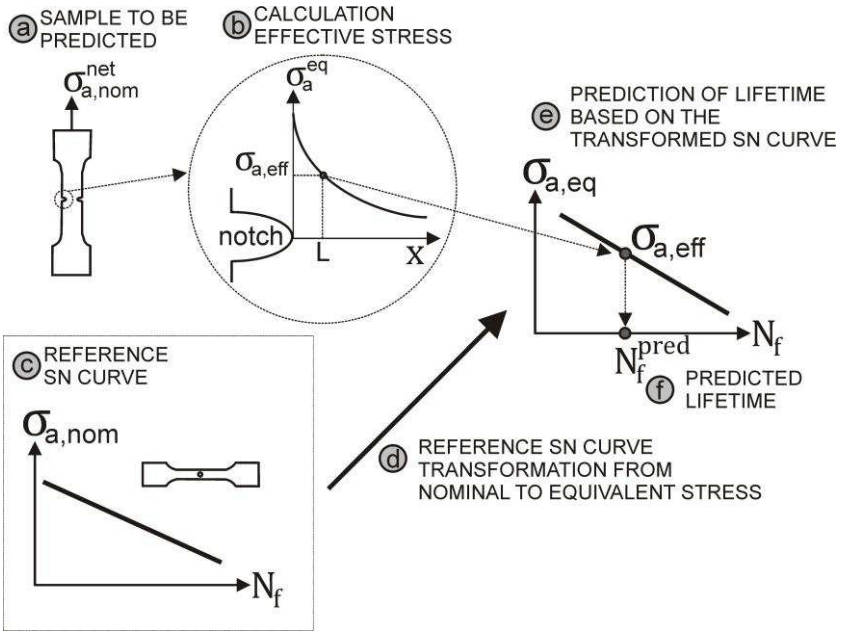

Figure 7.1 – Process of fatigue lifetime prediction using the stress-life approach considering the theory of critical distances

The steps of the process of lifetime prediction are described below:

a) The aim is to predict the lifetime of a sample subjected to a given input nominal stress ($\sigma_{a,nom}^{net}$).

b) The effective stress ($\sigma_{a,eff}^{net}$) related to this input nominal stress is calculated considering the TCD. For this, it is necessary to calculate the equivalent stress as a function of a distance from the notch root; this calculation depends on the choice of a suitable equivalent stress (σ_a^{eq}) and the critical distance (L).

c) A reference SN curve of total lifetime (obtained experimentally), that replicates the fatigue behaviour of the material, must be chosen in order to establish a relation between stress (fatigue strength) and the number of cycles to failure.

d) In the reference SN curve stresses are usually defined as nominal stresses. Therefore, the stresses on the reference SN curve need to be transformed from nominal to equivalent stress to ensure comparability.

e) The calculated effective stress is used to obtain the lifetime from the *transformed* reference SN curve.
f) The predicted number of cycles to failure (N_f) is determined.

Consequently, for the prediction of fatigue lifetime of the notched specimens of both adhesives the following decisions must be done: choice of reference SN curve, choice of equivalent stress, definition of critical distance parameters. Besides that, it is also necessary to define whether the stress is calculated considering 2D or 3D models. Discussions related to the determination of which equivalent stress, material model and critical distance provided the most accurate lifetime predictions for the structural adhesives are presented in **Section 7.3.**

7.2.1. Choice of reference SN curve

Regarding the choice of reference SN curve, the objective is to use just one type of SN curve for the prediction of all notched specimens. From experimental results (**Chapter 6**), five types of notches were common for both adhesives: internal notch (d10, d20) and external notch (r03, r05, r10). Hence, the reference SN curve should be selected among these types of notches.

The d10-notch has the most distinct fatigue behaviour among notch types (see **Table 3.3** and **Table 3.4)** because it has different cross-section and different stress concentration factor as compared to the other notches. If the predictions using the d10-notch are in a good agreement with experimental results it could indicate that the prediction method is robust. Therefore, the SN curve of total fatigue lifetime of the d10-notch was chosen as the reference SN curve for both adhesives.

7.2.2. Choice of equivalent stress

Two different kinds of equivalent stress were used for the lifetime predictions, namely, the maximum principal stress and the linear Drucker-Prager equivalent stress. The maximum principal stress (σ_{eq}^{MP}) is calculated as a function of the principal stresses ($\sigma_I, \sigma_{II}, \sigma_{III}$), see **Section 2.3.1**, according to **Equation (7.1)**:

$$\sigma_{eq}^{MP} = \max(\sigma_I, \sigma_{II}, \sigma_{III}) \tag{7.1}$$

The maximum principal stress is a hydrostatic stress-independent equivalent stress that has been widely used for lifetime prediction of adhesives [22,54,104].

The second equivalent stress applied in the research work was the linear Drucker-Prager. The use of this equivalent stress is based on the fact that the mechanical behaviour of some structural adhesives is dependent on the hydrostatic stress [65,67]. The linear Drucker-Prager equivalent stress is calculated from:

$$\sigma_{eq}^{DP} = \sigma_{VM} + \sigma_H \tan\beta \tag{7.2}$$

Where σ_{VM} is the von Mises equivalent stress, σ_H is the hydrostatic stress and β is the friction angle (a material property). A detailed description of these parameters is given in **Section 4.2.2.** For the lifetime prediction of notched specimens, the distributions of both equivalent stresses (σ_{eq}^{MP} and σ_{eq}^{DP}) as a function of the distance from the notch root were calculated using FE analysis.

7.2.3. Choice of geometrical model

The stress analysis by means of FEA could be carried out using 2D or 3D models. The use of 2D or 3D models is reflected on the amount of required computational power, simulation time and also post-processing time. 2D analysis are always desirable due their reduced requirements as compared to 3D analysis [11,23]. Nevertheless, in some cases, 3D analysis are necessary, especially for complex geometries (*i.e.* higher stress gradients) [140].

7.2.4. Choice of methodology of the theory of critical distances

In notched specimens due to the presence of stress concentrations, the distribution of equivalent stress in the vicinity of the notch root is not uniform (*i.e.* inhomogeneous) (**Figure 7.1**). In the process of lifetime prediction, a procedure must be applied in order to determine a representative value of the effective stress from the inhomogeneous distribution of equivalent stress [93,96].

The theory critical distances has been widely used for the determination of effective stress, providing support in the fatigue assessment of a wide range of materials, including polymers [94] and adhesives [22,98]. The theory of critical distances relies on a length parameter, the critical distance (L), which determines the size of the process zone in which fatigue takes place. The process of calibration of the critical distances is described in the next section.

The theory of critical distances comprises a group of methodologies that use the critical distance to determine the effective stress as a function of a point, a line, an area or a volume.

In the present work, two of these methodologies were employed: the point method and the line method (**Figure 7.2**). It was assumed, as proposed by Susmel [63], that the critical distance for the line method (L_{LM}) is twice the critical distance for the point method (L_{PM}).

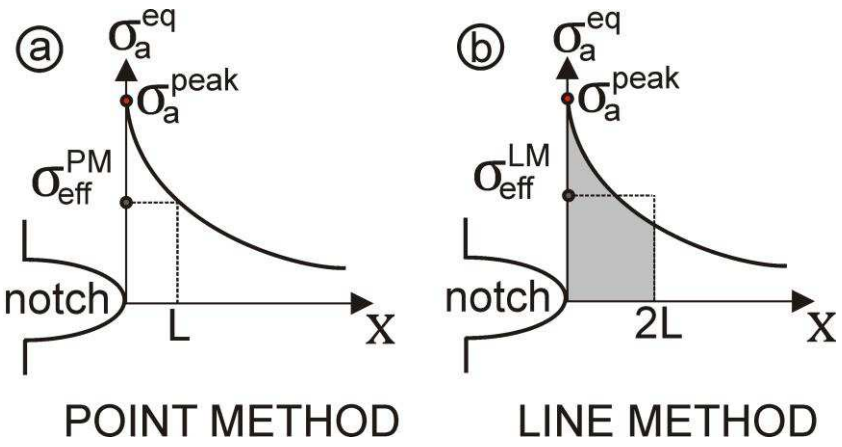

Figure 7.2 – Methodologies of the TCD: point method and line method

In the point method (**Figure 7.2a**), the effective stress (σ_{eff}^{PM}) is defined as function of the critical distance (L) and the distribution of equivalent stress (σ_{eq}) as follows:

$$\sigma_{eff}^{PM} = \sigma_{eq}(L) \tag{7.3}$$

In the line method, the effective stress (σ_{eff}^{LM}) is defined on the basis of the chosen equivalent stress (σ_{eq}) and critical distance (L) according to:

$$\sigma_{eff}^{LM} = \frac{1}{2L}\int_0^{2L} \sigma_{eq}(x)\,dx \tag{7.4}$$

7.2.5. Calibration of critical distance

In the present work it was assumed that the critical distance is a function of the type of material (*i.e.* type of adhesive) [95]. The linear-elastic properties of the structural adhesives under investigation are described in **Table 7.1**.

The process of determination of the critical distance for fatigue was done using a calibration process given by Hoey *et al.* [93]. It considers that "if the theory of critical distances is valid; then, for a given fatigue lifetime the curves for different notched specimens of equivalent stress as function of the distance from the notch root intercept at a certain distance, which is

the critical distance". The stress in which they intercept each other is the effective stress related to the given fatigue lifetime.

Table 7.1 – Linear-elastic properties of adhesives | RB-T and PU-T adhesives

	RB-T adhesive	**PU-T adhesive**
E [MPa]	1673	2289
ν [-]	0.4	0.4

To check the validity of this concept, the calibration process was carried out considering a linear-elastic material behaviour, the maximum principal stress as equivalent stress and the point method for applying the TCD. The process of calibration was done for un-notched and notched specimens (d10, d20, r03) of both adhesives. The curves of equivalent stress as function of distance from notch root are shown in **Figure 7.3**

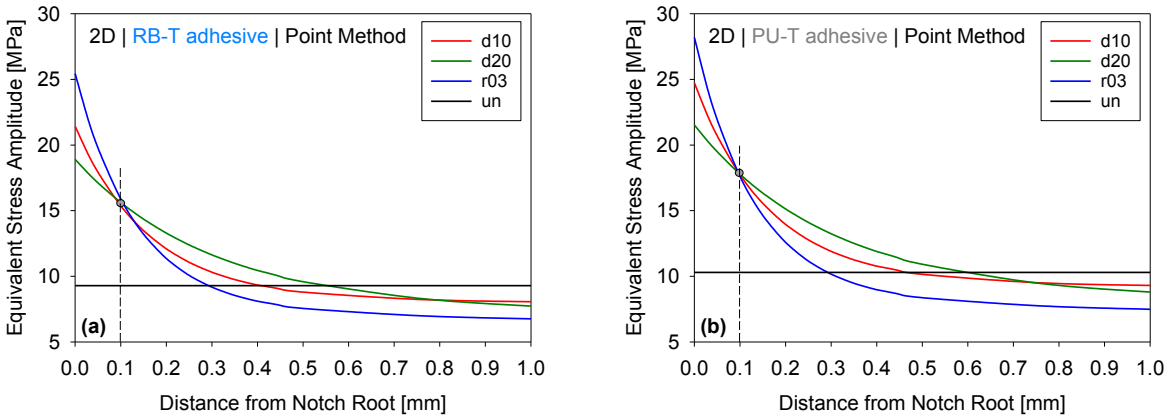

Figure 7.3 – Process of calibration of critical distance considering linear-elastic material behaviour and maximum principal stress [93] | Input nominal stress related to a fatigue lifetime of 10^5 cycles

These results demonstrate that the calibration process using the TCD is sensible since the equivalent stress-distance curves of notched specimens of both adhesives cross each other. For both adhesives, the curves crossed at a distance of 0.1 mm, which was assumed to be the critical distance (L). The un-notched specimen had a different behaviour compared to the notched specimens. This behaviour has been already reported in the literature [93], which suggests that the calibration process should be carried out using notched specimens.

After defining the critical distance, the parameters for lifetime prediction were calibrated for fatigue lifetimes of $N_f = (10^3, 10^4, 10^5, 10^6)$ using the d10-notch as reference SN curve. Two

types of equivalent stress were used in the calibration, namely the maximum principal stress and Drucker-Prager equivalent stress.

The calibration was done as follows: by means of FEA stress calculation, the distributions of equivalent stress regarding the nominal stresses related to the lifetimes of N_f = (10^3, 10^4, 10^5, 10^6) using the SN curves of the d10-sample were calculated. Then, the value of effective stress was defined by taking the value of equivalent stress (σ_{eq}^{MP} or σ_{eq}^{DP}) from a distance *L* of 0.1 mm from the notch root. A value of effective stress was determined for each fatigue lifetime and equivalent stress. The calibrated parameters to be used for the prediction of notched specimens are listed in **Table 7.2** (RB-T adhesive) and **Table 7.3** (PU-T adhesive).

Table 7.2 – Calibrated parameters for the prediction method - reference SN curve (d10-notch) and critical distance (L = 0.1 mm) | RB-T adhesive

N_f	σ_{eff}^{MP} [MPa]	σ_{eff}^{DP} [MPa]	L [mm]
10^3	24.1	29.7	0.1
10^4	19.2	23.7	0.1
10^5	15.4	19.0	0.1
10^6	12.3	15.1	0.1

Table 7.3 – Calibrated parameters for the prediction method - reference SN curve (d10-notch) and critical distance (L = 0.1 mm) | PU-T adhesive

N_f	σ_{eff}^{MP} [MPa]	σ_{eff}^{DP} [MPa]	*L* [mm]
10^3	26.1	32.2	0.1
10^4	21.5	26.5	0.1
10^5	17.7	21.9	0.1
10^6	14.6	18.0	0.1

The process of prediction for given fatigue lifetime (N_f^{pred}) using these calibrated parameters was carried out as follows: in the FEA simulation the input nominal stress ($\sigma_{a,nom}^{calc}$) was increased until the effective stress at a distance of 0.1 mm from the notch root reached the values given in **Tables 7.2** and **7.3**. Afterwards, the experimental lifetime ($N_f^{\exp}$) related to calculated input nominal stress ($\sigma_{a,nom}^{calc}$) was compared to the predicted lifetime (N_f^{pred}).

7.3. VALIDATION OF THE PREDICTION METHOD

The validation of the method was performed for both adhesives by predicting the fatigue lifetime of three types of notched specimens, namely d20, r05 and r03. These notched specimens were selected aiming to have a wide range of stress concentration factor (k_T) and highly stressed regions (L^{HS}) as detailed in **Table 7.4**. The values of k_T were defined analytically, whereas the values of L^{HS} were defined from the distributions of stress with the aid of the **Equation (2.20)**. The material model for the structural adhesives was considered to be linear-elastic.

Table 7.4 – Predicted notched specimens and related stress concentration factors (kT) and highly stress regions (L^{HS})

	d20	**r05**	***r03***
k_T [-]	2.52	3.16	3.90
L^{HS} [mm]	0.049	0.027	0.0172

The results of lifetime predictions for the RB-T adhesive, using 2D and 3D models, the Line and the Point Method and, the Maximum Principal (MP) stress and the Drucker-Prager (D-P) equivalent stress are given in **Figure 7.4** (prediction: d20-notch), **Figure 7.5** (prediction: r05-notch) and **Figure 7.6** (prediction: r03-notch).

The experimentally obtained SN curves (solid line) for each notch type along with the scatter bands of a life factor of 2 (dashed lines) are include in the images to provide a comparative basis for predictions.

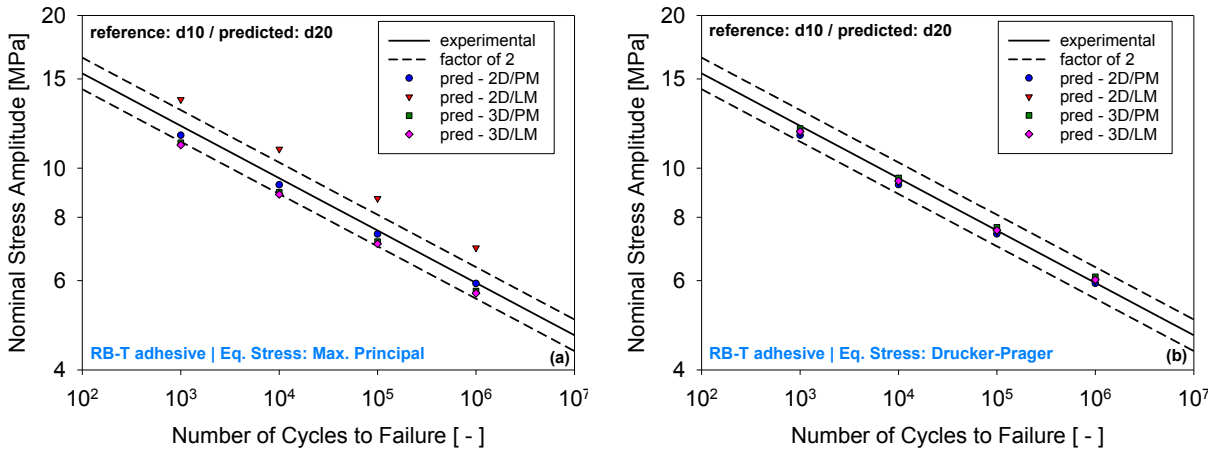

Figure 7.4 – Lifetime prediction (RB-T adhesive/d20-notch) | (a) MP and (b) D-P

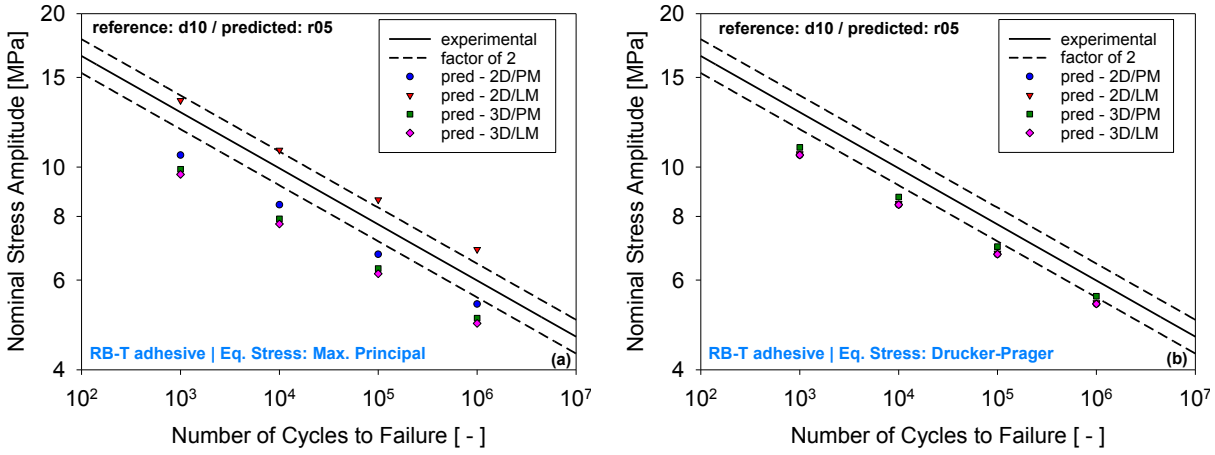

Figure 7.5 – Lifetime prediction (RB-T adhesive/r05-notch) | (a) MP and (b) D-P

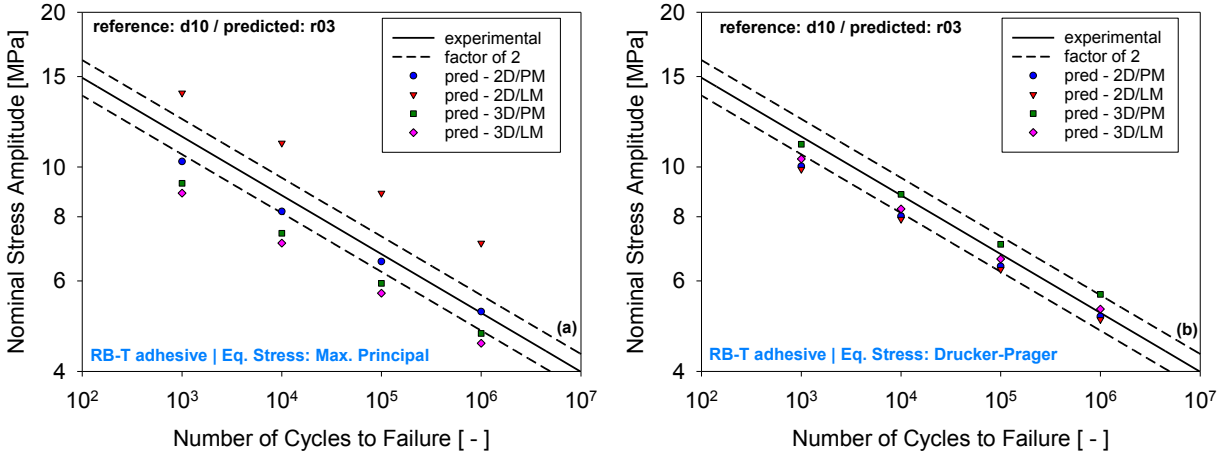

Figure 7.6 – Lifetime prediction (RB-T adhesive/r03-notch) | (a) MP and (b) D-P

The majority of predictions lied within a factor of 2 of the fatigue lifetime, especially considering the Drucker-Prager (D-P) equivalent stress. The best predictions were obtained for the d20-notch, followed by the r03-notch and the r05-notch.

Lifetime predictions for the PU-T adhesive, using 2D/3D models, the Line and the Point Method, and the Maximum Principal stress and the Drucker-Prager equivalent stress are given in **Figure 7.7** (prediction: d20-notch), **Figure 7.8** (prediction: r05-notch) and **Figure 7.9** (prediction: r03-notch). For comparison, the SN curves from experimental testing (solid line) for each notch type along with the scatter bands of a life factor of 2 (dashed lines) are include in the figures. These results indicate that lifetime predictions were generally more accurate for the PU-T adhesive than the RB-T adhesive. For instance, considering the Drucker-Prager equivalent stress every prediction lied within a factor of 2 of the lifetime

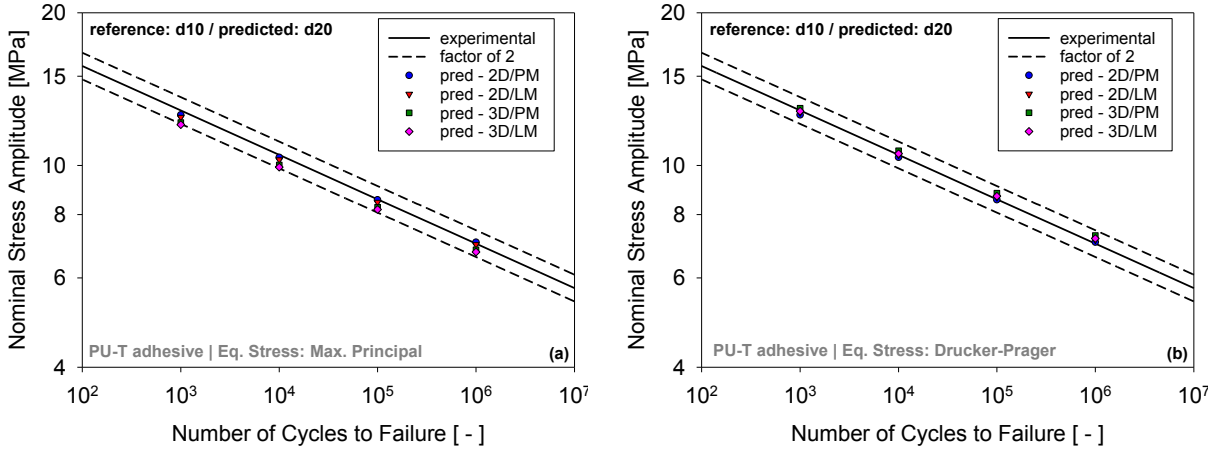

Figure 7.7 – Lifetime prediction (PU-T adhesive/d20-notch) | (a) MP and (b) D-P

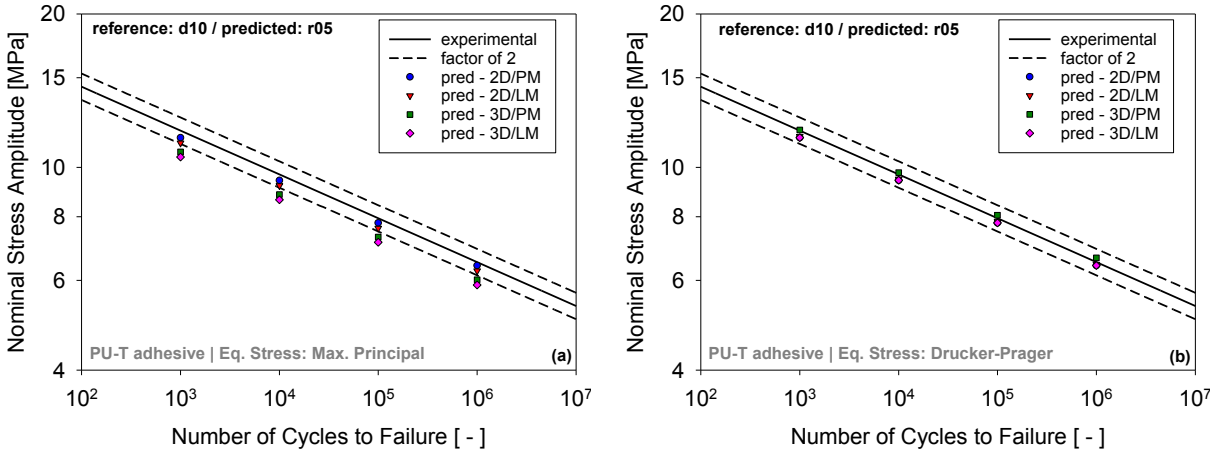

Figure 7.8 – Lifetime prediction (PU-T adhesive/r05-notch) | (a) MP and (b) D-P

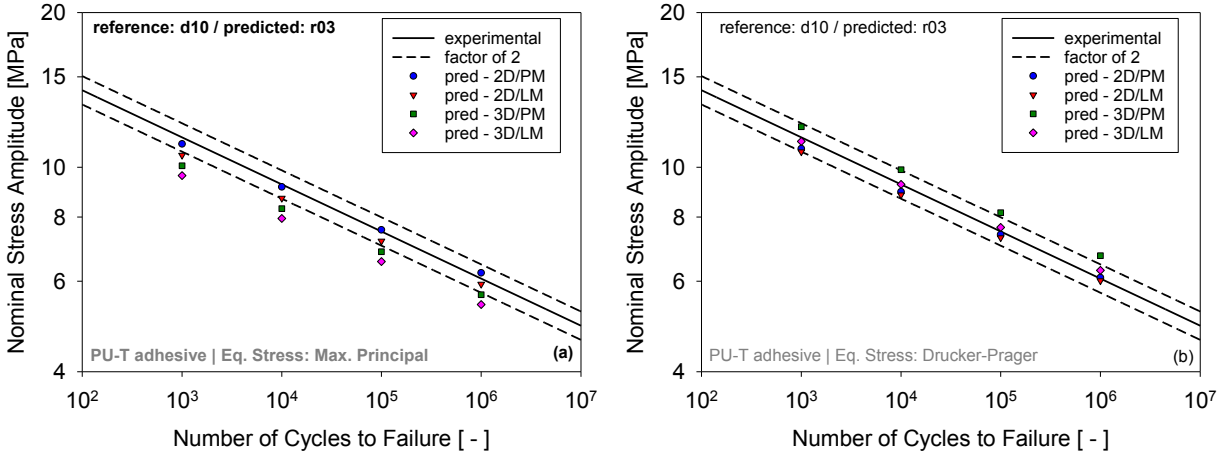

Figure 7.9 – Lifetime prediction (PU-T adhesive/r03-notch) | (a) MP and (b) D-P

The accuracy of lifetime predictions was assessed by comparing predicted lifetimes (N_i^{pred}) with experimental lifetimes (N_i^{exp}) for N_f = (10^3, 10^4, 10^5, 10^6). This fatigue range includes low cycle and high cycle fatigue. The parameter used to quantify the accuracy was the relative error of prediction ($\overline{ER}$) defined as follows:

$$\overline{ER} = \frac{1}{n}\sum_{i}^{n}\frac{\left|\log(N_i^{pred}) - \log(N_i^{exp})\right|}{\log(N_i^{exp})} \tag{7.5}$$

Here n is the number of predicted lifetimes (in the present case n = 4). Therefore, the smaller the values of $\overline{ER}$ are, the better the prediction is. The objective of the present analysis was to evaluate how the choice of equivalent stress (Drucker-Prager or Maximum Principal Stress), geometric model (2D or 3D), TCD methodology (Point Method-PM or Line Method-LM) would affect the accuracy of predictions.

The relative error of lifetime predictions for the notched specimens of the RB-T adhesive is presented in **Figure 7.10**. It is interesting to highlight that despite the use of a linear-elastic material model a good agreement with experimental results was obtained since the relative error of prediction was lower than 19% for all predictions. The best predictions were obtained for the d20-notch (smallest stress concentration).

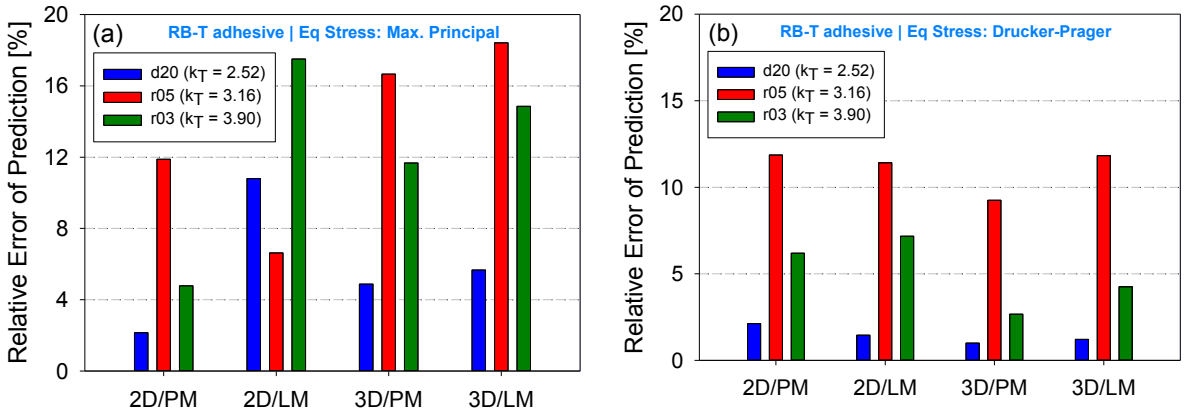

Figure 7.10 – Relative error of prediction (RB-T adhesive) | (a) Maximum Principal Stress and (b) Drucker-Prager Equivalent Stress

Predictions using the Drucker-Prager equivalent stress were more accurate ($\overline{ER}$ < 12%) than the ones with the Maximum Principal Stress. Considering the Drucker-Prager equivalent stress it could be inferred that: (i) 3D models provided lower prediction errors and (ii) no clear effect is seen with regards to TCD methodology (Point Method or Line Method). For the

Maximum Principal Stress, no clear trend regarding geometrical model or TCD methodology was observed.

The relative error of lifetime predictions for the notched specimens of the PU-T adhesive is shown in **Figure 7.11**. The predictions for the PU-T adhesive were more accurate ($\overline{ER}$ < 14%) than to the ones of the RB-T adhesive. Again, very good predictions ($\overline{ER}$ < 6%) were obtained considering the Drucker-Prager equivalent stress and 3D models. For the Maximum Principal Stress, the use 2D models provided better predictions ($\overline{ER}$ < 5%). The effect of TCD-methodology on the predictions showed no clear trend.

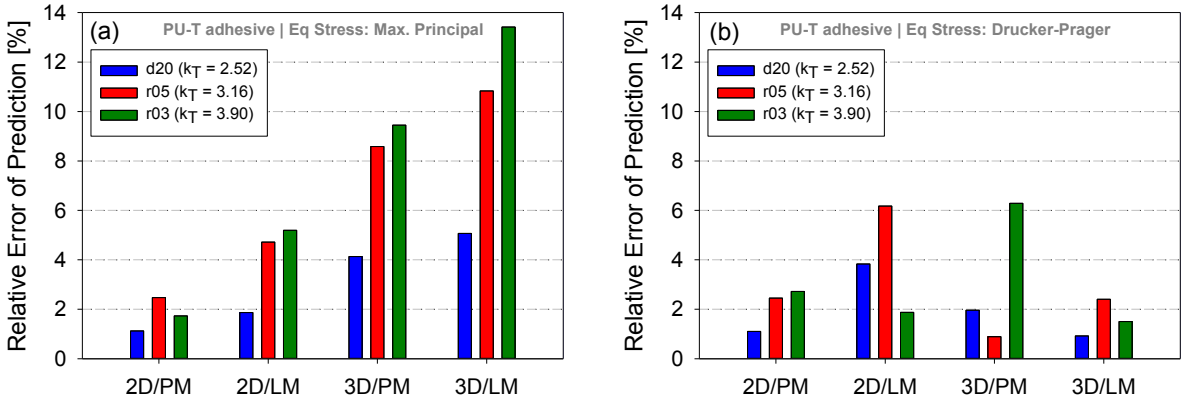

Figure 7.11 – Relative error of prediction (PU-T adhesive) | (a) Maximum Principal Stress and (b) Drucker-Prager Equivalent Stress

The relative error of predictions for both adhesives suggests that the choice of equivalent stress is a key aspect in the process of prediction. This is evidenced by the fact that the best predictions (for both adhesives) were obtained considering the Drucker-Prager equivalent stress. This could be related to the hydrostatic stress dependence of the mechanical behaviour of some structural adhesives [65,67]. Therefore, the Drucker-Prager equivalent stress, which takes into account the influence of hydrostatic stress, is likely more able to reproduce the fatigue behaviour of the adhesives. For both adhesives, regarding the geometrical model (2D or 3D) it was possible to achieve lower prediction errors for the Drucker-Prager equivalent stress by using 3D models. For the maximum principal, in the majority of cases, better predictions were obtained using 2D models. No clear trend was observed with regards to the TCD-methodology (Point Method or Line Method).

Due to the novel aspect of the present research, no other work dealing with the lifetime prediction of notched adhesive specimens has been found in the literature. However, to provide comparative values some other works dealing with different notched engineering

materials are described here. Taylor and Wang [152] predicted the fatigue limit of components containing stress concentration in a wide range of notch geometries, loading types, R-ratios and materials. The authors have stated than an error of less than 20% can be considered acceptable due to the scatter related to fatigue testing. Hoey and Taylor [93] predicted with a maximum error of 16% the fatigue strength of notched PMMA samples with stress concentration factor ranging from 1.4 to 11. Susmel and Taylor [153] predicted the fatigue limit of sharply notched specimens (stress concentration factor between 6.4 and 11.2) with an error usually less than 15%.

These results suggest that the values of maximum relative error obtained in the present research work considering the Drucker-Prager equivalent stress (12% for the RB-T adhesive and 6% for the PU-T adhesive) are below typical errors found in the literature (for other engineering materials).

Another potential approach for improving the prediction accuracy is to consider the critical distance not as a constant value, but rather as a function of the fatigue lifetime as suggested by Susmel *et al.* [154]. In **Figure 7.12** the relative error of prediction as function of the fatigue lifetime (N_f) is presented for the r03-notch (highest k_T) and the d20-notch (lowest k_T) of the RB-T adhesive.

The highest errors of prediction were obtained for the lowest values of N_f; especially, considering the Maximum Principal Stress. The higher values of relative error related to lower values of N_f are more evident for the r03-notch. For the d20-notch, the influence of N_f is smaller for the Maximum Principal Stress and nearly non-existent for the Drucker-Prager Equivalent Stress.

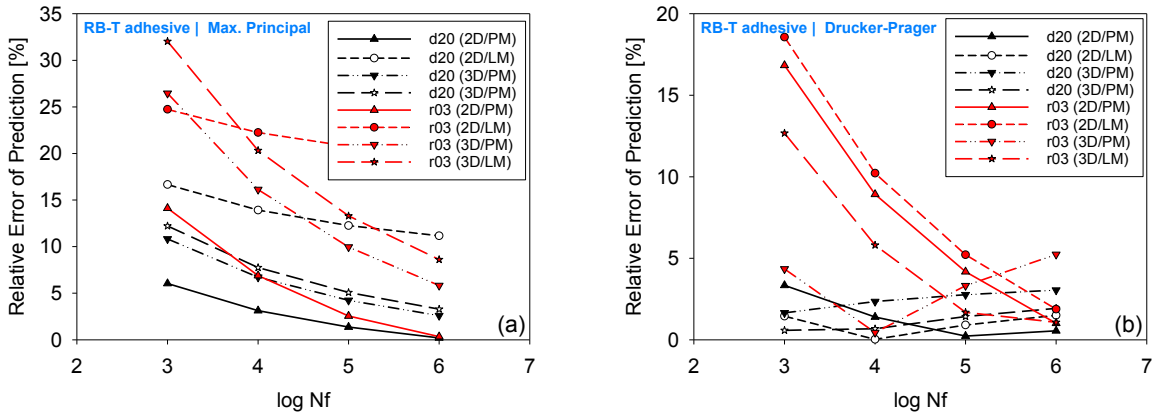

Figure 7.12 – Relative error of prediction as function of number of cycles to failure (RB-T adhesive) | (a) Maximum Principal Stress and (b) Drucker-Prager Equivalent Stress

The relative error of prediction as function of the fatigue lifetime (N_f) for the r03-notch and the d20-notch of the PU-T adhesive are shown in **Figure 7.13**. For the Maximum Principal stress, the relative error was higher for lower values of N_f, especially for r03-notch. Regarding the Drucker-Prager equivalent stress, the effect of the number of cycles on the relative error of prediction was evident for the r03-notch and unclear for the d20-notch (nearly constant value of relative error of prediction).

Based on these results where prediction errors tended to decrease for higher values of N_f it is possible to assume that varying the critical distance as a function of N_f could result in an improvement of prediction accuracy (which is already in a very good agreement with experimental results).

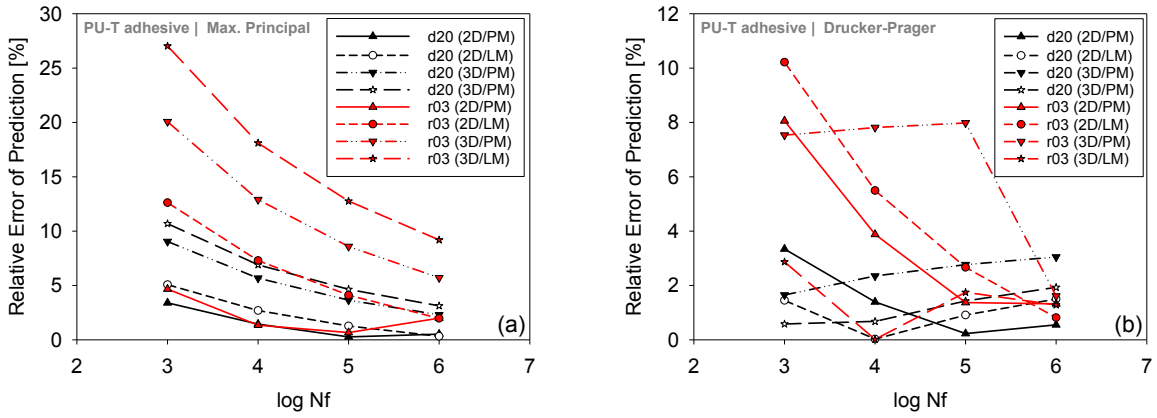

Figure 7.13 – Relative error of prediction as function of number of cycles to failure (RB-T adhesive) | (a) Maximum Principal Stress and (b) Drucker-Prager Equivalent Stress

7.4. LIFETIME PREDICTION CONSIDERING AN ELASTO-PLASTIC MATERIAL MODEL

In notched specimens with the combination of stress concentrations and high nominal stresses it is expected that plastic deformation takes place in the vicinity of the notch root [88,99]. Therefore, the use of an elasto-plastic material behaviour to predict the fatigue lifetime of structural adhesives under investigation is reasonable. However, in FE analysis the use of an elasto-plastic model is more complex than a linear-elastic model [11].

The aim of the present analysis is to evaluate whether the consideration of an elasto-plastic material behaviour improves the accuracy of predictions. The exact same procedure to set-up the prediction method (**Section 7.3**) was carried out, the only difference being the material

model. The process of implementation of an elasto-plastic material model is described in **Section 4.2.2** and material properties are listed in **Table 4.1.**

Since the choice of TCD-methodology (Point Method or Line Method) has not presented any clear influence in the prediction accuracy only the Point-Method was considered the following analysis. Relative error of prediction ($\overline{ER}$) was calculated by comparing predicted lifetime and experimental lifetime for N_f = (10^3, 10^4, 10^5, 10^6). The analysis was focused on the r03-notch and r05-notch because results for the d20-notch were already good ($\overline{ER}$ < 5% / **Figure 7.10-Figure 7.11**).

The relative errors of prediction for linear-elastic and elasto-plastic material models for the r03-notch and r05-notch of the RB-T adhesive are given in **Figure 7.14**.

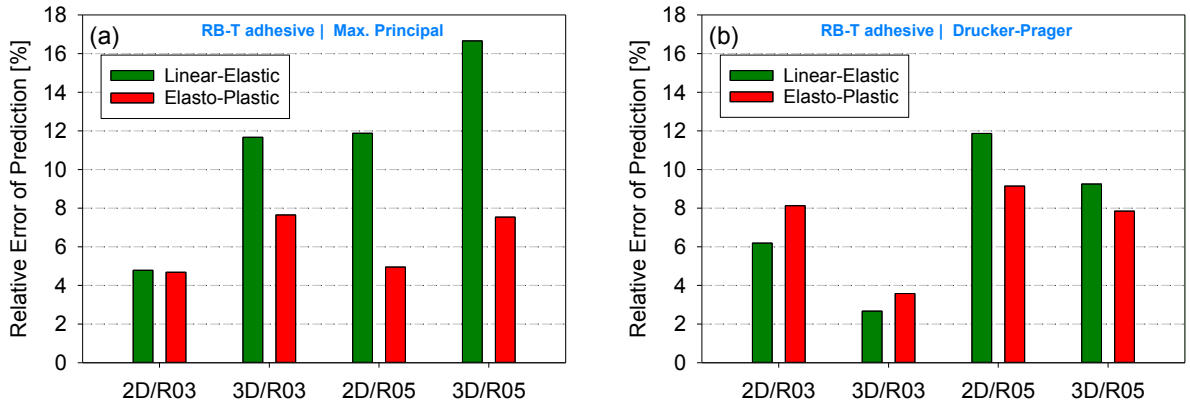

Figure 7.14 – Comparison of error of prediction between linear-elastic and elasto-plastic material models (RB-T adhesive) | (a) Maximum Principal Stress and (b) Drucker-Prager Equivalent Stress

For the Maximum Principal Stress the use of elasto-plastic model provided an error of prediction under 8% in all cases. In the case of the Drucker-Prager equivalent stress, the changes are less than 3% in the relative error: elasto-plastic model were slightly worse for the r03-notch and slightly better for the r05-notch.

In **Figure 7.15** the relative errors of prediction for the r03-notch and r05-notch of the PU-T adhesive for linear-elastic and elasto-plastic material models are presented. Surprisingly, for both Maximum Principal Stress and Drucker-Prager Equivalent stress, the relative error of prediction was slightly higher with the elasto-plastic model. Nevertheless, it is important to highlight that this error difference is very small (< 5%).

These results indicate that the accuracy of prediction of the elasto-plastic models depends on the type of structural adhesive. This could be associated with the distinct mechanical properties of the adhesives since it was possible to achieve higher accuracy levels, using elasto-plastic model, for the RB-T adhesive (more ductile adhesive). On the other hand, for the PU-T adhesive (more brittle), linear-elastic models provided better predictions.

The high prediction accuracy of linear-elastic models could be explained by the fact that the effect of peak stresses due to stress concentrations is addressed by considering the effective stress from a distance from the notch root.

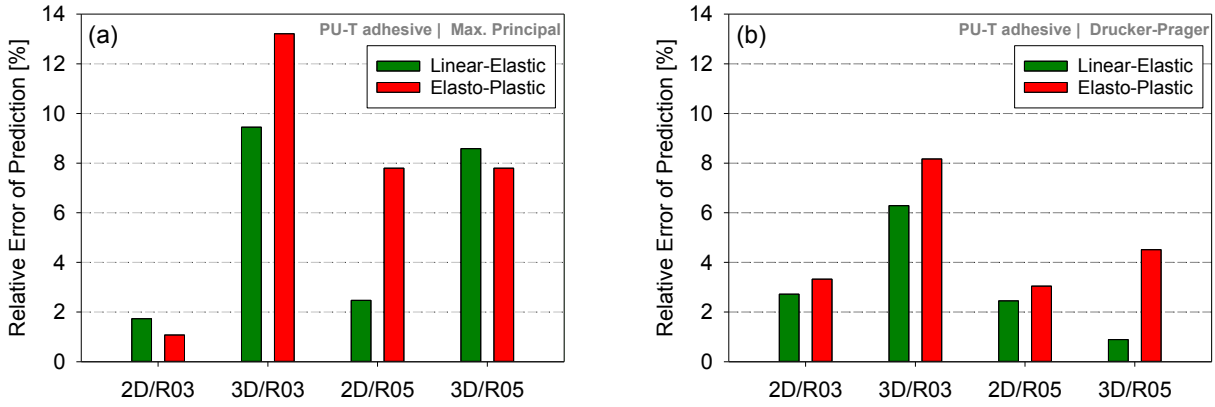

Figure 7.15 – Comparison of error of prediction between linear-elastic and elasto-plastic material models (PU-T adhesive) | (a) Maximum Principal Stress and (b) Drucker-Prager Equivalent Stress

7.4.1. Outlook and potential future works

The accuracy of lifetime predictions with regards to experimental results for different notched specimens and different structural adhesives suggest the effectiveness of the proposed method in accurately predicting the fatigue lifetime. Moreover, the proposed method was able to overcome the limitations of "transferability" of the stress-life approach by using just one reference SN curve (d10-notch) to predict the lifetime of all notched specimens.

An important aspect that was successfully addressed was the determination of the critical distance. In the present work the critical distance was determined by a process of calibration using experimental data (**Section 7.2.5**). It is important to highlight that the calibration requires the experimental data of only two samples (with different stress concentrations) at the same fatigue lifetime. The lower values of prediction error obtained with the calibrated critical distances suggest the validity of this process (**Section 7.3**). This calibration process

has been used in adhesives for quasi-static loading [101]. However, its usage for the fatigue of adhesive as done in the present work is innovative. Moreover, it was suggested that it is possible to reduce the prediction errors by considering the critical distance as a function of the fatigue lifetime [154].

For future research it could be interesting to expand the proposed method of lifetime prediction by enabling it to provide information on the state of the damage during the process of fatigue, which is interesting for predicting the evolution of damage. Moreover, it could be beneficial for design purposes to include in the method a feature to distinguish crack initiation lifetime and crack propagation lifetime.

7.5. SUMMARY

An accurate prediction of fatigue lifetime under stress concentration conditions is a fundamental aspect to expand the reliability of structural adhesives [23]. With a proper method for calculation of fatigue lifetime, it is possible to minimise experiments with real size structures allowing a reduction of development time and production costs [85].

In this regard the present chapter focused on the definition of a method for predicting the fatigue lifetime of notched specimens of the structural adhesives under investigation. The proposed method (**Section 7.1**) was based in the stress-life approach using the theory of critical distances (TCD) to account for the effects of stress concentrations on the fatigue lifetime.

The proposed method requires a reference SN curve related to total lifetime (obtained experimentally) to provide a relationship between stress amplitude and number of cycles to failure (**Section 7.2.1**). Then, a stress analysis using FEA is to be carried out to determine the information of the equivalent stress (**Section 7.2.2**) as a function of the distance from the notch root. Finally, the fatigue lifetime is obtained by correlating the results of stress calculations with the reference SN curve (defined in terms of equivalent stress).

Lifetime predictions were performed initially considering linear-elastic material behaviour. The chosen reference SN curve was the d10-notch, which has the most distinct behaviour as compared to the other notched specimens. This choice was done aiming to evaluate the robustness of the method. Two types of equivalent stress (**Section 2.3.1**) were used for predictions: Maximum Principal Stress (hydrostatic stress independent) and the Drucker-Prager Equivalent Stress (hydrostatic stress dependent). Regarding geometrical models

(**Section 4.1**) 2D and 3D model were employed. Two TCD-methodologies (**Section 2.4.3**) were applied, namely the Point and the Line Method. The critical distance was determined by a process of calibration that requires the experimental data of only two samples (with different stress concentrations) at the same fatigue lifetime.

The verification of the prediction method (**Section 7.3**) was performed for both adhesives by predicting the fatigue lifetime of three types of notched specimens: d20, r05 and r03. These notched specimens were selected aiming to have a wide range of stress concentration factor and size of highly stressed regions. The parameter used to quantify the accuracy was the relative error of prediction ($\overline{ER}$), which was defined by comparing predicted lifetimes with experimentally obtained lifetimes.

The results of relative error of prediction for both adhesives have shown the importance of proper choice of equivalent stress. This is evidenced by the fact that the best predictions for both adhesives ($\overline{ER}$ < 12%) were obtained considering the Drucker-Prager equivalent stress. This could be related to the hydrostatic dependence of the mechanical behaviour of structural adhesives [133,137]. Then, the Drucker-Prager equivalent stress was likely more able to reproduce the fatigue behaviour of the adhesives. The values of relative error obtained in the present research work considering the Drucker-Prager equivalent stress were below typical errors found in the literature (for other engineering materials). Regarding the geometrical model (2D or 3D) it was possible to achieve lower prediction errors for the Drucker-Prager equivalent stress by using 3D models. For the Maximum Principal stress, in the majority of cases, better predictions were obtained using 2D models. No clear trend was observed with regards to the TCD-methodology (Point Method or Line Method).

These lower values of prediction error obtained with the calibrated critical distances indicate the validity of the process of calibration. The calibration process has been used in adhesives for quasi-static loading [90]. However, its usage for the fatigue of adhesive as done in the present work is innovative. Moreover, it was revealed that it is possible to reduce even further prediction errors by considering the critical distance as a function of fatigue lifetime, especially for the Maximum Principal Stress and at a high stress concentration factor (r03-notch).

The results of lifetime predictions considering elasto-plastic material behaviour (**Section 7.4**) indicated that the accuracy improvement of the elasto-plastic models was dependent on the type of structural adhesives. This could be attributed to the mechanical properties of the

adhesives. For the RB-T adhesive (more ductile) with the use of elasto-plastic models it is possible to achieve higher accuracy levels. On the other hand, for the PU-T adhesive (more brittle), linear-elastic models provided better predictions. The prediction accuracy of linear-elastic models could be explained by the fact that the effect of stress concentrations is addressed by considering the effective stress from a distance from the notch root.

Based on the accuracy of lifetime predictions with regards to experimental results for different notched specimens (d20: $\overline{ER}$ < 4%, r05: $\overline{ER}$ < 12% and, r03: $\overline{ER}$ < 7%) and different structural adhesives (PU-T: $\overline{ER}$ < 6% and RB-T: $\overline{ER}$ < 12%) it is possible to assume the effectiveness of the proposed method in predicting the fatigue lifetime of notched specimens. In this sense, the proposed method was able to overcome the limitations of "transferability" of the stress-life approach by using just one reference SN curve to predict the lifetime of all notched specimens.

8. CONCLUSIONS AND OUTLOOK

This final chapter contains a summary of the results from the present research work. **Section 8.1** presents a brief review of previous sections including experimental and numerical methodology, quasi-static results, fatigue results and fatigue lifetime predictions. Besides that, concluding remarks are made to evaluate whether the research objectives were accomplished. **Section 8.2** provides an assessment of the novel contributions of the present work to the research field of fatigue of structural adhesives. Finally, some suggestions for future topics of research that could widen the present study are given in **Section 8.3**.

8.1. CONCLUSIONS

With the increasing demand for lightweight components, structural adhesives have been playing a major role providing multi-material constructions with high stiffness and low weight [1,25]. Under service conditions, structural adhesives are exposed to cyclic loads (*e.g.* rotating blades, engine vibration) that can lead to failure due to fatigue [8]. The phenomenon of fatigue, which involves the phases of crack initiation and crack propagation, is very complex [9]. In this regard, fatigue lifetime is considerably reduced in the presence of stress concentrations, which arise from notches (*e.g.* holes, corners, edges) that are inherent characteristics on the project of components [88]. The presence of stress concentrations make it difficult to accurately predict the fatigue lifetime of notched components. For this reason, designers often rely on large safety factors to ensure reliability of bonded structures. This over-conservative design could lead to cost and performance losses [7,10].

In this scenario the aim of present research work (**Section 1.2**) was to investigate the effect of stress concentrations on the fatigue behaviour of structural adhesives with focus on the prediction of fatigue lifetime of notched specimens.

Two different types of commercial structural adhesives (RB-T and PU-T) were employed in this study. Both are hot curing single component adhesives (**Section 3.1**). The RB-T adhesive is a rubber-toughened epoxy whereas the PU-T adhesive is a polyurethane-toughened epoxy. They have similar tensile strength. Nevertheless, their mechanical properties differ slightly in the stiffness and mainly in terms of plastic deformation prior to failure

It is important to highlight that the present work was focused on the investigation of notched bulk specimens. The notches introduced in the specimens were chosen to cover a wide range of stress concentrations, stress gradients, and stress triaxialities. Two fundamentally different

types of notches were used: (i) internal notches (with different diameters) and (ii) external notches (with different radii). With this approach it was possible to assess the effect of stress concentration without the influence of adherends (**Section 3.2**). However, the knowledge acquired in the present research work is to be used for the understanding of the effect of stress concentrations on adhesively bonded joints, which are the main application of structural adhesives.

An experimental set-up (**Section 3.3**) was built for quasi-static and fatigue tests. During testing the samples were monitored with cameras and the stiffness was calculated from displacement measurements of a clip-on extensometer. This experimental set-up provided insights into the progression of damage (*i.e.* degradation of stiffness) and evolution of stress whitening whilst allowing the detection of crack initiation. Fracture surface analysis was performed using optical microscopy.

Numerical investigations (**Section 4**) were carried out by means of Finite Element Analysis (FEA) using a commercial software (Dassault© Abaqus). The material behaviour of adhesives was modelled by an elasto-plastic behaviour combined with a failure criterion. The elastic behaviour of the adhesive was determined in terms of Young's modulus and the Poisson's ratio (**Section 4.2**). The plastic behaviour was assumed to be hydrostatic stress-dependent expressed by a linear Drucker-Prager model. The quasi-static failure was defined by a failure criterion based on the equivalent plastic strain. Regarding geometrical models, FEA was performed in 2D-plane stress and in 3D.

Quasi-static experiments were performed under displacement control with two displacement rates (2 mm/min and 10 mm/min). For un-notched specimens (**Section 5.1**), both adhesives presented great distinction with regard to plastic deformation prior to failure with an average strain at break of 15% for the RB-T adhesive and 8% for the PU-T adhesive. Moreover, the adhesives showed strain-rate sensitivity with an increase on tensile strength of around 6% for the highest strain rate (10 mm/min).

Furthermore, quasi-static experiments on internally and externally notched specimens (**Section 5.2**) revealed that tensile behaviour of adhesives changed due to the presence of notches. A strong reduction of elongation at break was observed for both adhesives. Regarding maximum net stress one adhesive has shown notch strengthening (RB-T) and the other notch weakening (PU-T). This distinct behaviour could be associated to the so-called

constraining effect that occurs under higher levels of stress and plastic deformation, which is more present in more ductile materials (*e.g.* RB-T adhesive).

This distinct behaviour was also observed in test monitoring images that revealed that the RB-T adhesive underwent widespread stress whitening (crazing) prior to failure, whereas in the PU-T adhesive this whitening was more localised. Fracture surface analysis demonstrated the presence of highly damaged regions with voids close to the notch regions. These regions were larger for the RB-T adhesive as compared to the PU-T. These findings were correlated to 2D-linear elastic FEA calculations that indicated that the stress whitening (*i.e.* high damage) and voids occur within regions with higher values of stress concentration and stress triaxiality.

Numerical simulation results (**Section 5.3**) for both adhesives indicate that the 3D models are suitable for modelling the quasi-static behaviour of the adhesives including very high levels of stress. 2D-plane stress models, although displaying slightly premature failure compared to experiments, could still be suitable for modelling the fatigue of the adhesives. Predictions considering 2D-plane stress models underestimated the values of failure stress between 13% and 25%. At the same time, predictions with 3D models showed excellent agreement regarding experimental results with an overall average error (for both adhesives) of 5.5% for all notch types. Compared to the accuracy of other works in the literature (for other notched materials), the accuracy obtained in the present work indicates the suitability of the proposed failure criterion (equivalent plastic strain) in predicting the failure stress of notched specimens of the adhesives under investigation

Fatigue experiments of un-notched, internally notched and externally notched specimens were tested under sinusoidal cyclic tension-tension load with constant amplitude and stress ratio of R = 0.1. The SN curves of un-notched specimens (**Section 6.1**) indicated higher fatigue strength of the PU-T adhesive in the entire fatigue range. Regarding damage evolution curves of un-notched specimens, higher values of stress amplitude caused faster damage evolution for both adhesives. Fracture surface analysis revealed that the mechanical properties of adhesives altered their fracture behaviour since RB-T adhesive (more ductile) had larger regions of stress whitening as compared to PU-T adhesive. Furthermore, fracture images seem more “rough” at high levels of stress. For low levels of stress fracture surfaces are more “flat”, especially for the PU-T adhesive (more brittle).

Fatigue experiments with internally notched specimens (**Section 6.2**) demonstrated a reduction of fatigue strength with an increasing notch size. Reduction of fatigue strength was

stronger at the high cycle fatigue range. Fatigue results revealed that under stress concentration conditions not only the value of the maximum peak stress (stress concentration factor) affects the fatigue strength, but the size of the highly stress volume plays a key role in the reduction of fatigue strength and on the change of the slope of the SN curves.

Damage curves of internally notched specimens showed gradual increase of damage in the beginning of cycles. Then, the slope of the damage curve started to increase with increasing number of cycles until the damage variable increased rapidly near the critical number of cycles corresponding to the fatigue lifetime. Moreover, there was a reduction of maximum damage prior to failure with an increasing notch size. Fracture surface analysis combined with 3D-FEA investigation revealed that the nucleation of voids is more present at regions with higher stress triaxiality ratios.

Fatigue experiments with externally notched specimens (**Section 6.3**) revealed that the reduction of fatigue strength was proportional to the stress concentration factors of the notches, *i.e.* higher values of stress concentration factor caused stronger fatigue strength reduction. The SN curves of different notched specimens had the same slope. However, the curves were translated according to the value of stress concentration factor of the samples.

The experimental set-up constructed for the present investigation enabled an accurate definition of crack initiation lifetime. The SN curves for crack initiation lifetime of both adhesives (**Section 6.3.2**) indicated that for both adhesives most of the fatigue lifetime was spent on the crack initiation phase (60 to 95%). Moreover, it was found that crack initiation phase is shortened by an increasing stress concentrations factor. The severity of this effect is influenced by the mechanical properties of the adhesives (the most ductile adhesive was more sensitive) and by the level of applied stress.

Damage curves of specimens with external notches showed that the crack initiation causes a sudden increase of damage (*i.e.* reduction of stiffness) in the specimens. For samples with different notches under the same level of stress the evolution of damage follows the same trend (same slope). However, for samples with higher stress concentration factor (sharp notch) the crack initiation occurred earlier.

Regarding fracture surface analysis, the size of the stress whitening region was larger for tests under lower stress amplitude. This could be explained by the fact that the propagation of cracks reduces the size of the effective area bearing the load. For lower values of stress the size of this effective area could be smaller as compared to higher values of stress. By

comparing the adhesives, once again the RB-T adhesive exhibited a larger stress-whitening region as compared to PU-T adhesive.

The understanding of the effect of stress concentrations on the fatigue behaviour provided a framework for defining the method for lifetime prediction of notched specimens. The proposed method for lifetime prediction is based on the stress-life approach using the theory of critical distances (TCD) to account for the effects of stress concentrations on the fatigue lifetime (**Section 7.1**). The proposed method (**Section 7.2**) requires a reference SN curve related to total lifetime (obtained experimentally) to provide a relationship between stress amplitude and fatigue lifetime. Then, a stress analysis using FEA is to be carried out to determine the information of the equivalent stress as a function of the distance from the notch root. Finally, the fatigue lifetime is obtained by correlating the results of stress calculations with the reference SN curve (transformed in terms of the equivalent stress).

Lifetime predictions were performed initially considering linear-elastic material behaviour (**Section 7.3**). Two types of equivalent stress were used for predictions: Maximum Principal Stress (hydrostatic stress-independent) and the Drucker-Prager Equivalent Stress (hydrostatic stress-dependent). Regarding geometrical models 2D and 3D model were employed. Two TCD-methodologies were applied, the Point Method and Line Method. The critical distance was determined by a process that required the experimental data of only two samples (with different stress concentrations) at the same fatigue lifetime.

The validation of the prediction method was performed for both adhesives by predicting the fatigue lifetime of three types of notched specimens. These notched specimens were selected aiming to have a wide range of stress concentration factor and highly stressed regions. The parameter used to quantify the accuracy of lifetime predictions was the relative error of prediction, which was defined in terms of predicted lifetimes and experimentally obtained lifetimes.

Prediction results showed the importance of proper choice of equivalent stress since the best predictions (for both adhesives) were obtained considering the Drucker-Prager equivalent stress. This could be related to the hydrostatic dependence of the mechanical behaviour of structural adhesives [133,137]. It was possible to achieve lower prediction errors for the Drucker-Prager equivalent stress by using 3D models. For the Maximum Principal stress, in the majority of cases, better predictions were obtained using 2D models. No clear trend was observed with regards to the TCD-methodology (Point Method or Line Method).

The lower values of prediction error obtained with the calibrated critical distances indicate the validity of the process of calibration. The calibration process has been used in adhesives for quasi-static loading [90]. However, its usage for the fatigue of adhesive as done in the present work is innovative. Moreover, it was revealed that it is possible to reduce prediction errors by considering the critical distance as a function of fatigue lifetime.

The improvement of accuracy obtained with the consideration of elasto-plastic models (**Section 7.4**) was dependent on the type of structural adhesives. This could be attributed to the mechanical properties of the adhesives. For the RB-T adhesive (more ductile) with the use of elasto-plastic models it is possible to achieve higher accuracy levels. On the other hand, for the PU-T adhesive (more brittle), linear-elastic models provided better predictions. The prediction accuracy of linear-elastic models could be explained by the fact that the effect of peak stresses due to stress concentrations is addressed by considering the effective stress from a distance from the notch root.

The accuracy of lifetime predictions (maximum error of 12%) indicates the effectiveness of the proposed method in predicting the fatigue lifetime of notched specimens. The values of relative error obtained with the proposed method considering the Drucker-Prager equivalent stress were below typical errors found in the literature (for other engineering materials). Besides that, the proposed method was able to overcome the limitations of "transferability" of the stress-life approach by using just one reference SN curve to predict the lifetime of all notched specimens.

8.2. NOVEL CONTRIBUTIONS OF THE PRESENT RESEARCH WORK

The present research work provides a framework for future investigations regarding the fatigue of structural adhesives under stress concentration conditions. This is one of the first works that offer a complete study of the effect of stress concentration on fatigue of adhesives, which includes influence of mechanical properties, stress concentration factor, stress triaxiality and size of highly stressed region.

The experimental set-up design including notched bulk specimens, test monitoring and stiffness measurements allowed the detection of crack initiation whilst providing reliable experimental data on: (i) quasi-static strength, (ii) total lifetime, (iii) lifetime for crack initiation, (iv) damage evolution and (v) fracture behaviour. The findings, conclusions and experimental data of the present investigation can be used by researchers in order to extend the prediction model proposed here. Moreover, the present investigation provides guidelines

for designers in how to make a proper choice of SN curves for lifetime prediction (regarding stress concentration factor and highly stressed region).

Furthermore, the following findings are considered highly relevant regarding the effect of stress concentrations on the quasi-static and fatigue behaviour of structural adhesives

- Equivalent plastic strain is a good failure criterion for notched specimens, especially considering 3D models. It showed excellent agreement with experimental results (overall average error of 5.5% for both adhesives).

- Experimental evidence was given to support the understanding of the occurrence of notch strengthening and its relation to the effect of constraining of the adhesive under higher levels of stress (plastic deformation).

- Fracture surface analysis enabled the understanding of the mechanisms of failure of adhesives under stress concentration conditions by revealing the presence of highly damaged regions (*e.g.* stress whitening) with voids close to the notch regions. These regions of stress whitening were larger for the most ductile adhesive. These findings were correlated to 3D-FEA calculations that indicated that these regions are associated with higher values of stress concentration and stress triaxiality.

- Fatigue results with internally notched specimens revealed that the size of the highly stressed region plays a key role in the reduction of fatigue strength.

- Fatigue results with externally notched specimens have shown that the fatigue strength is reduced with an increasing stress concentration factor.

- A model was proposed to explain the behaviour of SN curves of notched specimens in which the slope is controlled by the size of the highly stressed region and the stress concentration factor translates (shifts up and down) the position of the curve.

- The SN curves for crack initiation lifetime of both adhesives have indicated that most of the fatigue lifetime (60 to 95%) was spent on the crack initiation phase.

- The crack initiation phase is shortened by an increasing stress concentration factor. The severity of this shortening is influenced by the mechanical properties of the adhesives (the most ductile adhesive was more sensitive) and by the level of applied stress.

- Damage curves of externally notched specimens showed that the crack initiation causes a sudden increase of damage (*i.e.* reduction of stiffness) in the samples.

With regards to the proposed method for fatigue lifetime prediction of notched specimens the following information will be relevant for future researchers:

- Prediction results showed the importance of proper choice of equivalent stress: best predictions (for both adhesives) were obtained considering the Drucker-Prager equivalent stress.

- The process of calibration of the critical, which requires experimental data of only two samples (with different stress concentrations) at the same fatigue lifetime, has been proved valid. The process has been used in adhesives for quasi-static loading. Nevertheless, its application for fatigue lifetime predictions of adhesive as done in the present work is novel.

- Accuracy of lifetime predictions using the proposed method (maximum relative error of 12%) has shown that it is possible to overcome the limitations of "transferability" of the stress-life approach for notched specimens with a proper choice of equivalent stress, geometrical model and definition of critical distance.

8.3. SUGGESTIONS FOR FUTURE RESEARCH

The framework provided by the present research work that dealt with notched bulk specimens could be used for future investigations dealing with adhesively bonded joints, potentially focusing on the combined effect of adherends and stress concentrations. Since the present research revealed the effect of stress concentration factor and size of highly stressed region on the SN curves of bulk adhesive specimens, future studies should focus in developing methods to evaluate whether these effects are reproduced in adhesively bonded joints.

Fatigue experiments are costly and time-consuming. For this reason, the present work has focused on tests under constant amplitude with a fixed stress ratio, which provides future research opportunities for investigations under variable amplitude and different stress ratios.

For future research it could be interesting to expand the proposed method of lifetime prediction by enabling it to provide information of the state of damage during the process of fatigue, and to include a feature to distinguish crack initiation lifetime and crack propagation lifetime.

9. REFERENCES

[1] Adams RD. Adhesive bonding: Science, technology and applications. Boca Raton, Fla.: CRC Press; Cambridge Woodhead Publishing; 2005.

[2] Banea MD, da Silva LFM, Carbas R, Campilho RDSG. Effect of material on the mechanical behaviour of adhesive joints for the automotive industry. *J Adhes Sci Technol* 2016; 31(6):663–76.

[3] Heuss D, Müller N, van Sintern W, Starke A. Lightweight, heavy impact; 2012.

[4] Speth DR, Yang YP, Ritter GW. Qualification of adhesives for marine composite-to-steel applications. *Int J Adhes Adhes* 2010; 30(2):55–62.

[5] Viana G, Costa M, Banea MD, da Silva LFM. A review on the temperature and moisture degradation of adhesive joints. *Proc Inst Mech Eng L J Mater Des Appl* 2016.

[6] Stephens RI, Fuchs HO. Metal fatigue in engineering. 2nd ed. New York, Chichester: Wiley; 2001.

[7] da Silva LFM, Öchsner A. Modeling of adhesively bonded joints. Berlin: Springer; 2008.

[8] Abdel Wahab M. Fatigue in Adhesively Bonded Joints: A Review. *ISRN Mat Sci* 2012; 2012(3):1–25.

[9] Khoramishad H, Crocombe AD, Katnam KB, Ashcroft IA. Predicting fatigue damage in adhesively bonded joints using a cohesive zone model. *Int J Fatigue* 2010; 32(7):1146–58.

[10] Shenoy V, Ashcroft IA, Critchlow GW, Crocombe AD, Abdel Wahab M. An evaluation of strength wearout models for the lifetime prediction of adhesive joints subjected to variable amplitude fatigue. *Int J Adhes Adhes* 2009; 29(6):639–49.

[11] da Silva LFM, Campilho RDSG (eds.). Advances in Numerical Modeling of Adhesive Joints. Berlin, Heidelberg: Springer Berlin Heidelberg; 2012.

[12] Sobieraj MC, Murphy JE, Brinkman JG, Kurtz SM, Rimnac CM. Notched fatigue behavior of PEEK. *Biomaterials* 2010; 31(35):9156–62.

[13] Sobieraj MC, Kurtz SM, Rimnac CM. Notch sensitivity of PEEK in monotonic tension. *Biomaterials* 2009; 30(33):6485–94.

[14] Takano M, Nielsen LE. The notch sensitivity of polymeric materials. *J Appl Polym Sci* 1976; 20(8):2193–207.

[15] Huang Y, Kinloch AJ. The role of plastic void growth in the fracture of rubber-toughened epoxy polymers. *J Mater Sci Lett* 1992; 11(8):484–7.

[16] da Silva LFM, Pirondi A, Öchsner A. Hybrid adhesive joints. Berlin, New York: Springer; 2011.

[17] Burst N, Adams DO, Gascoigne HE. Investigating the Thin-Film Versus Bulk Material Properties of Structural Adhesives. *J Adhesion* 2011; 87(1):72–92.

[18] Morin D, Haugou G, Bennani B, Lauro F. Identification of a new failure criterion for toughened epoxy adhesive. *Eng Fract Mech* 2010; 77(17):3481–500.

[19] Abdel Wahab M, Hilmy I, Ashcroft IA, Crocombe AD. Evaluation of Fatigue Damage in Adhesive Bonding - Part 1: Bulk Adhesive. *J Adhes Sci Technol* 2010; 24(2):305–24.

[20] Chen Z, Adams RD, Silva LFM. Fracture toughness of bulk adhesives in mode I and mode III and curing effect. *Int J Fract* 2011; 167(2):221–34.

[21] Spaggiari A, Castagnetti D, Dragoni E, Bulleri S. The use of the theory of critical distance and the stress-gradient approach in the fatigue life estimation of notched components. *Proc Inst Mech Eng L J Mater Des Appl* 2016; 230(3):735–47.

[22] Schneider B, Beber VC, Brede M. Estimation of the lifetime of bonded joints under cyclic loads at different temperatures. *J Adhesion* 2015; 92(7-9):795–817.

[23] da Silva LFM, Öchsner A, Adams RD. Handbook of adhesion technology. Berlin: Springer; 2011.

[24] DIN EN. Adhesives - Terms and definitions(923); 2008.

[25] Adams RD, Comyn J, Wake WC. Structural adhesive joints in engineering. 2nd ed. London: Chapman & Hall; 1997.

[26] Habenicht G. Kleben: Grundlagen, Technologien, Anwendungen. 6th ed. Berlin, Heidelberg: Springer Berlin Heidelberg; Springer; 2009.

[27] Rösler J, Harders H, Bäker M. Mechanical behaviour of engineering materials: Metals, ceramics, polymers, and composites. Berlin, New York: Springer; 2007.

[28] Kinloch AJ. Toughening Epoxy Adhesives to Meet Today's Challenges. *MRS Bull.* 2003; 28(06):445–8.

[29] Zotti A, Zuppolini S, Zarrelli M, Borriello A. Fracture Toughening Mechanisms in Epoxy Adhesives. In: Rudawska A, editor. Adhesives - Applications and Properties. InTech; 2016.

[30] Kinloch AJ, Shaw SJ, Tod D, Hunston D. Deformation and fracture behaviour of a rubber-toughened epoxy: Part 1 - Microstructure and fracture studies. *Polymer* 1983; 24:1341-1354.

[31] Pearson RA, Yee AF. Toughening mechanisms in elastomer-modified epoxies: Part 2 - Microscopy studies. *J Mater Sci* 1986; 21(7):2475–88.

[32] Yee AF, Pearson RA. Toughening mechanisms in elastomer-modified epoxies: Part 1 - Mechanical studies. *J Mater Sci* 1986; 21(7):2462–74.

[33] Beber VC, Schneider B, Brede M. Influence of Temperature on the Fatigue Behaviour of a Toughened Epoxy Adhesive. *J Adhesion* 2015; 92(7-9):778–94.

[34] Pethrick RA. Design and ageing of adhesives for structural adhesive bonding - A review. *Proc Inst Mech Eng L J Mater Des Appl* 2015; 229(5):349–79.

[35] da Silva LFM. Testing adhesive joints: Best practices. Weinheim: Wiley-VCH; 2012.

[36] da Silva LFM, das Neves PJ, Adams RD, Spelt JK. Analytical models of adhesively bonded joints—Part I: Literature survey. *Int J Adhes Adhes* 2009; 29(3):319–30.

[37] Schijve J. Fatigue of structures and materials. 2nd ed. Dordrecht, London: Springer; 2009.

[38] Wöhler A. Bericht über die Versuche, welche auf der k6nigl. Niederschlesisch-märkischen eisenbahn mit Apparaten zum Messen der Biegung und Verdehung von Eisenbahnwagenachsen während der Fahrt angestellt wurden. *Zeitschrift für Bauweisen* 1858; 8:641–52.

[39] Schütz W. A history of fatigue. *Eng Fract Mech* 1996; 54(2):263–300.

[40] Basquin O. The exponential law of endurance tests. *Proc Am Soc Test Mat* 1910; 10:625–30.

[41] Griffith A. The phenomena of rupture and flow in solids. *Phil Trans Royal Soc Lond Part A* 1921; 221:163–8.

[42] Miner MA. Cumulative damage in fatigue. *J Appl Mech* 1945; 12:159–64.

[43] Coffin L. A study of the effects of cyclic thermal stresses on a ductile metal. *Transactions of the ASME* 1954; 76:931–50.

[44] Manson S. Behavior of materials under conditions of thermal stress. TN-2933; 1954.

[45] Neuber H. Theory of notch stresses: Principles for exact calculation of strength with reference to structural form and material. Springer, Berlin; 1958.

[46] Peterson RE. Notch sensitivity. *Metal fatigue* 1959:293–306.

[47] Paris PC, Gomez MP, Anderson W. A rational analytic theory of fatigue. *Trend Eng* 1961; 13:9–14.

[48] Elber W. Fatigue crack propagation: some effects Fatigue crack propagation: some effects of crack closure on the mechanisms of fatigue crack propagation and cyclic loading [PhD]: University of South Wales; 1968.

[49] Sauer JA, Richardson GC. Fatigue of polymers. *Int J Fract* 1980; 16(6):499–532.

[50] Sonsino CM. Course of SN-curves especially in the high-cycle fatigue regime with regard to component design and safety. *Int J Fatigue* 2007; 29(12):2246–58.

[51] Richard HA, Sander M. Ermüdungsrisse: Erkennen, sicher beurteilen, vermeiden. 3rd ed. Wiesbaden: Springer Vieweg; 2012.

[52] Hertzberg RW, Vinci RP, Hertzberg JL. Deformation and fracture mechanics of engineering materials. 5th ed. Hoboken, N.J., Chichester: John Wiley & Sons; 2013.

[53] Costa M, Viana G, da Silva LFM, Campilho RDSG. Environmental effect on the fatigue degradation of adhesive joints: A review. *J Adhesion* 2016; 93(1-2):127–46.

[54] Baumgartner J, Schmidt H, Rybar G, Melz T, Ernstberger, L, Jendrny, Teutenberg D et al. Auslegung von geklebten Stahlblechstrukturen im Automobilbau für schwingende Last bei wechselnden Temperaturen nter Berücksichtigung des Versaensverhaltens. 290; 2016.

[55] Crocombe AD. Predicting the response of adhesively bonded structures under a range of service load conditions using finite element methods. *Int J Mat Prod Tech* 1999; 14(5/6):411.

[56] Underhill PR, DuQuesnay DL. The dependence of the fatigue life of adhesive joints on surface preparation. *Int J Adhes Adhes* 2006; 26(1-2):62–6.

[57] Bornemann J, Schlimmer M. Methodenentwicklung zur Berechnung und Auslegung geklebter Stahlbauteile für den Fahrzeugbau. AiF-P593; 2005.

[58] Haigh BP. Experiments in the fatigue of brasses. *J Inst Metals* 1917; 18:55–86.

[59] Fatemi A, Shamsaei N. Multiaxial fatigue: An overview and some approximation models for life estimation. *Int J Fatigue* 2011; 33(8):948–58.

[60] Wang DY. Influence of stress distribution on fatigue strength of adhesive-bonded joints. *Exp Mech* 1964:173–81.

[61] Ishii K, Imanaka M, Nakayama H, Kodama H. Fatigue failure criterion of adhesively bonded CFRP/metal joints under multiaxial stress conditions. *Comp Part A: Appl Sci Manuf* 1998; 29(4):415–22.

[62] Imanaka M, Iwata T. Estimation of Fatigue Strength for Adhesively-Bonded Lap Joints Based on Fatigue Failure Criterion Under Multiaxial Stress Conditions. *J Adhesion* 1998; 65(1-4):7–24.

[63] Susmel L. The theory of critical distances: A review of its applications in fatigue. *Eng Fract Mech* 2008; 75(7):1706–24.

[64] Rodríguez RQ, Paiva WP de, Sollero P, Bertoni Rodrigues MR, Albuquerque ÉL de. Failure criteria for adhesively bonded joints. *Int J Adhes Adhes* 2012; 37:26–36.

[65] García JA, Chiminelli A, García B, Lizaranzu M, Jiménez MA. Characterization and material model definition of toughened adhesives for finite element analysis. *Int J Adhes Adhes* 2011; 31(4):182–92.

[66] Ward IM. Review: The yield behaviour of polymers. *J Mater Sci* 1971; 6(11):1397–417.

[67] Ward IM, Sweeney J. Mechanical properties of solid polymers. John Wiley & Sons; 2012.

[68] Volkersen O. Die nietkraftoerteilung in zubeanspruchten nietverbindungen mit konstanten loschonquerschnitten. 15, 41–47 (1938). *Luftfahrtforschung* 1938(15):41–7.

[69] Goland M, Reissner E. The stresses in cemented joints. *J Appl Mech* 1944; 11(1):A17-A27.

[70] Hart-Smith L. Adhesive bonded double-lap joints. CR-112235; January/1973.

[71] Bigwood DA, Crocombe AD. Elastic analysis and engineering design formulae for bonded joints. *Int J Adhes Adhes* 1989; 9(4):229–42.

[72] Hart-Smith L. Adhesive bonded single-lap joints. CR-112236; January/1973.

[73] Gleich DM, van Tooren MJL, Haan PJ de. Shear and peel stress analysis of an adhesively bonded scarf joint. *J Adhes Sci Technol* 2000; 14(6):879–93.

[74] Adams RD, Peppiatt NA. Stress analysis of adhesive-bonded lap joints. *Journal of Strain Analysis* 1974; 9(3):185–96.

[75] Crocombe AD, Adams RD. Influence of the Spew Fillet and other Parameters on the Stress Distribution in the Single Lap Joint. *J Adhesion* 1981; 13(2):141–55.

[76] Harris JA, Adams RA. Strength prediction of bonded single lap joints by non-linear finite element methods. *Int J Adhes Adhes* 1984; 4(2):65–78.

[77] He X. A review of finite element analysis of adhesively bonded joints. *Int J Adhes Adhes* 2011; 31(4):248–64.

[78] Pasha RA, Hammouda M. A model for notch fatigue life. *Mat Sci Eng A-Struct* 2008; 483-484:319–21.

[79] Mcevily A, Endo M, Yamashita K, Ishihara S, Matsunaga H. Fatigue notch sensitivity and the notch size effect. *Int J Fatigue* 2008; 30(12):2087–93.

[80] Schijve J. Stress gradients around notches. *Fat Frac Eng Mat Struct* 1980; 3(4):325–38.

[81] Siebel E, Steiler M. Dissimilar stress distribution and cyclic loading. *VDI Zeitschrift* 1955; 97:121–31.

[82] Irwin GR. Analysis of Stresses and Strains Near the End of a Crack Traversing a Plate. *J Appl Mech* 1957.

[83] Sonsino CM, Moosbrugger E. Fatigue design of highly loaded short-glass-fibre reinforced polyamide parts in engine compartments. *Int J Fatigue* 2008; 30(7):1279–88.

[84] Sonsino C. Multiaxial fatigue of welded joints under in-phase and out-of-phase local strains and stresses. *Int J Fatigue* 1995; 17(1):55–70.

[85] Baumgartner J, Lipp K, Bruder T, Kaufmann H. Design methods for reliable fatigue assessment of PM components. *Mat -wiss u Werkstofftech* 2011; 42(10):894–903.

[86] Imanaka M, Fujinami A, Suzuki Y. Fracture and yield behavior of adhesively bonded joints under triaxial stress conditions. *J Mater Sci* 2000; 35:2481–91.

[87] Kinloch AJ, Williams JG. Crack blunting mechanisms in polymers. *J Mater Sci* 1980; 15(4):987–96.

[88] Katnam KB, Comer AJ, Stanley WF, Buggy M, Young TM. Investigating tensile behaviour of toughened epoxy paste adhesives using circumferentially notched cylindrical bulk specimens. *Int J Adhes Adhes* 2012; 37:3–10.

[89] Rodríguez J, Salazar A, Gómez FJ, Patel Y, Williams JG. Fracture of notched samples in epoxy resin: Experiments and cohesive model. *Eng Fract Mech* 2015; 149:402–11.

[90] Weixing Y, Kaiquan X, Yi G. On the fatigue notch factor, Kf. *Int J Fatigue* 1995; 17(4):245–51.

[91] Mortazavian S, Fatemi A. Notch Effects on Fatigue Behavior of Thermoplastics. *AMR* 2014; 891-892:1403–9.

[92] Zhou Y, Mallick PK. Fatigue performance of an injection-molded short E-glass fiber-reinforced polyamide 6,6. I. Effects of orientation, holes, and weld line. *Polym. Compos.* 2006; 27(2):230–7.

[93] Hoey D, Taylor D. Fatigue in porous PMMA: The effect of stress concentrations. *Int J Fatigue* 2008; 30(6):989–95.

[94] Cicero S, Madrazo V, Carrascal IA. Analysis of notch effect in PMMA using the Theory of Critical Distances. *Eng Fract Mech* 2012; 86:56–72.

[95] Taylor D (ed.). The Theory of Critical Distances. Elsevier; 2007.

[96] Taylor D. Geometrical effects in fatigue: A unifying theoretical model. *Int J Fatigue* 1999; 21(5):413–20.

[97] Pluvinage G. Fatigue and fracture emanating from notch; the use of the notch stress intensity factor. *Nucl Eng Des* 1998; 185(2-3):173–84.

[98] Beber VC, Fernandes PHE, Fragato JE, Schneider B, Brede M. Influence of plasticity on the fatigue lifetime prediction of adhesively bonded joints using the stress-life approach. *Appl Adhes Sci* 2016; 4(1):26.

[99] Beber VC, Fernandes PHE, Schneider B, Brede M. Effect of notch size on the fatigue damage behaviour of toughened epoxy adhesive specimens. *J Adhesion* 2017; 93(1-2):113–26.

[100] Crocombe AD. Global yielding as a failure criterion for bonded joints. *Int J Adhes Adhes* 1989; 9(3):145–53.

[101] Khoramishad H, Akhavan-Safar A, Ayatollahi M, da Silva LFM. Predicting static strength in adhesively bonded single lap joints using a critical distance based method: Substrate thickness and overlap length effects. *Proc Inst Mech Eng L J Mater Des Appl* 2016.

[102] Akhavan-Safar A, Ayatollahi MR, da Silva LFM. Strength prediction of adhesively bonded single lap joints with different bondline thicknesses: A critical longitudinal strain approach. *Int J Sol Struct* 2017.

[103] Ashcroft I, Abdel Wahab M, Crocombe AD, Hughes D, Shaw S. The effect of environment on the fatigue of bonded composite joints. Part 1: Testing and fractography. *Comp Part A: Appl Sci Manuf* 2001; 32(1):45–58.

[104] Beber VC, Fernandes P, Schneider B, Brede M, Mayer B. Fatigue lifetime prediction of adhesively bonded joints: An investigation of the influence of material model and multiaxiality. *Int J Adhes Adhes* 2017; 78:240–7.

[105] Mesmacque G, Garcia S, Amrouche A, Rubio-Gonzalez C. Sequential law in multiaxial fatigue, a new damage indicator. *Int J Fatigue* 2005; 27(4):461–7.

[106] Kinloch AJ, Osiyemi SO. Predicting the Fatigue Life of Adhesively-Bonded Joints. *J Adhesion* 1993; 43(1-2):79–90.

[107] Abdel Wahab M, Ashcroft I, Crocombe AD, Smith P. Finite element prediction of fatigue crack propagation lifetime in composite bonded joints. *Comp Part A: Appl Sci Manuf* 2004; 35(2):213–22.

[108] Pirondi A, Moroni F. An investigation of fatigue failure prediction of adhesively bonded metal/metal joints. *Int J Adhes Adhes* 2009; 29(8):796–805.

[109] Abdel Wahab M, Ashcroft IA, Crocombe AD, Shaw SJ. Prediction of fatigue thresholds in adhesively bonded joints using damage mechanics and fracture mechanics. *J Adhes Sci Technol* 2001; 15(7):763–81.

[110] Imanaka M, Hamano T, Morimoto A, Ashino R, Kimoto M. Fatigue damage evaluation of adhesively bonded butt joints with a rubber-modified epoxy adhesive. *J Adhes Sci Technol* 2003; 17(7):981–94.

[111] Brede M, Heise F-J. Schwingfestigkeitsauslegung von geklebten Stahlbauteilen des Fahrzeugbaus unter Belastung mit variablen Amplituden: Design of adhesive joints with steel components at loading with variable amplitudes for vehicle construction. Düsseldorf: Verl. und Vertriebsges; 2012.

[112] Shenoy V, Ashcroft IA, Critchlow GW, Crocombe AD, Abdel Wahab M. Strength wearout of adhesively bonded joints under constant amplitude fatigue. *Int J Fatigue* 2009; 31(5):820–30.

[113] Shenoy V, Ashcroft IA, Critchlow GW, Crocombe AD. Unified methodology for the prediction of the fatigue behaviour of adhesively bonded joints. *Int J Fatigue* 2010; 32(8):1278–88.

[114] Graner Solana A, Crocombe AD, Ashcroft IA. Fatigue life and backface strain predictions in adhesively bonded joints. *Int J Adhes Adhes* 2010; 30(1):36–42.

[115] Katnam KB, Crocombe AD, Khoramishad H, Ashcroft IA. Load Ratio Effect on the Fatigue Behaviour of Adhesively Bonded Joints: An Enhanced Damage Model. *J Adhesion* 2010; 86(3):257–72.

[116] Shen F, Voyiadjis GZ, Hu W, Meng Q. Analysis on the fatigue damage evolution of notched specimens with consideration of cyclic plasticity. *Fat Frac Eng Mat Struct* 2015; 38(10):1194–208.

[117] Barenblatt G. The formation of equilibrium cracks during brittle fracture. General ideas and hypotheses. Axially-symmetric cracks. *Journal of Applied Mathematics and Mechanics* 1959; 23(3):622–36.

[118] Dugdale DS. Yielding of steel sheets containing slits. *Journal of the Mechanics and Physics of Solids* 1960; 8(2):100–4.

[119] Roe KL, Siegmund T. An irreversible cohesive zone model for interface fatigue crack growth simulation. *Eng Fract Mech* 2003; 70(2):209–32.

[120] Turon A, Costa J, Camanho PP, Dávila CG. Simulation of delamination in composites under high-cycle fatigue. *Comp Part A: Appl Sci Manuf* 2007; 38(11):2270–82.

[121] Ural A, Krishnan VR, Papoulia KD. A cohesive zone model for fatigue crack growth allowing for crack retardation. *Int J Sol Struct* 2009; 46(11-12):2453–62.

[122] Hilmy I, Abdel Wahab M, Ashcroft IA, Crocombe AD. Measuring of Damage Parameters in Adhesive Bonding. *KEM* 2006; 324-325:275–8.

[123] Zhang Z, Shang JK, Lawrence FV. A Backface Strain Technique for Detecting Fatigue Crack Initiation in Adhesive Joints. *J Adhesion* 1995; 49(1-2):23–36.

[124] Crocombe AD, Ong CY, Chan CM, Abdel Wahab M, Ashcroft IA. Investigating Fatigue Damage Evolution In Adhesively Bonded Structures Using Backface Strain Measurement. *J Adhesion* 2002; 78(9):745–76.

[125] Shenoy V, Ashcroft IA, Critchlow GW, Crocombe AD, Abdel Wahab M. An investigation into the crack initiation and propagation behaviour of bonded single-lap joints using backface strain. *Int J Adhes Adhes* 2009; 29(4):361–71.

[126] Dessureautt M, Spelt JK. Observations of fatigue crack initiation and propagation in an epoxy adhesive. *Int J Adhes Adhes* 1997; 17(3):183–95.

[127] Azari S, Papini M, Schroeder JA, Spelt JK. Fatigue threshold behavior of adhesive joints. *Int J Adhes Adhes* 2010; 30(3):145–59.

[128] Court RS, Sutcliffe M, Tavakoli SM. Ageing of adhesively bonded joints—fracture and failure analysis using video imaging techniques. *Int J Adhes Adhes* 2001; 21(6):455–63.

[129] Quaresimin M, Ricotta M. Life prediction of bonded joints in composite materials. *Int J Fatigue* 2006; 28(10):1166–76.

[130] Khoramishad H, Crocombe AD, Katnam KB, Ashcroft IA. A generalised damage model for constant amplitude fatigue loading of adhesively bonded joints. *Int J Adhes Adhes* 2010; 30(6):513–21.

[131] Tsuji, Iwase, Ando. An investigation into the location of crack initiation sites in alumina, polycarbonate and mild steel. *Fat Frac Eng Mat Struct* 1999; 22(6):509–17.

[132] Sobieraj MC, Kurtz SM, Rimnac CM. Notch strengthening and hardening behavior of conventional and highly crosslinked UHMWPE under applied tensile loading. *Biomaterials* 2005; 26(17):3411–26.

[133] Dow Automotive AG. Technical Datasheet - Betamate 1496 V; 2002.

[134] Sika AG. Sika Power-498 - Security Data Sheet.

[135] ISO EN. Adhesives - Methods of preparing bulk specimens - Part 2: Elevated-temperature-curing one-part systems(15166-2); 2000.

[136] Pilkey WD, Pilkey DF, Peterson RE. Peterson's stress concentration factors. Hoboken, N.J.: John Wiley; 2008.

[137] ISO EN. Metallic materials. Fatigue testing. Statistical planning and analysis of data(12107). London: BSI British Standards; 2012. doi:10.3403/02933174.

[138] E08 Committee. Practice for Statistical Analysis of Linear or Linearized Stress-Life (S-N) and Strain-Life (-N) Fatigue Data. West Conshohocken, PA: ASTM International; 2015. doi:10.1520/E0739-10R15.

[139] Lemaitre J. How to use damage mechanics. *Nucl Eng Des* 1984; 80(2):233–45.

[140] Abdel Wahab M, Hilmy I, Ashcroft IA, Crocombe AD. Damage Parameters of Adhesive Joints with General Triaxiality Part I: Finite Element Analysis. *J Adhes Sci Technol* 2012; 25(9):903–23.

[141] Chiminelli A, Breto R, Jiménez MA, Velasco F, Abenojar J, Martínez M. Experimental method for the determination of material parameters of plasticity models for toughened adhesives. *Int J Adhes Adhes* 2016; 68:182–7.

[142] Hua Y, Crocombe AD, Wahab MA, Ashcroft IA. Continuum damage modelling of environmental degradation in joints bonded with E32 epoxy adhesive. *J Adhes Sci Technol* 2007; 21(2):179–95.

[143] Dean G, Crocker L, Read B, Wright L. Prediction of deformation and failure of rubber-toughened adhesive joints. *Int J Adhes Adhes* 2004; 24(4):295–306.

[144] Hua Y, Kasavajhala ARM, Gu L. Elastic–plastic analysis and strength evaluation of adhesive joints in wind turbine blades. *Composites Part B: Engineering* 2013; 44(1):650–6.

[145] Christensen RM. Observations on the definition of yield stress. *Acta Mech* 2008; 196(3-4):239–44.

[146] Prabhakaran R, Nair EMS, Sinha PK. Notch sensitivity of polymers. *J Appl Polym Sci* 1978; 22(10):3011–20.

[147] Lemaitre J. A Continuous Damage Mechanics Model for Ductile Fracture. *J. Eng. Mater. Technol.* 1985; 107(1):83.

[148] Taylor D, Merlo M, Pegley R, Cavatorta MP. The effect of stress concentrations on the fracture strength of polymethylmethacrylate. *Materials Science and Engineering: A* 2004; 382(1-2):288–94.

[149] Gómez FJ, Elices M, Berto F, Lazzarin P. Local strain energy to assess the static failure of U-notches in plates under mixed mode loading. *Int J Fract* 2007; 145(1):29–45.

[150] Susmel L, Taylor D. On the use of the Theory of Critical Distances to predict static failures in ductile metallic materials containing different geometrical features. *Eng Fract Mech* 2008; 75(15):4410–21.

[151] Benedetti M, Fontanari V, Allahkarami M, Hanan JC, Bandini M. On the combination of the critical distance theory with a multiaxial fatigue criterion for predicting the fatigue strength of notched and plain shot-peened parts. *Int J Fatigue* 2016; 93:133–47.

[152] Taylor D, Wang G. The validation of some methods of notch fatigue analysis. *Fat Frac Eng Mat Struct* 2000; 23(5):387–94.

[153] Susmel L, Taylor D. Two methods for predicting the multiaxial fatigue limits of sharp notches. *Fat Frac Eng Mat Struct* 2003; 26(9):821–33.

[154] Susmel L, Taylor D. A novel formulation of the theory of critical distances to estimate lifetime of notched components in the medium-cycle fatigue regime. *Fat Frac Eng Mat Struct* 2007; 30(7):567–81.